IANCAS Bulletin

INDIAN ASSOCIATION OF NUCLEAR CHEMISTS AND ALLIED SCIENTISTS

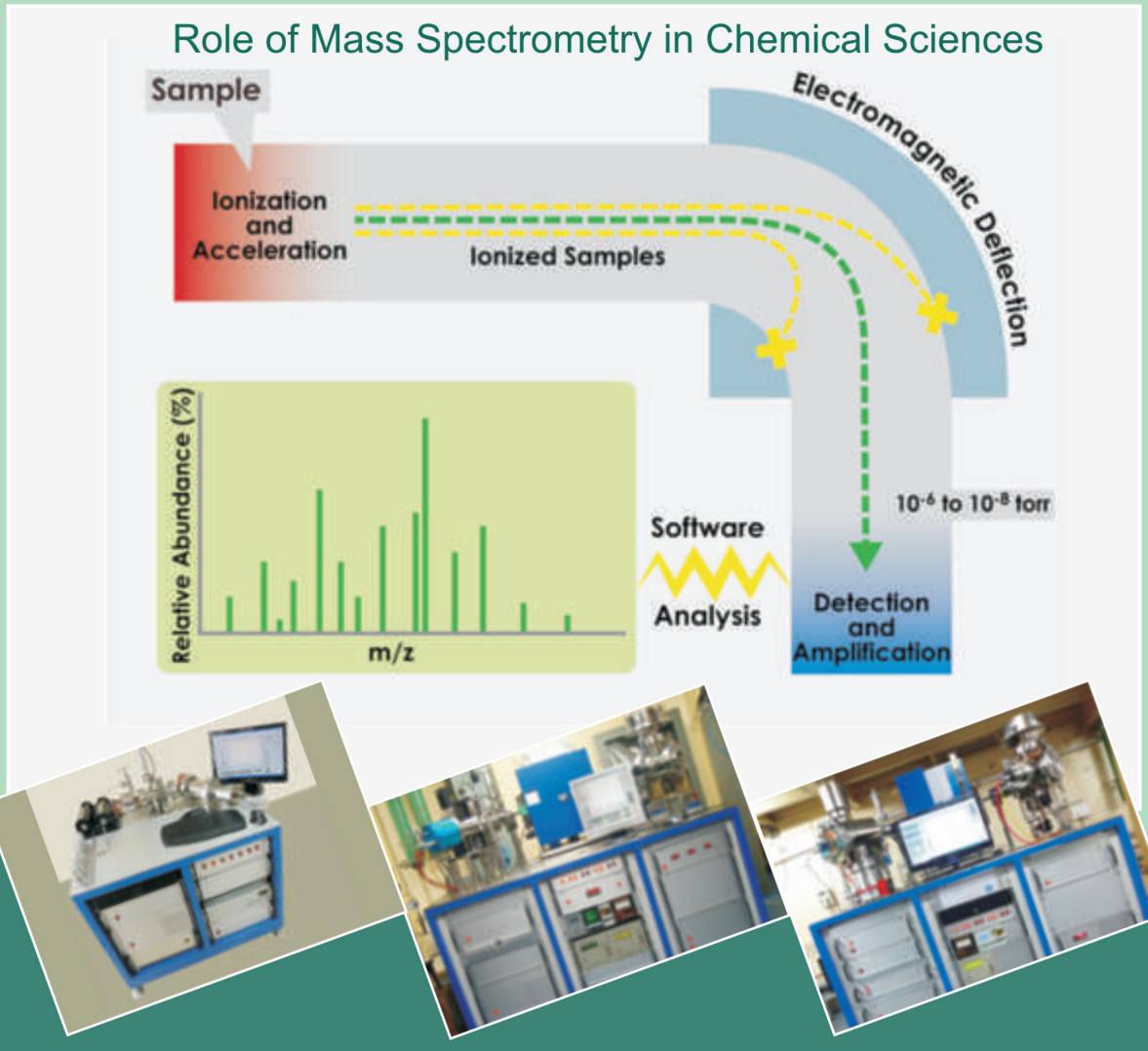

www.iancas.org

December 2016 Vol. XIII No. 2

Vol. XIII No. 2 **December 2016**

CONTENTS

From Secretary's Desk

Dear Members,

Greetings from BARC, Mumbai.

I am very happy to let to know that thematic bulletin on "Role of Mass Spectrometry in Chemical Sciences" is ready for circulation. Mass spectrometry has become an indispensable analytical tool and has played a pivotal role in a number of scientific breakthroughs such as the exact determination of atomic weights, characterization of new elements, stable isotope labeling and identification of trace pollutants and drugs. Mass spectrometry also contributed to the understanding of the structure of elementary matter including the isotopic nature of the chemical elements, isotopic abundance, nuclear binding, and the investigation of nuclides far-off stability. Precision measurements of isotopic masses and abundances by mass spectrometers drove researchers to new international standard for atomic mass. Due to the good sensitivity and precision, inorganic mass spectrometry is playing a critical role in the characterization of nuclear materials, post-irradiation examinations of nuclear fuels, environmental monitoring, nuclear material accounting and radioactive waste management. Mass spectrometry is being employed in the identification of complex natural products and of metabolic pathways. The capabilities of detecting and identifying trace constituents in small size samples have led to use of mass spectrometers in toxicology, drug abuse diagnosis, environmental pollution monitoring and pharmaceutical industries. Mass spectrometry is now the most widely used anlytical technique in almost all areas of science & technology. I am sure that the present thematic bulletin would be able to promote mass spectrometry and its applications in research and various areas of societal applications.

With the help of many active members, various activities of IANCAS are being done very smoothly. With kind support of BRNS, we are able to organize National and Local Workshops in various educational institutes in India. On behalf of IANCAS, I thank BRNS, DAE for the financial support towards bringing out the thematic bulletins.

With best wishes & regards.

R. Acharya
Radiochemistry Division, BARC
Email : racharya@barc.gov.in

FOCUS

Dr. B. S. Tomar
Director, Radiochemistry and Isotope Group, BARC
& Vice President, IANCAS

The history of mass spectrometry began with Sir J. J. Thomson when he constructed an instrument then called a parabola spectrograph for the determination of mass-to-charge ratios of ions. Thomson's associate, F. W. Aston designed a mass spectrometer in which ions were dispersed by mass and focused by velocity which significantly improved resolving power. Subsequent developments in the fields of instrumentation, electronics and applications transformed mass spectrometry into a powerful analytical technique used to quantify known materials, to identify unknown compounds and to elucidate the structure of molecules.

In view of its capability to provide precise data on the isotopic composition and concentration, mass spectrometry has become an indispensable analytical technique for the measurements at different stages of the nuclear fuel cycle including quality control of fuels, nuclear material accounting, nuclear safeguards, nuclear forensics, environmental monitoring etc. A variety of mass spectrometric techniques such as thermal ionization mass spectrometry, electron impact ionisation mass spectrometry, inductively coupled plasma source mass spectrometry, glow discharge mass spectrometry, knudsen effusion cell mass spectrometry, accelerator mass spectrometry, secondary ion mass spectrometry, electrospray ionisation mass spectrometry etc are being employed to obtain data at various stages of nuclear fuel cycle. Precise measurement of isotopic ratios finds applications in a variety of fields such as age determination of rocks and meteorites based on Sm-Nd dating, verifying the provenance of food materials based on $^{87}Sr/^{86}Sr$, unraveling the past climatic change using $^{18}O/^{16}O$, to name a few applications.

Developments in technology have expanded mass spectrometry from a tool for characterizing small molecules to its current manifestation as one of the most powerful technique for characterizing large molecules in proteomics, lipidomics, metabolomics etc. The advent of soft ionization techniques like electrospray and matrix assisted laser desorption/ionization in combination with the high resolution mass analysers pawed the way for mass spectrometry to become an indispensable tool for molecular and cellular biology and for the emerging field of systems biology.

I thank all the contributors for providing excellent articles towards this important bulletin on "Role of Mass Spectrometry in Chemical Sciences". I am sure that both novices & general research community would find this bulletin useful and enjoyable. I thank Shri. M. K. Saxena, RACD, BARC & Dr. P. G. Jaison, FCD, BARC (Guest Editors) for sparing their time and makeing this bulletin possible in present from. On behalf of IANCAS, I thank BRNS, DAE for the continued financial support.

Guest Editorial

M.K. Saxena
RACD, BARC

Jaison P.G.
FCD, BARC

Mass spectrometry is a multi-disciplinary science and has established as an indispensable analytical tool due to its sensitivity, specificity and universality. Mass spectrometry plays vital roles in a variety of scientific disciplines of chemistry, physics, biology, archaeology, material science etc. Developments in the field of mass spectrometry in the recent past has led to the advent of new ionisation techniques, improvements in existing mass analyzers and introduction of hybrid mass analyzers. As the technique continues to advance, many new applications have emerged particularly in health sciences, material science and forensic applications. The current scenario demands determination of concentration or isotopic composition at extremely low levels with high degree of confidence.

It is a matter of great pleasure to the Editors to present this Thematic Bulletin containing the articles illustrating the impact of mass spectrometry on various fields of research. In order to appreciate various aspects of mass spectrometry, well established practitioners were requested to contribute in the areas of their specialization. It is a matter of privilege for us that the prominent experts from different fields readily agreed to share their rich experience in the field of mass spectrometry. We profusely thank all the contributors for providing their articles for this thematic bulletin.

The first chapter gives an overview of various types of ionisation techniques, mass analyzers and detectors along with their instrumentation aspects. Readers especially novices would find this chapter useful to appreciate the specific mass spectrometric techniques/applications described in the subsequent chapters.

The potential of elemental mass spectrometry for the characterization of materials for composition and isotopic abundance with a high degree of precision and accuracy is highlighted in the next two chapters. These articles illustrate how the techniques such as inductively coupled plasma mass spectrometry (ICP-MS) and thermal ionisation mass spectrometry (TIMS) have become the work horse for quality assurance of fuel materials.

Overviews of laser-mass spectrometric techniques that are used in nuclear energy research are described in the fourth chapter. The in-house developed laser based mass spectrometers were employed in the analyses of refractory materials with high levels of radioactivity and under hostile environment.

Fifth chapter describes the use of mass spectrometry for generation of thermodynamic data corresponding to both condensed and vapor phases. Studies on the rate of vaporisation also help to obtain kinetics of vaporisation and condensation processes and also insight to bonding in molecules.

Chapter six deals with the use of accelerator based mass spectrometry to provide data on very low levels of cosmogenic nuclides which is used to understand various Earth processes and to determine the age.

Application of stable isotope ratio mass spectrometry in oceanography is described in detail in chapter seven.

Organic mass spectrometry played a key role in bringing out a paradigm shift in the drug discovery and development process. Chapter eight highlights the role of mass spectrometry in drug discovery process and its advancements.

The last chapter highlights the role of organic mass spectrometry especially electrospray ionization (ESI) and matrix assisted laser desorption/ionization (MALDI) in the analysis of polypeptides and other biological molecules to overcome the challenges of proteome analysis

We hope that the readers would find this thematic bulletin both enjoyable and valuable and we welcome comments and suggestions from the readers. It was indeed an enjoyable and learning experience for us to compile this thematic bulletin and we wish to thank IANCAS for giving us this opportunity.

Mass Spectrometry: Principles and Instrumentation

V. Nataraju

Advanced Mass Spectrometry Section, Technical Physics Division, BARC, Mumbai 400085, India
Email: vogirala@barc.gov.in

Introduction

Mass spectrometry is a highly powerful and useful analytical technique for assaying a material on the basis of mass to charge ratio of the analyte ions [1-4]. When compared with other analytical techniques viz. spectroscopy and radio-active emission counting etc., mass spectrometry is a more sensitive, precise and selective technique [5,6]. The technique provides highly valuable information in various fields viz. nuclear technology, geochronology, chemistry, biology, planetary science, pharmaceutical industry, petrochemical industry etc.

Some of the typical applications of mass spectrometry in different fields are as below:

- Characterization of various materials employed in different stages of nuclear energy generation is carried out by the isotopic ratio measurement of various elements, eg. the reactor fuel (U), the spent fuel (Pu), the activity controlling material (B), moderator (H) and structural materials (Pb) etc. In geochronology the isotopic ratio composition of Sr,Rb, Nd, Os, and Pb etc. helps in age determination of various rock samples.
- In environmental science, mass spectrometry is employed for the trace elemental detection of toxic elements like Pb, As, Hg etc. for the health and safety purpose. The isotopic ratios of various elements like Sr, C, S, O and N etc. are used as signatures specific to a region or system and helps in studying the migration of substance from one region/system to another, eg.the ground water studies, crop production, soil erosion, meteorological studies etc. In planetary science, the isotopic studies of any planetary object are carried out to ascertain its origin of composition.
- The accelerator mass spectrometry [1] is employed for the age determination of various organic or planetary species consisting of long lived radio nuclides e.g. radio isotopes of C, Be, Al and I etc.
- In organic chemistry [4] mass spectrometry is used in the determination of molecular weights, structural and speciation studies of compounds, detection of various drugs in the blood samples of athletes, identification of drugs and their metabolites in human body fluids etc.

Principle

A mass spectrometer consists of mainly three parts: (a) the ion source, (b) analyzer and (c) detector. The analyte material is introduced in the ion source where the neutral atoms/molecules undergo ionization. The ions so formed are accelerated and passed through or trapped inside the analyzer where they get separated as per their m/q ratio. The ion current corresponding to respective ion species are measured using suitable detector and the spectrum of ion intensity versus m/q is generated. There are variety of ion sources, analyzers and detectors which are used in different combinations as per demand of the application. A mass spectrometer is characterized by the parameters like resolution, mass range, sensitivity and precision etc. Typical examples of a mass spectrometers are- thermal ionization mass spectrometer (TIMS), electron impact mass spectrometer (EIMS), quadrupole mass spectrometer (QMS), inductively coupled mass spectrometer (ICPMS), glow discharge mass spectrometer (GDMS), time of flight mass spectrometer (TOFMS), secondary ion mass spectrometer (SIMS), resonance ionization mass spectrometer (RIMS), accelerator mass spectrometer (AMS) etc.

The mass spectrometers for inorganic applications are mainly employed for the measurements related to elemental species. The ionization technique is selected based on the effective ionization of the atoms of an element present in the analyte material and the molecular integrity of the analyte species is not important. The main applications covered in this category are – isotopic ratio measurement of an element, compositional analysis of material, trace elemental detection and surface and bulk imaging of the solid materials etc.

The organic applications include mass spectrometers with soft ionization techniques [2, 4] so that the integrity of the molecules of organic or bio-organic analyte remains intact. Mostly used techniques are Matrix Assisted Laser Desorption Ionization (MALDI) [4, 9] and Electro Spray Ionization (ESI) [10, 11] with RF quadrupole [12], time of flight [4, 13] and ion trap analyzers [14]. The applications involve the molecular weight measurements, molecular structural characterization and speciation studies of etc.

Ion sources

- Electron impact / bombardment (EI / EB)
- Thermal ionization (TI)
- Inductively Coupled Plasma (ICP)
- Glow Discharge (GD)
- Secondary Ion induced ionization
- Matrix assisted laser desorption ionization (MALDI)
- Electro-spray ionization (ESI)
- Resonance Ionization (RI)

Above techniques are explained in the following pages.

i Electron impact /bombardment ion source

beam to increase the path length of the electrons, leading to enhancement of the ionization efficiency of the ion source.

The electron impact ion source [1, 2] is used for the ionization of samples in gaseous phase. The principle is based on the ionization of neutral atoms or molecules of analyte by collision with the energetic electrons. The ionization can take place by following processes. Removal of electrons from outermost orbit of an atom (A) or molecule (M):

$$A + e \rightarrow A^+ + 2e$$

$$M + e \rightarrow M^+ + 2e$$

Molecules may also undergo fragmentation along with ionization.

$$M + e \rightarrow A^+ + (M\text{-}A)^0 + 2e$$

The ion source consists of an ionization box (also called as case box) which uses tungsten filament for producing electrons and other electrodes *viz*. repeller, trap, electron focus and shield as shown in the Fig. 1. A magnetic field in the range of 150 – 200 gauss is also employed in the direction of electron beam to increase the path length of the electrons, leading to enhancement of the ionization efficiency of the ion source.

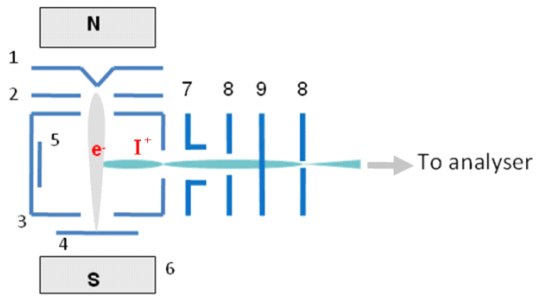

Fig. 1. Schematic of Electron impact ion source. 1.Filament, 2. Electron Focus, 3.Case Box, 4. Trap, 5. Repeller, 6. Magnet, 7. Y Plate, 8. Ground Plate, and 9. Z Plate.

The filament is heated to very high temperature by ohmic heating emitting electrons by thermionic emission. The emission is governed by Child Langmuir's Law as given below:

$$N_e = AT^2 \exp(-\Phi/kT) \quad (1)$$

where N_e is the number of electrons emitted per unit area per unit time from the filament surface, A *is a* constant (material property), Φ is the work function of the filament, k is Boltzman's constant and T *is* absolute temperature.

These electrons accelerated to an energy of 70 eV, undergo inelastic collision with the gas molecules/atoms introduced into the ion source and ionize them by knocking out outermost electrons or by breaking the chemical bonds of the molecules. The ion beam intensity (I^+) obtained from the ion source is given by following equation.

$$I^+ = \beta I^- L_e \sigma n_g \quad (2)$$

where β *is* transmission factor of ion source, I^- is electron current (also called as emission current of filament), L_e is path length of electron, $\acute{o}$ is ionization cross section of gas particle for a given energy of electron and n_g is gas density.

The ionization cross section $\acute{o}$ is dependent on ionization potential of analyte species and the energy of electron as shown in Fig. 2. It is evident from this figure that the ionization is maximum in the range of 50 -100 eV for various analyte species. The probability of in-elastic collision (and hence the ionization) increases with kinetic energy in lower energy limits as the the electrons do not possess sufficient energy for undergoing in-elastic collision with the gas particles. However with increasing kinetic energy, the time spent by the electron in the vicinity of analyte molecule reduces thereby reducing the interaction between the ionizing electron and analyte, leading to reduced probability of ionization. Hence after a certain limit, the ionization probability reduces with the kinetic energy of the electrons. In the intermediate region (50 – 100 eV) the interaction time and the energy of electron are optimum for maximum ionization.

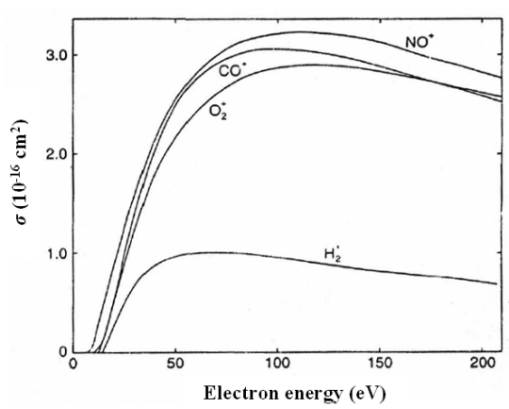

Fig. 2. Dependence of ionization cross section on kinetic energy of electron in an EI source

The ionization cross section s is dependent on ionization potential of analyte species and the energy of electron as shown in Fig. 2. It is evident from this figure that the ionization is maximum in the range of 50 -100 eV for various analyte species. The probability of in-elastic collision (and hence the ionization) increases with kinetic energy in lower energy limits as the the electrons do not possess sufficient energy for undergoing in-elastic collision with the gas particles. However with increasing kinetic energy, the time spent by the electron in the vicinity of analyte molecule reduces thereby reducing the interaction between the ionizing electron and analyte, leading to reduced probability of ionization. Hence after a certain limit, the ionization probability reduces with the kinetic energy of the electrons. In the intermediate region (50 – 100 eV) the interaction time and the energy of electron are optimum for maximum ionization.

The electron impact ion source is known for its reliability, stability and sensitivity. It is suitable for magnetic

sector (for precise isotopic ratio analysis) and quadrupole analyzers (for compositional analysis of gas mixture and organic samples). Subsequent to the ionization in EI source, the ions are accelerated to 5 – 10 keV for a magnetic sector and to 2-20 eV for a radio frequency (RF) quadrupole analyser. The ions exhibit moderate energy spread in the range of 1 – 5 eV and therefore for certain applications may require high resolution using double focusing (magnetic sector in combination with electrostatic analyser) arrangement. Being a hard ionization (fragmentation of molecules) technique it is not suitable for bio-organic molecules as the molecular integrity is lost due to fragmentation.

ii Thermal ionization source

In this technique ionization of a given analyte occurs when it is adsorbed on a hot surface of high work function material [1-4, 6]. Source consists of single or plurality of filaments of a high work function material in the form of a ribbon. The solid sample dissolved in acidic medium is deposited on one or two filaments called sample filament. The sample filament is heated electrically under vacuum and the ionization is achieved by surface ionization of the sample vapors on same filament (single filament assembly) or the other filament (double or triple filament assembly) called as ionization filament.

The ionization efficiency is governed by Saha Langmuir equation:

$$n^+/n_i = g_i/g_{\bar{i}} [(1-r_i)/(1-r_{\bar{i}})] \exp\{(W-I)/kT\} \quad (3)$$

where n^+& n_i are the number of positive ions formed and neutral species evaporated, r_i & $r_{\bar{i}}$ are reflection coefficients and g_i & $g_{\bar{i}}$ are the statistical weights of the ionic and atomic states, W is the work function of the filament, I is the ionization energy of the element, T is the temperature of the surface and k is the Boltzmann constant.

The ionization efficiency (β) is defined as the relative number of neutral species converted to ions as follows:

$$\beta = n^+ / N \quad (4)$$

where N is total number of species given as:

$$N = n_o + n^+ + n^-$$

For negligible negative ions:

$$N \sim n_o + n^+ \quad (5)$$

Using equation 4 and 5:

$$\hat{a} = 1/(1+1/\acute{a}) \quad (6)$$

where $\acute{a} = n^+/n_{\bar{i}}$

Equation 3 shows that the ionization efficiency is dependent on ionization potential of the analyte species, work function of the filament material and the temperature. In case of elements with low ionization potential (IP< W), W-I term in equation 3 is positive which implies that the ionization efficiency increases with reduced temperature. In this case single filament is sufficient for sample deposition as well as ionization. The filament is heated to a temperature just enough for the sufficient vaporization of sample to get the ions in gas phase.

In case of elements with high ionization potential (IP >W), the term W-I becomes negative so that the ionization efficiency increases with the temperature. In this case the sample is required to be heated at much higher temperature for high sensitivity that can lead to evaporation of the sample before sufficient ionization takes place if single filament is used. This leads to the use of multiple filament assembly whereby double or triple filaments are employed to decouple the evaporation and ionization processes. The double filament assembly consists of one sample and one ionization filament facing each other as shown in the Fig. 3(a). The triple filament assembly incorporates two sid)e filaments and a centre filament as shown in Fig. 3(b). The decoupling helps in controlling the evaporation and ionization processes independently and hence optimizing the ionization efficiency. Generally Rhenium (Re) filament (single or multiple) is used for ionization because of its high work function (~5.2 eV) and high melting point (3180° C). Other used filament materials are tungsten, tantalum and platinum etc.

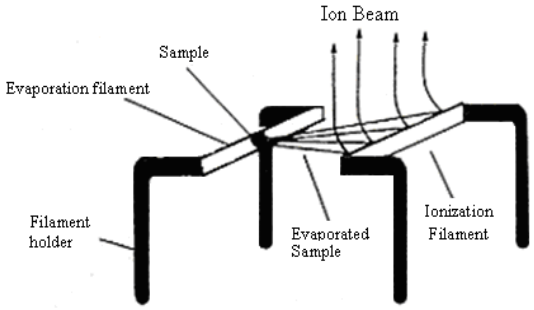

Fig. 3(a). A double filament assembly

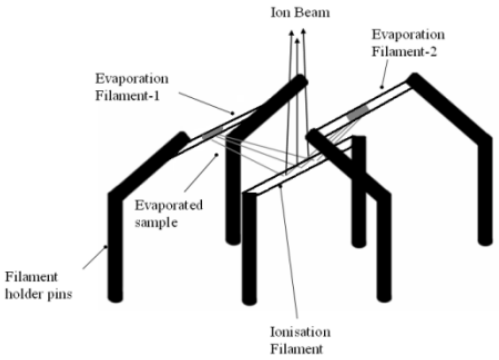

Fig. 3(b). A triple filament assembly

As the ionization efficiency is dependent on the work function of the filament, there are various techniques used for enhancing the work function for an element with very high IP (>7 eV). To mention a few techniques - graphite coating of the filament for enhancing ionization of actinides, deposition of silica gel/phosphoric acidic on the filament before sample loading for Pb, Fe, Cr etc. and resin bead technique to analyse nanograms of U and Pu samples.

Some of the elements (with high IP) exhibit sufficiently high probability of negative ionization which is governed by following equation:

$$n^-/n_i = g_i/g_i[(1-r_i)/(1-r_i)] \exp\{(W-EA)/kT\} \quad (7)$$

where EA denotes electron affinity and other terms represents same meanings as for eq. 3. The elements with high EA produce negative ions in excess than positive ions during thermal ionization and are analysed by negative thermal ionization mass spectrometry (NTIMS) e.g. Osmium (Os), Boron (B) and Rhenium (Re) etc.

The thermal ionization source is known for its sensitivity, stability, selectivity and low energy spread (1 – 2 eV). It is used in combination with a magnetic sector analyzer for precise isotopic ratio measurement of elements.

iii Inductively coupled plasma ion source

This technique exhibits very high ionization efficiency [4,6,7,32] and is employed for the trace elemental detection for more than 90% of the elements in periodic table. The technique is known for very low detection limit (up to 10^{-15} for some of the elements), high sample throughput, very simple sample preparation and sample introduction systems. It is used in combination with RF (radio frequency) quadrupole for trace elemental detection. It can also be coupled with combination of electrostatic and magnetic analysers for precise isotopic ratio measurements. The ionization is based on the evaporation, atomization and ionization of aqueous sample by the high temperature (> 8000 K) atmospheric plasma generated by inductive coupling between the RF field from coil and the electrons present inside the coil.

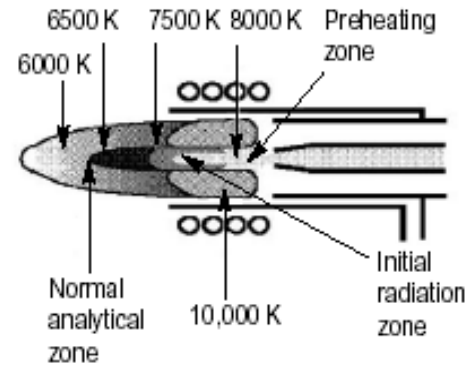

Fig. 4(a). Schematic of ICP

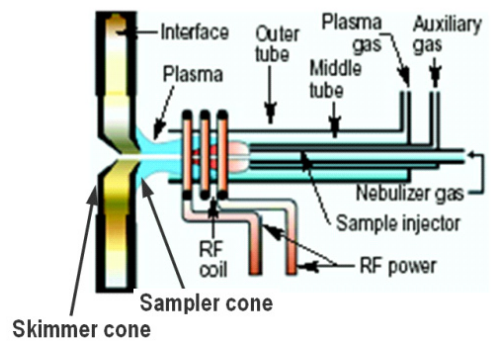

Fig. 4(b). Different temperature zone in plasma

An ICP source consists of a plasma torch, an RF coil and RF power supply as shown in Fig. 4(a) and(b). The plasma torch is made of three hollow co-axial quartz tubes (with different radii) fused together. Argon gas is introduced in the outer most (region between outer tube and the middle tube) at a flow rate of 12 – 15 L/min (plasma flow) to generate plasma and for cooling the inside of the outer most tube. An auxiliary flow of ~ 1 L/min is introduced in the mid region and carrier flow of ~ 0.5 L/min is maintained in the inner most tube. An RF power of 1-1.5 kW with frequency of 27.12 MHz is supplied to the coil. Electrons produced by spark from a Tesla coil get coupled to the RF field (produced by RF coil surrounding the torch) and get energized and ignite intense plasma (8000 K) in the region near to the opening of the torch. The sample introduced by the carrier gas gets evaporated, atomized and ionized in the central region of the plasma.

As the ions are produced in atmosphere, the introduction inside the vacuum is achieved by differential pumping using water cooled sampler and skimmer cones made up of Nickel. The sampler cone with orifice of around 1 mm is placed ~10-20 mm from the torch and the skimmer cone with orifice of 0.85 mm is placed at a distance of ~ 9 mm downstream of the sampler.

The region between sampler and skimmer cone is evacuated up to 1 – 0.1 torr. The hot gas from plasma while passing through the sampler cone aperture undergoes hydrodynamic expansion and gets cooled down within a distance of less than an aperture diameter. This leads to freezing the reactions which can change the composition of the plasma gas. The sudden cooling at reduced pressure directs the gas along the axis leading to the free jet formation that is bound radially by shock wave known as barrel shock and terminated by perpendicular shock known as Mach disc. The skimmer cone is placed at a distance just before the formation of Mach disc. The region beyond skimmer cone has high vacuum in the range of (2^{nd} Stage) which also houses the electrostatic lens followed by the third vacuum stage (< 10^{-6} torr) having the mass analyser.

iv Glow Discharge

Glow discharge ionization [1,6] is a powerful analytical technique for the trace elemental detection in solid samples. It is a complementary technique to ICP with advantages of lower detection limits and lower cost of the instrumentation. However, lower throughput and presence of matrix effects (as compared with ICP) are the drawbacks of this technique. The ionization is based on sputtering and ionization of the molecules by Argon ions generated by glow discharge. The glow discharge is obtained by various methods namely direct current (DC) glow discharge (mostly employed), radiofrequency and pulsed mode glow discharge.

The ionization is based on sputtering and ionization of the molecules by Argon ions generated by glow discharge. The glow discharge is obtained by various methods namely direct current (DC) glow discharge (mostly employed), radiofrequency and pulsed mode glow discharge.

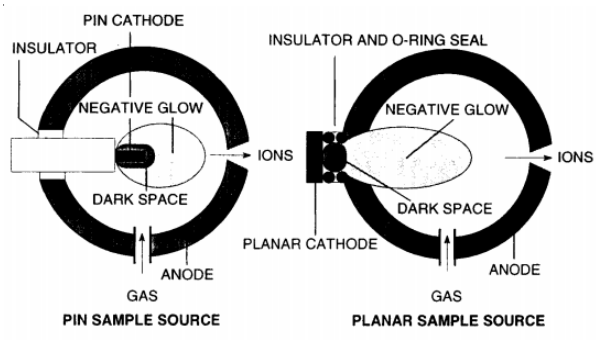

Fig. 5. Schematic of the GD ion source with (a) Pin cathode and (b) Planer cathode

In DC glow discharge, the solid sample in form of a disc or a pin is used as cathode in the ion source as shown in Fig. 5. The plasma is struck between cathode and anode under low pressure atmosphere (0.1 – 10 torr) of Argon gas by applying negative DC voltage (500 volts – 1000 volts) on cathode with respect to anode at ground potential. Different discharge regions are generated as shown in the Fig. 6.

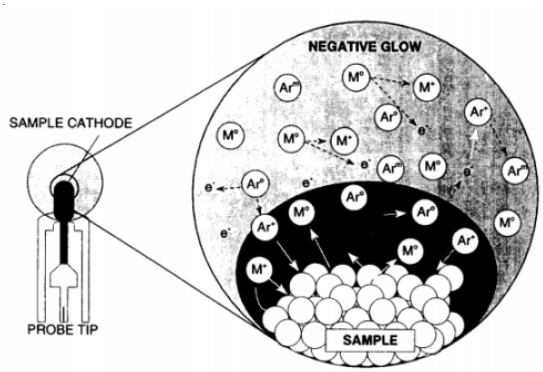

Fig. 6. Schematic showing different regions in glow discharge

The cathode is surrounded by a narrow dark space which is extended up to one mean free path away from the cathode surface and hence is free form collision induced excitation and recombination involving electrons. Around 80% of the voltage (between electrodes) falls across this region that leads to the maximum acceleration of electrons and Ar^+ ions to gain maximum kinetic energy. Beyond this region, the negative glow region prevails. The characteristic glow is provided by the relaxation of the metastable species in this region. The atomization of the sample is provided by sputtering of the cathode by Ar^+ ions generated in negative glow region. The atoms thus liberated get ionized in negative glow region by Penning ionization which is the dominant process. The de-coupling of atomization and ionization processes makes the ionization less dependent on matrix effects. However, the sample should be electrically conducting which otherwise can accumulate static charge affecting the discharge process. The non conducting sample is converted to powder form and a conducting mixture is prepared using conducting binders *viz*. Ag, Cu, Ta etc. Subsequently, the mixture is molded in form of pin or disk to be used as cathode in GD source. However the mixing of conducting binders can lead to diluting the analyte signals and contaminating the sample with extra impurities thereby affecting the analysis adversely.

The alternate way is to use RF Glow Discharge. The technique uses RF voltage (2 kV peak to peak at 13.56 MHz) on the cathode instead of dc voltage. The charging of cathode in first half cycle of the RF voltage is neutralized by opposite polarity of the other half cycle. This circumvents any accumulation of charges on the time averaged cathode with half of the peak to peak voltage developing across the electrodes.

The pulsed mode of operation is used along with DC or RF glow discharge. This includes the application of high voltage for short duration (micro seconds) which leads to higher peak voltages and peak currents for the same average power. This increases sputtering and hence higher sensitivity. This also helps in distinguishing the analyte of interest from interfering ions by using time resolving methods.

v Secondary ion induced ionization

This technique is used in secondary ion mass spectrometry and is a versatile analytical technique [4, 33] for the compositional characterization of the surface and bulk of the solid materials. It also provides the measurement of spatial and depth dependent concentration of analyte material in solid matrix by sputtering them with energetic primary ions followed by mass spectrometric measurements of secondary analyte ions using suitable mass analyzers *viz*. magnetic sector, time of flight or quadrupole. There are varieties of primary ion sources and the modes of operation employed in this technique and their selection is application dependent. The material under investigation undergoes bombardment with the energetic primary ion beam (Fig. 7) which is selected based on the electrochemical nature of the analyte material. The typically used primary ions for various analyte elements are as given below:

Primary ion	**Type of element /application**
O_2^+	Electropositive element
Cs^+	Electronegative element
O^-	Less conductive material
Ga^+	High lateral resolution

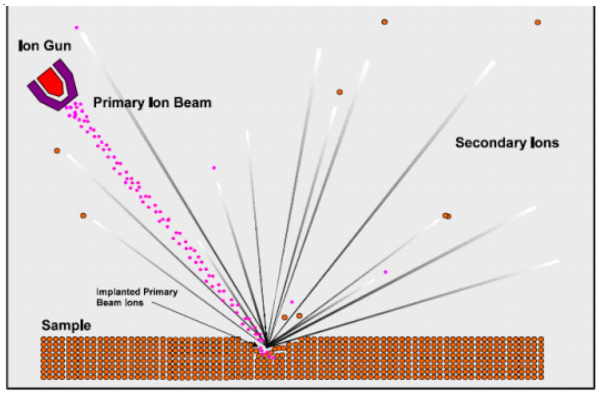

Fig. 7. Schematic showing the secondary ionization

The primary ions sputter out the analyte material which consists of positive or negative secondary ions along with the neutral atoms or molecules. The secondary ion current (I_s) can be expressed in terms of charge state (q), primary ion current (I_p), sputtering yields (Y), analyte concentration (C) and transmission of the instrument (T) and ionization cross section ($\acute{a}$) as follows:

$$I_s = q.\, I_p .\, Y .\, \alpha .\, C .\, T \qquad (8)$$

Typical values for some of the above parameters are: $Y = 0.1 - 10$, $T = \sim 0.3$, $\alpha = 0.1 - 10^{-6}$. The large variation in $\acute{a}$ is mainly responsible for the inaccuracy in the quantitative measurements.

Some of the major advantages of SIMS are its very high sensitivity in ppb range and very high depth resolution of the order of 0.1 nm. It can also be used to analyse light elements like H, C, O and N which are generally difficult to be analysed with other techniques.

The different types of modes for the operation of SIMS are: Static, dynamic, line/ gate scan, mass spectrometry mode, isotope ratio and imaging mode. The static mode is used for the compositional analysis of few top layers of the material. It uses very low primary currents (~ nA/cm^2) and ultra high vacuum conditions (10^{-9} - 10^{-10} torr) so that soft desorption of the top layers can take place at very low sputtering rate (~0.1 nm/hr). Dynamic mode is used for the depth profile of the material. It uses higher primary currents (~ µA to mA/cm^2) which can generate a sputtering rate of 0.1 nm/s. High sensitivity measurements (sub ppb) with depth resolution of 0.1 nm can be carried out in this mode. The line / gate scan provides concentration profiling along a line over the surface of the material. It uses microscope mode for line scan and microprobe mode for gate scan. In case of microscope mode the primary ion beam is focused on very small area of the specimen which is moved to take scan. In case of gate scan the larger area (500 µm x 500 µm) of the specimen is exposed to ion beam whereas the analysis area is defined by electronic gate which is moved to take scan. The mass spectrometry and isotope ratio modes are used for the compositional analysis and isotopic ratio measurements of very small amount of material loaded in the ion source of SIMS. In imaging mode the surface and depth profiling are combined to generate 3d images of the specimen in terms of various concentrations of constituent elements.

vi Matrix assisted laser desorption ionization

Matrix assisted laser desorption ionization (MALDI) is a soft ionization technique [4, 31,34] used for the ionization of bio-organic molecules such as DNA, proteins, peptides, sugars and large organic molecules such as polymers and other macromolecules. It provides very high resolution and mass range in combination with time of flight (TOF) analyser. The ionization is based on absorption of laser energy by matrix and transferring it to analyte for ionization with negligible fragmentation.

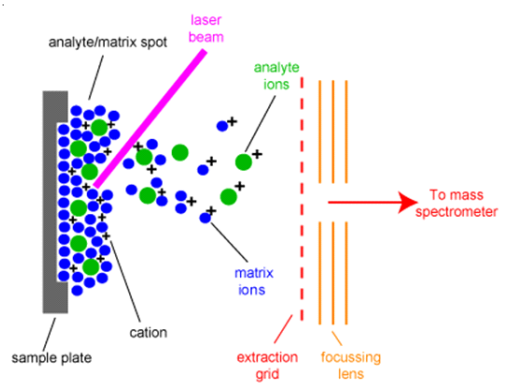

Fig. 8. Schematic presentation of ionization process in MALDI

The ion source (Fig. 8) consists of laser system with wavelengths ranging from ultraviolet (UV) to infrared (IR) e.g. Nitrogen lasers (337 nm), excimer lasers (193, 248, 308 and 351 nm), Q-switched, frequency tripled and quadrupled Nd: YAG lasers (355 and 266 nm), Er:YAG lasers (2.94 µm) and TEA-CO_2 (10.6 µm) lasers. The laser fluence and irradiance are important parameters to be controlled for the efficient generation of ions. This is achieved by employing optical lens with beam attenuator in the laser's optical path. The laser beam with shorter pulse width in the range of a few nanoseconds and spot size of 100 – 200 µm is preferred. The shorter duration of pulse inhibits the degradation of the sample matrix due to heating and provides high resolution for analysis with TOF. Most of the MALDI instruments use UV nitrogen lasers (337 nm, 3 ns pulse width) whereas IR lasers (with pulse width 6 – 200 ns) are restricted to applications where its deeper penetration offers advantages e.g. for the direct desorption of analytes from sodium dodecyl sulfate gets or thin layer chromatographic plates.

The analyte material is mixed with suitable matrix exhibiting high absorption efficiency for laser employed for the analysis. The mixture of analyte and the matrix is deposited on sample plate and dried to solid form. The laser energy is absorbed by the matrix molecules and transferred to the analyte molecules thereby desorbing them in form of ions. The matrix to analyte molar ratio is optimised for the generation of ions with lower laser fluence. In case of high molar ratio of matrix to analyte the less availability of analyte molecules requires large fluence for the production of ion. However for lower ratio the efficiency of energy absorption is reduced due to lower concentration of matrix molecules.

In case of UV-MALDI, matrix is based on some aromatic core with a suitable functional group to achieve desired properties. In case of IR-MALDI, the requirements are not stringent as wavelengths up to 10 µm are easily absorbed by O-H and N-H stretch vibrations or C-O and O-H bending vibrations. Some of the commonly used matrices for UV-MALDI are- picolinic acid (PA), 3 hydroxy picolinic acid (HPA), 3-amino picolinic acid (APA) for DNA ; 2,5-hydroxy benzoic acid (DHB) for oligosaccharides; a-cyano-4-hydroxycinnamic acid for peptides and smaller proteins; dimethoxy-4-hydroxycinnamic acid (sinapinic acid) for proteins etc. In general a polar matrix is used for a polar

analyte and a non polar analyte is preferably combined with a non polar matrix.

vii Electrospray ionization

Electrospray ionization (ESI) is a soft ionization technique [34] employed for the analysis of large, non-volatile, chargeable molecules such as proteins and nucleic acid polymers. It incorporates desorption of analyte ions from solution to gas phase. The solution is composed of a volatile solvent and the ionic analyte molecules. It is an alternative technique to MALDI with an added advantage of higher mass range owing to very high charge state achieved with ESI. Moreover, the ionization occurs in atmospheric pressure which circumvents the restriction imposed on the solvent required to make the analyte solution in case of ionization under vacuum.

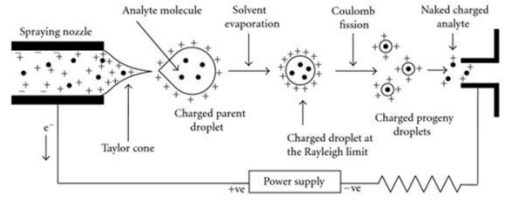

Fig. 9. Schematic showing the ionization mechanism in ESI source

An ESI ion source consists of hypodermic needle held at a voltage of 3 - 4 kV with respect to a surrounding cylindrical electrode (Fig. 9). The dilute sample solution is pumped through the needle at a flow rate of 5 – 20 µL/min. The solution is electro- sprayed out of the needle in the form of aerosol and expands into counter current stream of dry nitrogen gas that helps in evaporation of the volatile solvent from the aerosol droplets. With the evaporation of the volatile solvent from the large droplets, the charge density increases thereby increasing the electrostatic repulsion among charged molecules in the droplets leading to the coulomb fission of the droplets into molecular ions. A small portion of the sprayed material enters the aperture of a short capillary (0.2 mm diameter) that interfaces the atmospheric pressure region to the first pumping stage (~1 mbar). In this region, the rate of dessolvation of aerosol is increased and most of the gas is pumped out. The analyte ions are further taken by the skimmer cone and passed to the high vacuum portion where by complete dessolvation of the droplets occur and the molecular ions of analyte are available for the further analysis using mass analyse and detector.

The conventional ESI ion source has some limitations in terms of limited flow rate, volatility and polarity of the solvent thereby restricting its use as liquid chromatography (LC) MS interface. These limitations are circumvented in different types of modified ESI sources. Some of them are: pneumatically assisted ESI, ultrasonic nebulizer and nano-Electrospray. In case of pneumatically assisted ESI larger flow rates up to 10-200 µl min^{-1} can be handled. The ultrasonic nebulizer handles flow rates of 50 - 100 µl min^{-1}. The nano electro spray produces droplets of size less than 200 nm (much smaller than 1 – 2 µm as produced by conventional ESI) and allows for high polarity solvents such as pure water with smaller consumption of sample as compared with conventional ESI.

viii Resonance Ionization

It is a highly sensitive analytical technique based on ionization induced by Lasers for sample in gas phase [1,2,4,34]. The ultra high sensitivity along with high selectivity make this technique very useful for the detection of very small traces of analyte in a sample by circumventing any isobaric interference from other species present in the sample. It employs tunable laser with small bandwidth in the range of 0.1 to 0.5 cm^{-1} (3 to 15 GHz). The sample atom in gas phase is excited with photon of suitable energy matching with characteristic energy state of the atom. Due to resonance absorption of the photon energy the atom gets excited to the higher energy state and stays there for time of around tens of nanoseconds before de-excitation by photo emission or collision with another atom. During this time, the transfer of energy by another photon can further excite the atom to higher energy state. Conditions can be generated, by which the excitation process can continue till the atom gets ionized. There are certain schemes by which excitation and ionization can take place as shown in Fig. 10. Each element has its characteristic ionization potential (I.P.) ranging from 3.89 for Cs to 24.48 eV for He. For *n* photons of frequency *í* the ionization occurs when $n.hí \geq$ I.P. However due to single color multi-photon ionization the selectivity reduces due to non-resonant excitation of the closely matching energy states for elements in a given group of periodic table. The non-resonant excitation and ionization is the source of noise that is undesirable. For higher selectivity multi-color excitation and ionization process is employed. After excitation of the atom to desired state the ionization can be achieved by different types of processes namely photo-ionization, field ionization and by excitation to auto-ionising states. The photo-ionization is carried out by using photon of suitable frequency usually more than the excitation frequency to achieve saturation i.e. ionization of each atom of the sample under study. In case of field ionization suitable electric field is applied to excite the atom to Rydberg states (high energy states). The pulse of electric field is applied soon after the application of excitation laser pulse. In case of ionization using auto-ionising states, another tunable laser is required to excite the atom to its characteristic auto ionising states present in the ionization continuum. The added advantage with this technique is the additional selectivity during ionization along with the selectivity provided during the excitation process.

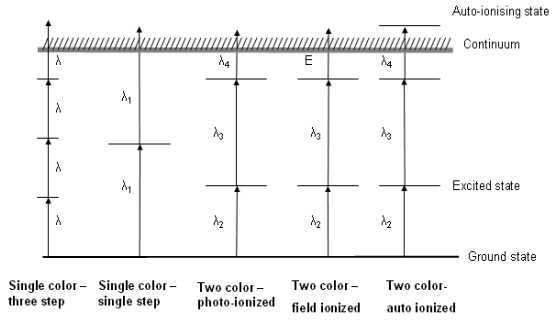

Fig. 10. Schemes for excitation and ionization in Resonance Ionization

The actual scheme adopted for a given analysis depends upon the ionization cross section of element under study and the extent of selectivity required. The necessary and the sufficient condition for the saturation to occur is to transfer the electron to ionization state before the excited state is destroyed by other process. This requires fluence (number of photons per unit area) and the flux (number of photons per unit area per unit time) to be higher than particular values.

Flux condition: $\sigma_i . F >> \Gamma_{10} + \beta$ (9)

Fluence condition: $s_i . F g' T = g' \Phi \sigma_i >> 1$ (10)

where σ_i is the cross section for photo-ionization of state 1, F is flux of laser photons, Γ_{10} is cross section for stimulated emission, $\hat{a}$ is rate of decay of state 1 by other processes, $g' = g_1/(g_0 + g_1)$; g_i is statistical weight of i^{th} state, Φ is fluence.

The different types of resonance ionization sources (RIS) are: thermal atomization RIS (TARIS), Laser ablation RIS (LARIS), sputter initiated RIS (SIRIS). In case of TARIS, the sample is deposited electrolytically in a high purity filament of Re or Ta. The sample is evaporated by heating the filament at high temperature in a cavity. The laser beam is introduced in the cavity for ionization. The LARIS incorporates ablating atoms from solid sample by imparting laser beam on it. In case of SIRIS the sputtering of solid sample is carried out using energetic ion beams.

The most commonly employed laser for RIMS is dye laser pumped by either Nd: YAG laser or XeCl excimer laser. The pulse width is in the range of 2 – 20 nsec with energy in the range of tens of mJ per pulse. The band width is in the range of 0.1 – 0.5 cm^{-1} (3 to 15 GHz). The pumping with Nd:YAG is more useful than excimer laser in the sense that same can be used for ionisation of the excited atoms.

Analyzers

i Magnetic Sector

The magnetic sector analyser [2-4] is employed in mass spectrometers used for the precise isotopic ratio measurements of the analyte elements. It is a prime component of the mass spectrometer that decides the resolution and overall foot print of the instrument. It exhibits unique feature of passing ions (within given mass range) simultaneously thereby enabling simultaneous collection on different collectors of a multi-collector system which increases the precision of given analysis. The separation of ions with different m/q ratio is achieved due to different Lorentz forces applied by the magnetic field on the analyte ions with different m/q ratio. The ion traverses a circular path of radius (r) which is related to mass 'm' and charge 'q' of the analyte ion by following equation.

$$m/q = (B^2 . r^2 / 2V) \quad (11)$$

where, B is the magnetic field in the magnetic analyser and V is the accelerating potential of the analyte ion.

The ions produced in the ion source of a mass spectrometer are accelerated by an accelerating potential of 5 - 10 kV in the ion source and introduced to magnetic analyser in form of diverging ion beam. The ion beam undergoes deflection and separation (as per m/q) during its passage through the magnetic sector and aftr leaving the magnetic field it re-focuses at a location dependent on the geometry of the magnetic sector as shown in the Fig. 11(a). The magnetic sector geometry is characterized by parameters: radius of curvature, deflection angle and entry/ exit angles of ion beam with respect to entry/ exit boundary of the magnetic field. The system parameters like resolution, dispersion and magnification are decided by the geometry of the magnetic sector.

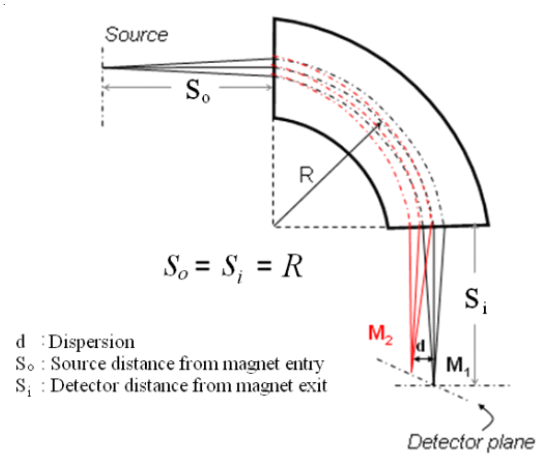

Fig. 11 (a). Ion beam focusing in case of normal geometry magnetic sector with 90° deflection angle

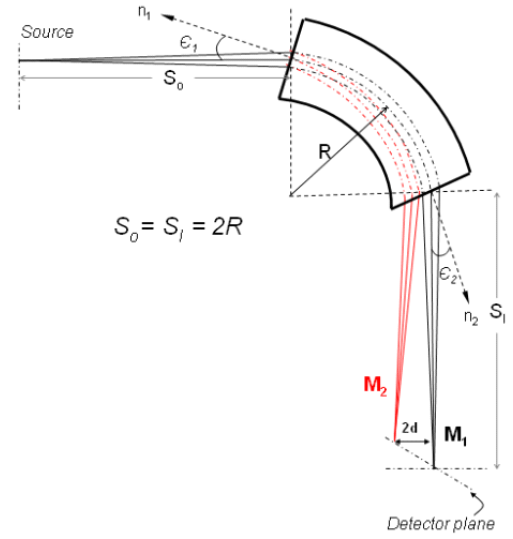

Fig. 11 (b). Ion beam focusing in case of stigmatic geometry for a 90° deflection angle; the entry angle ($\in_1$) and exit angle ($\in_2$) of the ion beam with respect to entry and exit boundaries of the magnet are 26.5° each.

The dispersion is defined as the separation between the ions of two different masses (say m and m + "m) at the refocusing points of the respective ion beams. It is given by the product of relative mass difference "m/m (between given ion beams) and the dispersion factor (d) as shown in equation below.

$$D_m = d . \Delta m/m \quad (12)$$

The dispersion factor *d* is dependent on the geometry of the magnetic sector. For example in normal geometry the value of *d* is one. However in case of stigmatic geometry it is two i.e. double of that for normal geometry.

In early development period of mass spectrometry, normal geometry was employed where ion beam entrance and exit in the magnetic sector was normal to the boundaries of the magnetic sector i.e. entry and exit angles were 0° as shown in Fig. 11(b). In this case the distances of object (source slit) and image (detector slit) from entry and exit boundary of magnetic sector respectively are equal to the radius of curvature of the analyser. The normal geometry provides limited dispersion and resolution. The focusing of the ions occur in a plane (median plane) orthogonal to the magnetic field so that the ions diverging in the plane parallel to magnetic field are not collected by the detector which leads to loss of sensitivity of the mass spectrometer. These limitations were circumvented by extended geometry or stigmatic geometry.

In case of stigmatic geometry the ion beam entry and exit from the boundary of magnetic sector are inclined at some specific angles. In case of symmetric stigmatic geometry the entry and exit angles are 26.5° with respect to normal at entry and exit boundaries of the magnetic sector as shown in Fig. 11(b). In this case, the object and image points of ion beam (with respect to entrance and exit boundary of magnetic sector respectively) are located at distance equal to double the radius of curvature of magnetic sector. The dispersion and hence resolution for this geometry also become double of those in case of normal geometry. Moreover, the stigmatic geometry also provides focusing of the ion beam in a plane along the magnetic field along with the focusing in median plane and the re-focusing points for both the planes occur at same location. This results into higher transmission of the magnetic analyser thereby providing higher sensitivity of MS.

The magnification is defined as the ratio of cross sectional width of ion beam at refocusing point to that at the source point. In case of symmetric normal and stigmatic geometries it is unity i.e. magnification is not affected by changing geometry from normal to stigmatic as long as it is symmetric.

The resolution of any mass spectrometer is related to the ratio of dispersion to the magnification of the ion beam. As in case of stigmatic geometry dispersion is doubled with same magnification of unity, the resolution also gets doubled. For two adjacent ion beams with masses of ions as *m* and $m + \Delta m$, resolution conventionally defined as $m/\Delta m$ and is given by:

$$R = d \,.\, r / (W_c + W_i) \qquad (13)$$

where r is the radius of curvature of magnetic sector, W_c is the width of detector entry slit, W_i is the width of ion beam cross section, d is the dispersion factor.

The ion beam width W_i is mainly decided by the source slit width but owing to various factors *viz*. instability in the power supplies related to acceleration and analyser magnetic field, energy spread of ions and in-homogeneity of the magnetic field of magnetic analyser various aberrations are introduced to the focusing of ion beam which increase the cross sectional width of ion beam and hence reduce the resolution of mass spectrometer.

ii Radio frequency (RF) Quadrupole

The RF quadrupole [8] is a widely used analyser in mass spectrometers employed for compositional analysis of materials. Because of its rapid scanning capabilities it has gained importance for gas/liquid chromatography-mass spectrometry (GM-MS and LC-MS) systems where fast scanning is required. The advantages of RFQ (radio frequency quadrupole) are: (i) high transmission, (ii) light weight and compactness, (iii) more economic than other type of analyzers, (iv) low acceleration voltage than magnetic analyser and (v) very fast scanning speed. The various applications of RFQ includes: residual gas analyser for partial pressure measurement, elemental and isotopic analysis in combination with ICP, EI and secondary ion sources, organic analysis in GC and LC chromatography, tandem mass spectrometry for the structural analysis of organic molecules.

A quadrupole consists of four hyperbolically or cylindrically shaped rods placed parallel to each other on the vertices of square with inter rod distance dependent on the radius of rods as shown in the Fig. 12(a) and (b). The pairs of opposite rods are shorted electrically and both the pairs are held at DC and RF potential of opposite polarity. Considering the case when positive DC potential is applied on the rods along *x-z* plane and negative DC potential is applied on rods along *y-z* plane, the electrostatic field is generated in the region between the rods in such a way that the positively charged particles undergo focusing along *x-z* plane and de-focusing along *y-z* plane. The focusing and defocusing of charged particles as produced by DC fields are mass independent. The application of RF potentials on the same sets of rods generates oscillations in the path of charged particles and deviate them from the stable paths traversed in the pure DC field. In *x-z* plane, the RF field will try to deviate the charged particles from focusing and the deviations are more effective for lower masses as compared to higher masses thereby making it a high (mass) pass filter in *x-z* plane. In *y-z* plane the RF field deviates the charged particles from defocusing and here again lower masses are more deviated from the defocusing action thereby making it a low (mass) pass filter along *y-z* plane. The combined effect of focusing and defocusing of charged particles in both the planes (*x-z* and *y-z*) allows only certain mass range to pass through thereby making it a mass filter. The deviations produced by RF field are mass dependent and for given values of DC and RF field charged particles only within particular mass band are allowed to pass through the quadrupole. Hence for charged particles with given charge state, RF quadrupole works as mass filter. The mass scanning is carried out by changing the value of RF and DC potentials while maintaining the same ratio of DC and RF potential.

(a)

Fig. 12 (a). Photograph of a Quadrupole analyzer

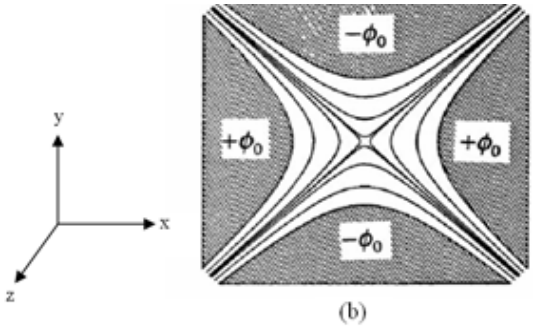

(b)

Fig. 12 (b). Electric field distribution in xy plane

The field distribution (Ö) inside the quadrupole consisting of hyperbolic rods with DC (U) and RF (V) potentials is given by:

$$\Phi(x,y) = \frac{(x^2 - y^2)}{r_0^2}\phi_0$$

$$\Phi_0 = U + V\cos\omega t$$

where x and y are the co-ordinates in x and y axis, r_o – radius of inscribed circle in x-y plane with centre at z axis, $Ö_o$ – potential on one pair of rods with respect to other pair, U – DC potential, V – amplitude of RF potential.

The electric field (E) and force (F) at charge particle with charge (e) at any point (x, y) is given by:

$$\vec{E} = -\nabla\Phi(x,y)$$

$$\vec{F} = e\vec{E}$$

The equations of motion (Matheiu's equations) of charged particle are given by:

$$\frac{d^2x}{dt^2} + \frac{2e}{m_i r_0^2}(U + V\cos\omega t)x = 0$$

$$\frac{d^2y}{dt^2} - \frac{2e}{m_i r_0^2}(U + V\cos\omega t)y = 0$$

$$\frac{d^2z}{dt^2} = 0$$

The solution of above equations for the stable trajectories of charged particles inside quadrupole exist for particular values of parameters a and q defined as:

$$q = \frac{4eV}{m\omega^2 r_0^2} \qquad a = \frac{8eU}{m\omega^2 r_0^2}$$

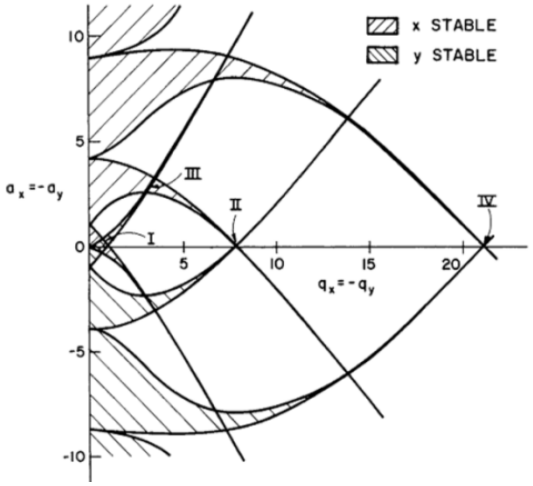

Fig. 13 (a). The stability region of quadrupole

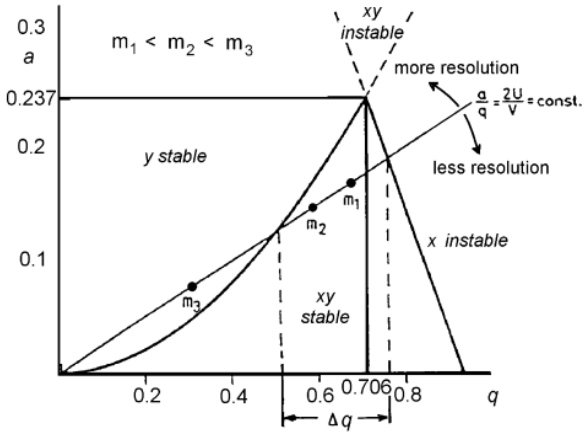

Fig. 13(b). Conditions for high resolution in 1st stability zone

The set of values for a and q for stable trajectories are shown in Fig. 13(a). Considering the 1st stability region, the stable trajectories of charged particles exists only for the set of a, q values as shown in Fig. 13(b). For given geometry of quadrupole and frequency of RF field the values a and q are decided by the DC potential, the RF potential and m/q of ion. The plot of a against q for given ratio of DC and RF potential is called as load line. For higher resolution, the values of DC and RF potentials are selected in such a way that the load line passes through a region near the tip of the stability zone. The stable region for both x and y trajectories will allow charged particles to pass through the quadrupole and hence

it will decide the mass resolution.

The resolution is also decided by the number of oscillations undertaken by the charged particle within quadrupole field and in turn depends on time spent by charged particle in the same region. The parameters contributing to these requirements are kinetic energy of charged particle as decided by the accelerating potential (V_z) in the ion source used for generating charged particle, length of quadrupole rod (L) and frequency of RF field. The mass resolution of quadrupole with rod diameter (r_o), RF potential V_m is given by:

$$M_m / \Delta M_{min} = \frac{L^2}{r_o^2} \frac{V_m}{V_Z} \frac{1}{290}$$

The design parameters of quadrupole like radius, length of rods and the mechanical tolerances involved in their fabrication and assembly are very critical parameters affecting the mass range and resolution of the quadrupole.

iii Time of Flight (TOF) analyser

The TOF analyser [4, 13] is widely employed for the applications which require very high resolution and mass range to analyse molecules or molecular clusters of very high molecular mass. Owing to very large mass range and resolution provided by TOF, it is mostly used with MALDI and ESI ion source in biological applications. The principle of separation of ions (as per their mass to charge ratio) is based on mass dependent arrival times of ions with same kinetic energy after passing through field free drift space of given length, Fig.14. The arrival of respective ions is recorded by the fast response detector and is calibrated in term of their masses.

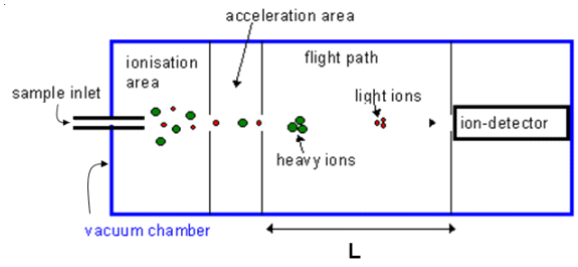

Fig. 14. Schematic showing the separation of ions in TOF analyser

The time (t) taken by any charged particle in a field free region of length 'L' is given by:

$$t = L/v \quad (14)$$

$$v = \sqrt{(2 e V / m)} \quad (15)$$

where v, m are the velocity and mass of charged particle; V is the accelerating potential of the charged particle

Eliminating v from equation 14 and 15 above:

$$t = L \sqrt{[m / (2 e V)]} \quad (16)$$

Above equation shows that the arrival time of a charged particle is directly proportional to square root of its mass. The lighter mass takes less time to travel a given distance in the TOF and hence reaches the detector earlier than the heavier masses. The difference in the arrival times of the ions with different masses is exploited by using a fast response detector that can detect ions reaching with short time intervals in between. The pre-requisite for TOF measurements is a detector with very fast response on the time scale of nano-seconds. This was the main hurdle in achieving good resolution in the early period of development of TOF instruments. The dependence of resolution on smaller detectable time intervals is further explained below.

Taking logarithm and then differentiating eq. 16 for t and m.

$$m/\Delta m = ½ t /"t \quad (17)$$

i.e. mass resolution ($m/\Delta m$) is inversely proportional to Δt, the difference in the arrival time between two ions with Δm mass difference at mass m. This implies that the resolution depends on the response time of the detector. The faster is the response time of the detector, smaller will be the detectable time interval between ions of adjacent masses and hence higher resolution. At very high mass the time difference per unit mass difference decreases which puts limit on the resolution of TOF. For example the Δt per unit mass is 114 ns at mass 20 amu, 36 ns at 200 amu and 11 ns at mass 2000 amu for ions accelerated to 19.5 kV and the flight path of 2 m.

The equation 17 also implies that resolution depends on the arrival time of given mass m which in turn depends on length L of flight tube and kinetic energy of the ion. For t to be higher requires the larger length of flight tube and lower kinetic energy. However larger L will increase the transmission losses along with the foot print of the instrument. The lower kinetic energy will also result into lower sensitivity and higher relative energy spread of the ions. Therefore the length and kinetic energy are optimised to certain values. In general, flight tube length of 2-5 meter and accelerating potential around 5 - 20 keV are used in a TOF instruments.

Apart from fast detector, other requirements for obtaining higher resolution in TOF are:

The starting time of the ions should be same. This requires the generation of ions in pulses of very short duration (less than the time resolution of the detector). The pulsed laser ionization is most suitable for TOF. In case of other ionization i. techniques vis. electron impact the extraction of ions is executed with very short pulses of extraction potential in the ion source. The advent of laser source with femto second pulse size makes MALDI-TOF an ideal combination for the analysis of bio molecules with very large molecular masses.

ii. The ions in a given pulse should exhibit same kinetic energy i.e. smaller energy spread. The main reasons for the higher energy spread are: (a) The random thermal energy of analyte particles which is added to the kinetic energy of ions after their acceleration and hence produces energy spread. 2) Generation of ions at

different locations with different electrostatic potential so that they acquire different kinetic energy during their acceleration within the ion source.

The energy spread can be circumvented by different techniques viz. supersonic jet technique, delay extraction technique and reflectron type TOF. In super sonic jet technique the gas sample is introduced under high pressure difference so that formation of supersonic jet takes place and the sample molecules get cooled to very low temperature thereby reducing the energy spread. In delayed extraction technique, the difference in thermal energies is compensated by the different potentials applied at the time of their extraction from the ion source. The ions are allowed to spread for short duration before their extraction so that ions with higher thermal energy moves towards the exit slit faster than the low energy ions. At the time of extraction the field distribution near the exit slit is such that the higher energy ions are accelerated to lower potential and vice versa thereby the energy spread is reduced. The reflectron is electrostatic mirror which is placed at one end of the TOF (Fig. 15). The ions penetrate against the repelling electric field in such a way that ions with higher energy travels longer distance as compared to that with lower energy. This allows the ions to reach the detector at same time irrespective of their energies and hence energy focusing takes place.

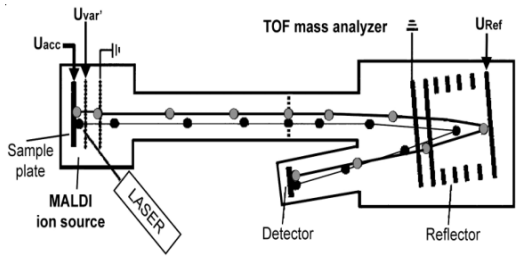

Fig. 15. Schematic showing the Reflectron type TOF analyser

During early development period of TOF the resolution was limited to 50 - 100 mainly because of unavailability of fast detector. The development of fast response detectors could increase the resolution but the higher energy spread still limited it up to 1000. The advent of techniques for cooling of sample could increase the resolution to around 4000. Nowadays a resolution of as high as 50000 – 100000 is achievable with the help of Reflectron TOF, delayed extraction technique and lasers with femto seconds pulse width.

iv Ion trap analyser

The ion traps [8,13] are widely used for applications related to biological and chemical sciences. These are suitable for the studies of large bio-organic molecules due to high mass resolution, mass range and sensitivity. Owing to the confinement capability of the charged particles, they are employed for the gas phase ion chemistry and elucidation of molecular structures by the use of repeated stages of mass selection known as tandem mass spectrometry or MS/MS techniques. The technique is advantageous over other competitive MS-MS techniques by the fact that different MS steps can be executed in the same set up in shorter duration of time as compared to other techniques which involve different setups for each MS stage.

There are two types of ion traps: linear quadrupole ion trap and three dimensional quadrupole ion trap. The linear (quadrupole) ion trap (LIT) consists of quadrupole (as explained in earlier section) with electrodes of higher potential on both the ends as shown in Fig. 16. The RF potential at quadrupole rods and DC potential of same polarity on the end electrodes enable the trapping of ions along the axis of the quadrupole. It is capable of scanning the mass of ions, the radial and axial excitation of ions and precursor ion selection for MS/MS experiments. It is used in combination with other quadrupoles or Fourier transform ion cyclotron resonance analyser to enhance the sensitivity of the measurements related to molecular ion studies.

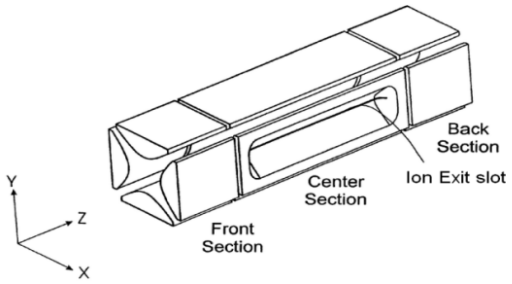

Fig. 16. Schematic of a linear Q'pole ion trap

The quadrupole ion trap (QIT) creates a three dimensional RF quadrupole field to store ions within defined boundaries. It consists of two hyperbolic electrodes serving as end caps and a ring electrode placed in between as shown in the Fig. 17(a), (b) and (c). The end caps are electrically shorted and DC and RF potentials are applied on them with respect to the ring electrode.

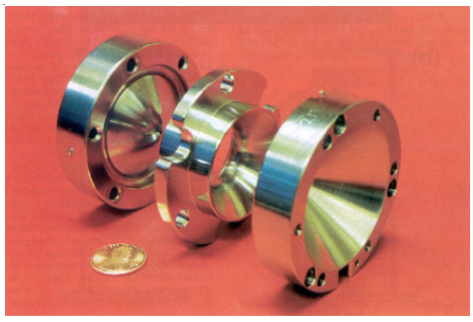

Fig. 17(a). Three electrodes of ion trap in open array

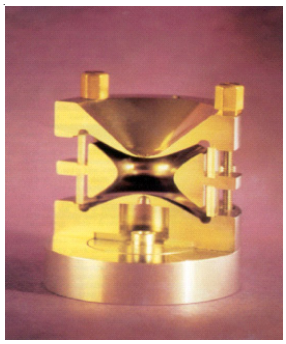

Fig. 17(b). Ion trap cut in half along the axis of cylindrical symmetry

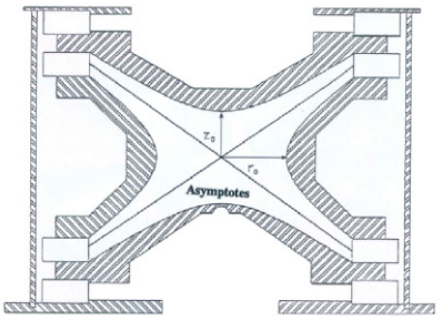

Fig. 17(c). Schematic of ion trap showing the asymptotes and dimensions r_o and z_o

The working principle of QIT is based on creating stable trajectories of ion with certain *m/q* or with in some *m/q* range by generating trapping potential region within the QIT with the help of suitable DC and RF potentials applied on the ring and the end caps. The basic theory of motion of charge particles in QIT is similar to that for RF quadrupole as explained in earlier section with a difference of using *a* and *q* parameters in radial and azimuthal co-ordinates instead of x and y co-ordinates earlier.

The different modes of operation of QIT are: the mass selective stability mode, mass selective instability mode, resonant ejection and axial modulation. In mass selective stability mode, ions of desired mass range are trapped by setting suitable parameters followed by their ejection by applying negative pulse across the end caps. The mode is rarely used because of its slow speed and low sensitivity. In case of mass selective instability mode ions of all masses are firstly trapped. Subsequently, with the end caps grounded, an RF voltage scan is applied to the ring electrode causing consecutive ejection of ions in the order of their *m*/*q* values. This mode is relatively faster than mass selective stability mode but suffers from poor efficiency because of space charge effects. The resonant ejection is the mostly used mode in QIT. It is based on ejection of ions with particular axial secular frequency by applying a supplementary RF voltage (of few milli volts) across the end electrode. The scan can be carried out in forward or reverse manner allowing for the selective storage of ion of a certain *m*/*q* value by eliminating ions below and above particular *m*/*q* value. Axial excitation can also be used to cause collision induced dissociation (CID) of the ions. The axial modulation incorporates application of modulation voltage with a fixed amplitude and frequency between the end caps during RF scan. The frequency is chosen slightly below the half of fundamental frequency. The mode is mainly employed to facilitate the efficient ejection of ions in mass selective instability mode during RF scan to circumvent the problems related to space charge effect.

In early developments, QIT were used with internal ion sources whereby ionization occurs inside the region of QIT limiting its applications. However the development of techniques to interface ions generated outside has increased its versatility. In present MS systems QIT can be combined with a number of ionization techniques like electron impact, chemical ionization, atmospheric pressure ionization and electrospray ionization etc. The resolution as high as 10^6 and mass range up to 70,000 amu by QIT has been reported.

Detectors

i Faraday collector

The simplest of all ion detectors used in Mass Spectrometers, is the Faraday Cup. The Faraday detector [1-3,6,25,35] handles ion beam intensity $>10^{-14}$ A only. It is typically used in applications related to precise isotopic ratio measurements on magnetic sector mass spectrometers. The major advantage of the detector is the precise measurement of ion current because of absence of any mass discrimination effects as present in other types of detectors like electron multiplier. However when connected to a pre-amplifier with high resistance in the feedback loop, it shows very slow response because of high *RC* (resistance-capacitance) time constant.

A Faraday collector consists of a main collector, a secondary electron suppressor and entry aperture at ground potential as shown in the Fig. 18. The components are assembled together using proper insulations in between. The combination is covered with another metallic cover at ground potential to screen the collector from any stray charged particles. The principle of detection is based on measurement of the ion current using electrometer amplifier connected to the main collector. The charged particles impinge on the surface of main collector thereby transferring the charge to the collector surface that is connected to an electrometer amplifier. The rate of charging is neutralized by an equivalent electronic current passing through the high resistance (typically 10^{11} ohm) connected in the feedback loop of the electrometer amplifier. The ion current is measured in terms of voltage drop across the resistor. For the isotopic ratio measurement a series of Faraday collectors are used. The ion beams corresponding to the different isotopes are collected in the respective Faraday collectors and the isotopic ratio is calculated using ion currents measured for the respective isotopes.

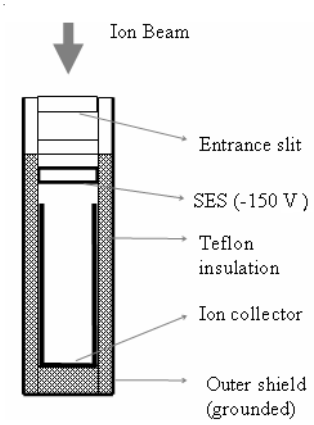

Fig. 18. Schematic of Faraday collector

The measurement by Faraday collectors suffers from various errors *viz*. Johnson's noise due to high resistor in amplifier, non uniform amplifier gain from one collector to another. The noise of the amplifier can be circumvented by putting the amplifiers under low vacuum and controlling the temperature of the amplifiers within +/- 0.1°. The amplifiers

are calibrated using stable current source on daily basis prior to analysis schedule to circumvent the error due to time varying gains. Apart from this, various methodologies have been developed to address the errors viz. using multi-dynamic mode of ratio measurements and virtual amplifier concept [26]. Using Faraday collectors the precision of the order of 5 ppm can be achieved for the isotopic ratio measurements for some of the elements like Sr and Nd.

ii Electron Multiplier detectors

The Electron Multiplier detector [1-3,35] is used for the measurement of very small ion currents below 10^{-14} A that are not measurable by Faraday collector. It is mainly employed for trace elemental detection or compositional analysis involving concentration of analyte in the range of ppm or below. The detection principle is based on the amplification of ion current by multiplication of secondary electrons at different stages of the multiplier so that the total electron current produced at the last stage is high enough to be measured by an electrometer amplifier. The major advantages of the detectors are their high gain, high dynamic range and fast response. The limitations of electron multipliers are: (i) gain variation with time and (ii) gain dependence on mass of the ions under measurement. The different types of electron multiplier detectors are: Discrete dynode electron multiplier, Continuous dynode or Channeltron, Micro-channel plate (MCP) and Daly detector.

iii Discrete dynode electron multiplier detector

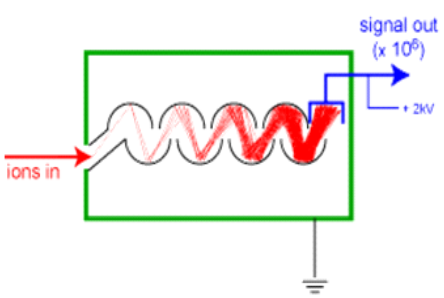

Fig. 19(a). Schematic showing the working of discrete dynode electron multiplier

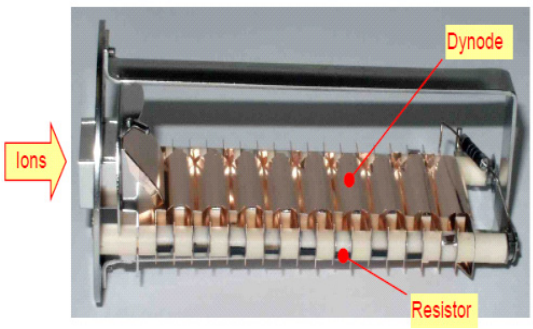

Fig. 19(b). Photograph of a discrete dynode EM

It consists of series of dynodes (Fig. 19) [1-3] made of materials with high secondary emission coefficient *viz.* Copper-Beryllium or Aluminium. The dynodes are electrically biased in such a way that electrons generated at first dynode get accelerated and directed towards adjacent dynode down the line. The first dynode (conversion dynode) is kept at negative potential and the last dynode at ground potential for the measurement of positive ions. In case of negative ions the conversion dynode is at ground potential and the last dynode is kept at positive voltage. The incident ions under measurement are allowed to hit at the conversion dynode to generate secondary electrons with a multiplication factor of b. These electrons are accelerated to second dynode due to positive electrical bias and further generate secondary electrons with multiplication factor G. The process of electron multiplication continues till the last dynode where total number of secondary electrons produced is b. G^N where N is the number of dynodes. This corresponds to the ratio of output current to the input current of the detector and is called as gain. Along with the dependence on design and material characteristics of the detector the gain also depends on the bias voltage, mass and energy of the ion under measurement. A discrete dynode electron multiplier can produce a gain as high as $10^7 - 10^8$ with a dark noise < 0.1 counts/sec. The main limit to the highest achievable gain is posed by non linearity due to the space charge effect and the emission of secondary ions at the dynodes (ion feedback effect) in the last stages of the detector.

There are two modes of measurements of ion currents - Analog mode and ion counting/ pulse counting mode. The analog mode is used for the ion currents generally above 10^{-16} A. It incorporates the measurement of output electron current integrated over time. In case of pulse counting mode, each ion is counted in terms of the pulses produced by the secondary electrons at the output. The detector is set at high gain and the numbers of pulses produced per unit second are recorded by the pulse counting unit. This can generate very accurate results as compared to analog mode for the ion current below 10^{-14} A. In the higher ion current region the measurement accuracy is limited due to dead time effects.

Another advantage of the detector is higher dynamic range due to the high bias current (> 100 μA) which extends the measurable range of the detector to higher ion currents. The main drawback of the detector is gain variation with time due to change in surface conditions. Another disadvantage is the mass discrimination i.e. gain variation with mass of the ion. This limits the use of this detector in mass spectrometer for precise isotopic ratio measurements. The detector must be shielded from any magnetic or electric field (in the surrounding) which can disturb the paths of secondary electrons and hence affect the gain.

iv Continuous dynode detector/ Channel electron multiplier (CEM /Channeltron)

It is an alternative to the discrete dynode electron multiplier [32,35]. The main advantage is its compactness, durability and better gain stability as compared to discrete dynode type. However it exhibits lower dynamic range as compared to discrete dynode multipliers due to lower bias current.

CEM consists of tubular structure made of specially formulated lead silicate glass with inner diameter of 1mm and outer diameter in the range of 2 – 6 mm. The electro-emissive surface of SiO_2 with thickness 200 nm is responsible for

emission of secondary electrons. Beneath this the conductive layer of lead (thickness around 2 μm) helps to electrically bias CEM and generating bias current. The input end of the tube is given conical shaping and the body is shaped in curve as shown in Fig. 20. During operation, the input and output ends of the detector are electrically biased with high voltage in the range up to 3 kV. The primary ion beam is allowed to fall on the input end of the detector to produce secondary electrons. An ion striking the input face of the device typically produces 2-3 secondary electrons which get accelerated towards the out put end due to positive bias. The electrons get multiplied due to further collisions within the electro-emissive surface of the detector to produce multiple electrons in the range of 10^7-10^8 (typically for a voltage of 2-3 kV applied across the multiplier). For the detection of positive ions, the input end is at negative potential and the out put end is kept at ground potential. In case of negative ions, input end is kept at ground potential and positive potential is applied on output end.

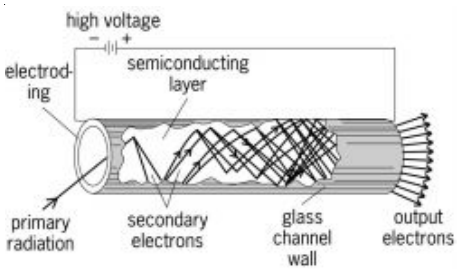

Fig. 20(a). Straight Channeltron

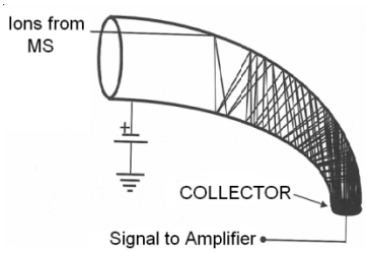

Fig. 20(b). Channeltron with curved shape

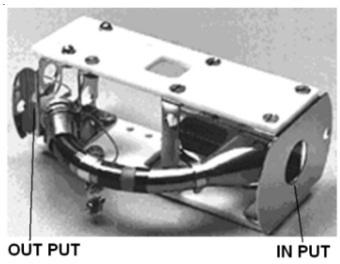

Fig. 20(c). Photograph of Channel electron multiplier

The gain of CEM depends on various factors *viz*. secondary emission coefficient of glass, the applied voltage to CEM and the length to diameter ratio of the CEM tube. The variation of gain of the CEM with applied voltage is shown in Fig. 21. The gain at higher voltage becomes non linear due to space charge effect. The ion feedback due to emission of secondary ions near the output end also limits the gain in the range of 10^4-10^5 in straight CEM. The curved shape helps in minimizing ion feedback and extends the gain to a range of 10^7-10^8.

Similar to discrete dynode type, it also suffers from mass discrimination effect which reduces the efficiency of the detector for higher masses causing errors in the concentration measurement of elements with different masses present in an analyte material. It can be circumvented up to some extent by introducing separate dynode at the input end of the detector. This also extends the life of the detector as the direct exposure can damage the surface of detector in case of ions of very high energy.

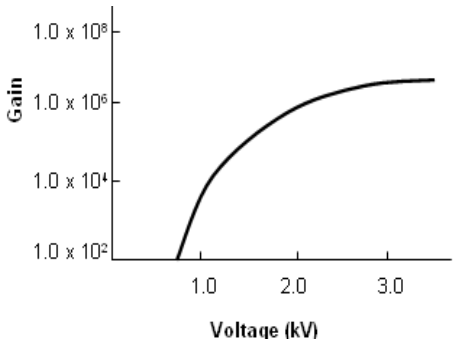

Fig. 21. Variation of gain with applied voltage

v Micro-channel plate (MCP)

It is a two dimensional array of many small sized Channeltrons stacked together as shown in Fig. 22(a) and (b) [32,35].

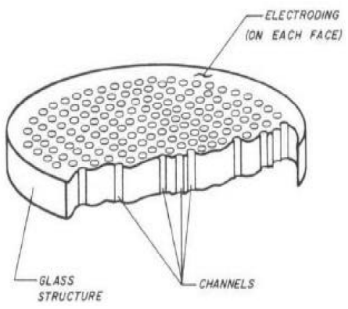

Fig. 22(a). Cut view of MCP

Fig. 22(b). Photograph of MCP

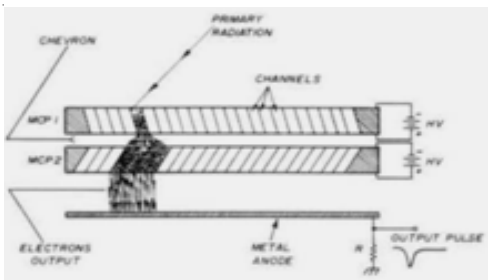

Fig. 22(c). Chevron type MCP

The detector is mainly employed for the measurement of ion currents in TOF-MS due to its fast response time in the range of 0.1 ns (much better than Channeltron). It can also be used for intensity profiling of the cross section of ion beams when used in combination with phosphor screen.

The detector is fabricated of glass fibers consisting of chemically dissolvable core glass and wall glass as lead silicate. The fibers are stacked together in lead glass substrate to form a boule which is sliced along a plane at an angle 8° - 15° with respect to normal to the channel axis. The core glass is removed by chemical etching leaving hollow lead silicates fibers. Subsequently, the reduction in hydrogen atmosphere converts the surface of fibers to semi conducting layer of lead. Each channel has cross section of 10 – 20 μm diameter and length of around 0.5 mm. The channels are placed uniformly with separation of around 5 - 10 μm from each other. Each channel is provided with a parallel electric contact by coating of a thin layer of Nichrome or Inconnel on the front and rear surfaces of MCP, which also serves as the input and output electrodes of MCP. The total resistance between the electrodes is of the order of 10^9 &!. The MCP can generate electron multiplication (gain) in the range of 10^4 - 10^7 with ultra high time resolution < 0.1ns and spatial resolution around 10 μm.

Each channel in the MCP works as individual electron multiplier. The primary ions falling on the input surface of MCP generate secondary electrons that get multiplied within each channel. The secondary electrons exiting from the output surface are collected on metallic electrode and measured using electrometer amplifier. Ion beam profiling can also be carried out using phosphor screen just beneath and parallel to the output surface of MCP. The phosphor screen is raised to positive potential around 3 kV to accelerate the secondary electrons (from MCP out put end) towards it to generate scintillation.

The gain of single stage MCP is limited to 10^4-10^5 due to the ion feed back and space charge effect. This is circumvented by using two stages MCP (also called as Chevron type MCP) with configuration of channels as shown in Fig. 22(c). The Chevron MCP is capable of generating maximum gain of more than 10^7, around two orders more than single stage MCP.

The main advantages of MCP are its higher gain and very fast response. Along with charged particles, it is also sensitive to UV radiations and X rays. The operation of MCP is not affected by the external magnetic field as in case of other detectors. However it also suffers from gain variations with time and mass discrimination and hence is not applied in precise isotopic ratio measurements. It is more delicate than other electron multiplier detectors and prone to any sudden changes in pressure and humidity of environment in which it is operated and hence has to be handled very carefully.

vi Daly detector

The Daly detector [6,35] is used as an alternative to other electron multiplier detectors. It has very low detection limits ranging up to 10^{-20} A. It consists of a metallic knob, a scintillator and photo multiplier tube as shown in Fig. 23.

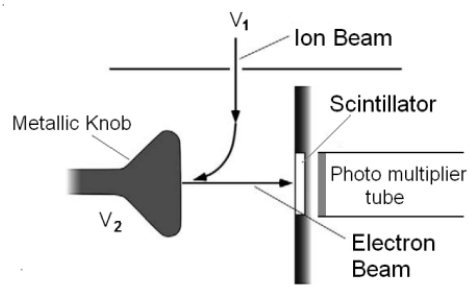

Fig. 23. Schematic of Daly Detector

The metallic knob (stainless steel make coated with aluminium) is raised to high negative potential of 40 kV. The detection process consists of three steps of conversion. Firstly, the ion beam accelerated at V_1 potential from the mass spectrometer is further accelerated to fall on the knob to emit secondary electrons from the surface. Because of the higher momentum of the ions impinging on the conversion knob and high secondary emission coefficient of the knob material, a large number of secondary electrons are released. In the second step these electrons are accelerated to the phosphor screen at ground potential. The high energy electrons lose part of their energy in the phosphor to emit photons. In the third step, the emitted photons are introduced to photo multiplier tube (PMT) and are converted to photo electrons that get multiplied and measured in PMT. The application of high negative potential and using energetic electrons enhances the emission efficiency of the phosphor material thereby improving the detection efficiency of the detector. This detector is mainly suitable for the detection of positive ions. In case of negative ions, the polarity of knob has to be positive and the very high positive potentials are to be applied on scintillator and PMT. This generates very high electric field in the vicinity of PMT and can generate noise. Therefore the Daly detectors are typically employed for the detection of positive ions.

The major advantage of this detector with respect to other electron multiplier detectors is the absence of mass discrimination when used in pulsed counting mode. However, the requirement of very high voltage, larger size of the detector and its inability to measure negative ions make this detector less preferable over other electron multiplier detectors.

References

1 Introduction to mass spectrometery, Ed. S.K.Aggarwal, H.C.Jain, Indian Society for Mass spectrometry (1997).

2 Modern isotope ratio mass spectrometry, Ed. I.T.Platzner, John Wiley & Sons (1997).

3 Introduction to mass spectrometry, J. Roboz, John Wiley & Sons (1968).

4 Mass spectrometry, Jurgen H. Gross, Springer.

5 M.E. Wieser, J.B. Schwieters, *International Journal of Mass Spectrometry* **242** (2005) 97.

6 J. Sabine Becker, Inorganic Mass Spectrometry- Principle and Applications, John Wiley (2007).

7 J.W. Coburn, W.W. Harrison, *Appl. Spectroscop. Rev.* **17** (1981) 95.

8 Quadrupole Mass Spectrometer and its application, Peter H. Dawson, Elsevier Scientific Publishing Company, (Netherland) 1976.

9 L.F. Marvin, M.A. Roberts, L.B. Fay, *Clinica Chemica Acta* **337**(2003)11.

10 S. Banerjee and S. Mazumdar, *International Journal of Analytical Chemistry* **2012**, Article ID 282574

11 A.P. Bruins, *Journal of Chromatography A*, **794** (1998) 345.

12 R.K. Bhatia, R. Datta, R. Chandak, M.M. Gulhane, P.R. Kasina, A.M. Kasbekar, N. Ved, V.K. Yadav, M. Gopalakrishna, E. Ravisankar, R.K. Saha, V. Nataraju and V.K. Handu, 11th ISMAS-TRICON-2009, 493

13 S. Maher, F.P.M. Jjunju, S. Taylor, *Reviews of Modern Physics* **87** (2015).

14 S.N.Bindal et.al. 8th ISMAS Symposium 1999.

15 S.K. Aggarwal, A.I. Almaula, P.S. Khodade, A.R. Parab, R.K. Duggal, C.P. Singh, A.S. Rawat, G. Chourasiya, S.A. Chitambar and H.C. Jain, J. *Radioanal. Nucl. Chem. Letters*, **87**, (1984) 169.

16 K.L. Ramakumar, P.S. Khodade, A.R. Parab, S.A. Chitambar, H.C. Jain, *J. Radioanal. Nucl. Chem*. **107** (1985) 215.

17 R.K. Bhatia, P.K. Reddy, V. Yadav, V. Nataraju, E. Ravisankar, T.K. Saha, V.K. Handu and S.K. Gupta, 14th ISMAS Workshop-2011

18 R.K. Bhatia, V.K. Yadav, M.M. Gulhane, R. Dutta, R. Chandak, K.D. Joshi, M. Murali, A.M. Kasbekar, V. Mahadeswar, E. Ravisankar, A. Verma, T.K. Saha, V. Nataraju, V.K. Handu and S.K.Gupta, 14th ISMAS Workshop 2011.

19 R.M. Rao, A.R. Parab, K. Sasibhushan, S.K. Aggarwal, *International Journal of Mass Spectrometry* **273** (2008) 105.

20 D.A.Dahl, "SIMION version 7.0", Idaho National Engineering Laboratory, 2000

21 E. Ravisankar, R.K. Bhatia, V.V. Katke, A.M. Kori, V.K. Yadav, V. Nataraju and V.K. Handu, Proceedings of 11th ISMAS-TRICON-2009.

22 The Focusing of Charged Particles, H.A. Enge, Academic Press, New York, (1967) 203.

23 H. Hintenberger and L.A.König, Advances in Mass Spectrometry, Pergamon Press, New York (1959) 16.

24 H.H. Tuithof and A.J.H. Boerboom, *International Journal of Mass Spectrometry and Ion Physics* **20** (1976), 107.

25 L. A. Konig, H.Hinterberger, *Nuclear Instruments*, **3** (1958) 133I. and Chavet, *Nuclear Instruments and Methods* **99** (1972) 115.

26 V.V.K. Rama Rao, *International Journal of Mass Spectrometry* **145** (1995) 45.

27 R.K. Bhatia, V.V.K. RamaRao, N. Padma and A.D. Kulkarni, 9th ISMAS Symposium (2003).

28 R.K. Bhatia, S.N. Bindal and V.K. Handu, 13th ISMAS symposium cum workshop (2008).

29 M. Ishihara, United states patent, Patent no. 4998015

30 M. Ishihara, United states patent, Patent no. 5118939

31 MALDI MS: A Practical Guide to Instrumentation, Methods and Applications, F. Hillenkamp, J. . Katalinic, Wiley Blackwell (2013).

32. Practical Guide to ICP-MS: A Tutorial for Beginners, R. Thomas, CRC Press (2003).

33. Secondary Ion Mass Spectrometry: An Introduction to Principles and Practices, Paul van der Heide, Wiley (2014).

34. Mass Spectrometry: Principles and Applications, 3rd Edition, E. de Hoffmann, V. Stroobant, Wiley (2013).

35. A review of Mass Spectrometry Detectors, K. Neetu et. al., *IRJP* **10** (2012) 3.

Sh. V. Nataraju is Heading the Advanced Mass Spectrometry Section of Technical Physics Division, BARC. He secured Ist position in M.Sc. (Physics) from Government College, Rajahmundry of Andhra University in 1986 with specialization in Electronics. He was graduated from 31st batch of BARC Training school and joined Technical Physics Division in 1988. Since then he has been associated with mass spectrometry activity and has a vast experience of nearly three decades. He is presently responsible for indigenous development of different mass spectrometers such as Quadrupole MS, Thermal ionization MS, Process Gas MS and ICP MS etc. in BARC. He has published more than 12 research papers in reputed international Journals on the design and improvement aspects of mass spectrometer instrumentation. He is the recipient of Science and Technology Excellence Award (2014) and Group Achievement Awards (2006, 2010 & 2015) by the Department of Atomic Energy. Currently he is the Vice -President of Indian Society for Mass Spectrometry and the Joint Secretary of Indian Vacuum Society.

Applications of Mass Spectrometer for the Trace Elemental Analyses of Nuclear Materials

S.B.Deb and M.K.Saxena

Radioanalytical chemistry Division, Bhabha Atomic Research Centre, Trombay, Mumbai 400085, India
(Email: sbdeb@barc.gov.in; Fax: +91-22-25505151; Phone: +91-22-25590633)

Introduction

A trace element is an element present in low concentration in a system. A concentration of 100 ppm is commonly accepted as an upper limit. Although trace elements may not be plentiful within the object of interest, yet they can play extremely important roles in understanding the history of things and can also be extremely important to certain biological functions. In nuclear industry the trace elements play a critical role as their presence above the specified limits may lead to failure of fuels and structural materials. Hence all the nuclear materials including fuels undergo stringent quality control (QC) and quality assurance (QA). The trace elements of importance in nuclear industry include metallic elements like B, Cd, Co, Dy, Gd, Mn, Mo, Ni, W, etc., and non metals like C, Cl, D, F, H, O, etc. There are many techniques which have been employed for their determination.

The competence to, accurately and precisely, determine element concentration at trace and ultra-trace level and isotope ratios is the main characteristic of inorganic mass spectrometry. The basic principle in mass spectrometry is generation of ions of the analytes, separating the ions according to their m/e and finally detecting them. All mass spectrometers have an ion source, a mass analyzer and an ion detector. The nature of these components varies based on the type of mass spectrometer, the type of data required, and the physical properties of the sample. Mass spectrometers are classified by the type of their ionisers and analyzers as shown in Fig. 1. They are extremely involved machines. To avoid the lowering of sensitivity due to loss of ions by scattering or neutralization, a high vacuum of 10^{-6} to 10^{-9} Torr is desirable in these systems.

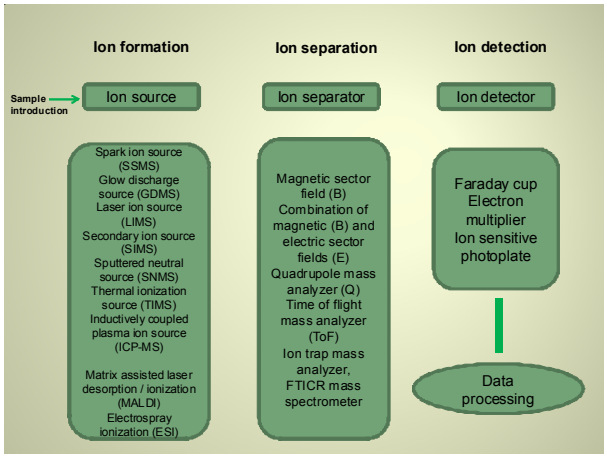

Fig.1. Basic diagram of a mass spectrometer

The unique feature of these instruments is their high sensitivity and low detection limit. In addition, one of the main features of mass spectrometry is, and this is the major advantage in comparison to other atomic and molecular non-mass spectrometric techniques, that it offers the possibility of determining isotope ratios and abundances of isotopes with high precision and accuracy in all types of samples (in solid, liquid and gaseous materials as well).

Their applications in nuclear industry embrace quality assurance of nuclear materials, determination of burn-up of fuel in a nuclear power plant, environmental monitoring and health, for studying radionuclide migration, for determination of isotope ratios of radiogenic materials in nuclear materials, nuclear material accounting and radioactive waste control.

The characterization of radioactive waste is required, for nuclear waste management, especially in respect to long lived transuranics ^{237}Np ($t_{1/2}$= 2.1x10^6 y), ^{239}Pu ($t_{1/2}$= 2.4x10^4 y), ^{240}Pu ($t_{1/2}$=6.6=10^3 y), ^{242}Pu ($t_{1/2}$=3.8x10^5 y), ^{243}Am ($t_{1/2}$=7.4x10^3 y) and fission fragments and activated products ^{79}Se ($t_{1/2}$= 7x10^3 y), ^{93}Zr ($t_{1/2}$= 1.5x10^6 y), ^{99}Tc ($t_{1/2}$=2.1x10^7 y), ^{107}Pd ($t_{1/2}$= 6.5x10^6 y), ^{126}Sn ($t_{1/2}$= 1.0x10^4 y), ^{129}I ($t_{1/2}$= 1.57x10^7 y) and ^{135}Cs ($t_{1/2}$=10^6 y). The complete record of fission products and actinides can be obtained using, mass spectrometry (very good detection limits) as compared to radiometric methods. The characterization of radioactive waste, environmental scrutinizing, monitoring of the health of exposed personnel is also very important. For this various types of samples like blood, urine, feces, hair and tissue need to be analyzed and this requires a powerful and fast analytical technique that can cope with the analysis of a large number of samples within a very short time frame and give accurate and precise results. The constant improvements in sensitivity and interference suppression in inductively coupled plasma mass spectrometry (ICP-MS) have enabled the determination of cesium and strontium. The fission product ^{90}Sr is released into the environment primarily from leaks, nuclear bomb testing etc. ^{90}Sr has a high fission yield (~6%), half life of 29 years, high biological uptake and slow excretion thus making it difficult to use radiometric determination due to various disadvantages including interferences from the daughter product ^{90}Y. The procedure adopted takes time and the sample throughput is very low. However, when fast and accurate determinations are needed in crucial situations, mass spectrometry is the ultimate technique that comes to rescue of researchers. The analysis time is very short and the interferences are very less. Besides the analysis of radioactive waste the determination of contamination and enrichments of selected radioactive nuclides e.g. ^{129}I, which is one of the most important environmental indicator of nuclear accidents at ultralow concentration levels is useful for environmental monitoring due to fallout from nuclear weapons testing, nuclear power plants or nuclear accidents. Isotope speciation is very important in environmental radiochemistry for understanding transfer/

migration mechanisms and age determinations and bioavailability. Long-lived radionuclide tracers are also been used for tracer experiments in biological, medical and geological research and can also be applied for determining the concentration of monoisotopic elements (e.g. iodine using ^{129}I) by the isotopic dilution method (IDMS) . The presence of elements like B, Cd and some rare earths such as Sm, Eu, Gd and Dy as impurities in the fuel 'meat', even at ultratrace levels is detrimental to their efficient utilization in the nuclear reactor due to the high thermal neutron absorption cross section of these elements. Some of the rare earth elements, i.e., Ce, Nd, Tb etc., and transition elements, i.e., Mn, Co and Ni, can form activation products whereas others like W, Mo, etc. can modify the metallurgical properties of the fuel. The presence of hydrogen in certain metals (e.g., titanium, vanadium, zirconium) and alloys (e.g., steel, zircaloy) beyond certain limit leads to embrittlement resulting in loss of structural integrity of the material. Consequently fuel and other nuclear materials have specifications for these elements. The specifications differ for different nuclear materials e.g., oxide fuel, carbide fuel, clad, etc. The quality assurance of the nuclear materials for trace elements are preferably done by mass spectrometry. Fig.2 summarizes the different applications of mass spectrometers in determination of concentration and isotope ratio of radionuclides.

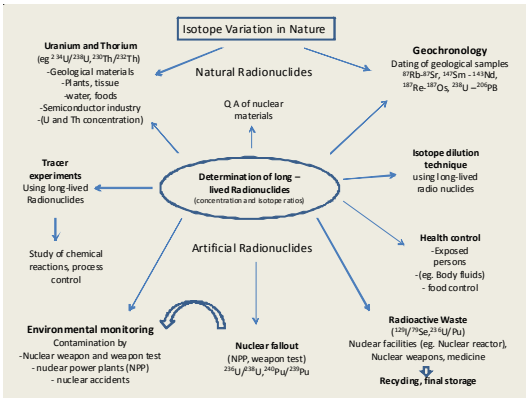

Fig.2. Summary of the applications of mass spectrometers

The history of mass spectrometry is intimately intertwined with the early history of nuclear physics. J.J. Thomson's pioneering experiments on the mass-to-charge ratio of the electron, led to the discovery that neon possessed at least two isotopes. He used what could be called the world's first mass spectrometer (Thomson, 1912). Shortly thereafter, F.W. Aston, a graduate student of Thomson's at the Cavendish Laboratory at the University of Cambridge, built a mass spectrograph with a resolving power of 130 to confirm Thomson's work on neon, and showed that the mass of a proton exceeded unity by approximately 0.08% (Aston, 1919). This result had far-reaching consequences for nuclear astrophysics (Eddington, 1926). A.J. Dempster, who had trained under Wilhelm Wien, constructed a mass spectrograph in 1918 and used it to measure the isotopic composition of Mg, K, Zn, Ca, and Li by heating salts of these elements and ionizing them by electron impact (Dempster, 1918). Consequently lots of work had been done to develop the state of the art mass spectrometers.

Since its beginning about 100 years ago, mass spectrometry (MS) has become a virtually ubiquitous research tool. Scientific breakthroughs made possible by MS have included the discovery of isotopes, the exact determination of atomic weights, the characterization of new elements, quantitative gas analysis, stable isotope labeling, fast identification of trace pollutants and drugs, and the characterization of molecular structure. With the hyphenation of separation techniques (e.g., Capillary electrophoresis, ion chromatography etc) to mass spectrometers the research in speciation studies has boosted up.

Since a mass spectrometric method is primarily determined by the choice of evaporation and ionization method, the different mass spectrometric techniques can be classified according to the evaporation and ionization method used. The mass spectrometric techniques could be divided into methods with simultaneous evaporation (atomization) and ionization processes in the ion source e.g. Spark Source Mass Spectrometer (SSMS), ICP-MS, Secondary Ion Mass Spectrometer (SIMS) and methods with "postionization" processes e.g. secondary neutral mass spectrometry (SNMS), Glow Discharge Mass Spectrometer (GDMS), Laser Ablation ICP-MS (LA-ICP-MS), Thermal Ionization Mass Spectrometer (TIMS). With the "postionization" methods, the processes of evaporation and atomization or sputtering of the sample material are separated in time and space from the processes of ionizing the atomic species. The ionization method applied in turn determines the ion separation system to be employed, which is essentially defined by the physical properties of the ions formed (e.g. initial energy) and the ionization itself (e.g. formation of molecular and cluster ions often with great intensity). Both static magnetic sector fields or combinations of electric and magnetic sector fields (e.g. Mattauch–Herzog mass spectrometer, Nier–Johnson mass spectrometer or the reverse geometry) are used for ion separation as well as dynamic ion separation systems (e.g. quadrupole mass spectrometer, time-of flight (TOF) mass spectrometer, Fourier transform mass spectrometer and ion trap mass spectrometer). Ion detection is usually done by electron multiplier, channel plates, channeltron, Faraday cup, daly detector or charge coupled device (CCD).

In the trace analysis of solids, preference is given to the very sensitive multi-element analytical methods which permit a direct analysis of the sample material without any chemical sample preparation i.e., GDMS, LA-ICP-MS, SIMS, etc. A possible danger of contamination during sample preparation and the occurrence of numerous interferences in the mass spectra of aqueous solutions after digestion of sample with acids (in comparison to ICP-MS) can thus be reduced to a minimum. However, quantification in solid-state mass spectrometry generally proves difficult if no suitable matrix matched standard reference materials are available. For this reason, ICP-MS has become the work horse for analysis of trace metallics in nuclear materials. The calibration of the measuring technique can thus be significantly improved and inhomogeneity problems avoided. The most important techniques for mass spectrometric trace element analysis on inorganic solids and for the determination of trace impurities in aqueous solutions and their applications are compared in Table 1.

Inorganic mass spectrometric techniques, such as ICP-MS, LA-ICP-MS, GDMS and SIMS have been established in the last few decades as the most important and sensitive analytical techniques for elemental, surface and isotope

analysis at the trace and ultra-trace concentration level and for analysis of species. Furthermore, special mass spectrometric techniques i.e., SIMS - have achieved significance as reliable surface analytical techniques with spatial resolution in µm and sub-µm range and depth resolution in the nm range, respectively. The capabilities and applications of different inorganic mass spectrometric methods have to be judged with respect to their advantages and drawbacks, also in comparison to non-mass-spectrometric analytical techniques.

The following paragraphs will be highlighting some of the applications of different mass spectrometric techniques for trace element analysis of nuclear materials.

Table 1: Different types of mass spectrometers

Method	Detection limit (µg/g)	Calibration/reproducibility	Strengths of the method	Limitations of the method
SSMS	0.001-0.1	Using SRM/ ±20%	High sensitivity	Expensive experimental arrangement
GDMS	0.0005-0.1	Using SRM/ ±10%	High sensitivity, good precision	Analysis restricted to electrically conducting samples (dc GDMS)
LA-ICP-MS	0.0005-0.5	Using SRM/ ±10-20%	No charge –up effects, High sensitivity	Problem with inhomogenous samples
SIMS	0.001-1.0	Using ion implantation standards/ ±30-40%	High sensitivity, imaging, depth profiling	Great variation in element sensitivity, matrix effects
ICP-MS	0.0001-0.1	Using calibration solution/ ±10%; isotope dilution / ±0.5%	Good calibration possibility, no problems with inhomog-eneity, good precision	Solution steps necessary, matrix effects
ID-TIMS	0.000005-0.1	±0.5%	Excellent quantification possibility, highest precision and accuracy	No multi element capability, trace separation necessary

Inductively Coupled Plasma Mass Spectrometry

Mass spectrometry with inductively coupled plasma ionization is probably the most sensitive analytical technique for fast multi-element determination of elements in the trace and ultra-trace concentration range in aqueous solutions. This powerful analytical technique is increasingly used in nuclear forensic science. In contrast to conventional inorganic solid mass spectrometric techniques, inductively coupled plasma mass spectrometer (ICP-MS) allows a simple sample introduction in a normal pressure ion source and an easy quantification procedure using aqueous standard solutions. In ICP-MS the ion source is the plasma. An atmospheric inductively coupled plasma is formed when an inert gas, usually argon, is introduced into a Fassel torch [1] surrounded by three turns of a coaxial water cooled induction copper coil. The details of the plasma formation and instrumentation are described elsewhere [2-5]. The resulting plasma is a dense annular shaped ball of highly excited electrons, ions, metastable and neutral species. The operating temperature of an ICP is between 5000 to 10000 K. At such high temperatures most of the elements in the periodic table, having their first ionization potential of less than 9 eV, are singly ionized to the extent of 90% and there is negligible molecular species and doubly charged ions. Ions are produced in a reproducible manner and ion characteristics of the dissolved solids are formed. Hence multi-elemental analysis can be carried out by ICP-MS. Most of the metallic elements can be detected quantitatively by ICP-MS. This technique is applicable to the determination of analytes in solution form only and hence solid samples have to be dissolved prior to analysis by ICP-MS. An inherent limitation of the ICP-MS is that this instrument can tolerate solutions containing total dissolved solid concentration of only 0.1 % and in most of the cases the matrix has to be separated from the trace elements before injecting the solution into the ICP-MS [6-9]. The background in ICP-MS is almost clean beyond mass No. 80 [9, 10-12]. Most of the interferences had been resolved over time [13-18] since the inception of ICP-MS. Commercially the ICP ion source is commonly coupled to the Quadrupole / Time of Flight / Magnetic Sector mass analyzers. The detectors used in these instruments are Channeltron / ion multiplier tube / faraday cup / dally detectors etc. The extreme element sensitivity of double- focusing sector field ICP-MS (ICP-SFMS) permits ultratrace analysis down to the sub-femtogram per milliliter concentration range in aqueous solution [19]. For sensitive measurements of transient ion signals ion trap and TOF mass spectrometers with detection limits in the low ng L^{-1} concentration range and lower are generally used [20].

It is well known that the rare-earth elements (REE) concentration (relative to uranium) will change during ore processing but the REE pattern (i. e. their relative concentration compared to each other) and isotopic composition are assumed to remain unaltered during uranium production processes. In consequence, the REE are considered as one of the most useful nuclear forensic signature for origin assessment of natural uranium. Recently in an article [21] the authors had reported a chemical separation method involving co-precipitation and extraction chromatography (EXC) for ultra-trace levels of REE in high

purity uranium matrix. This was followed by ICP-SFMS analysis. Fig. 3shows the REE pattern in UO_3 from plant A and B and that in UO_2 from plant B. The limits of detection for different elements in question are in the pg/g range.

Binary and/or ternary metallic alloys of uranium (U) and plutonium (Pu) with transition metals are considered to be promising fuels for fast breeder reactors due to their high fissile atom content, high breeding ratio with lower doubling time, dimensional stability at high burn-up and high thermal conductivity, etc. A method was reported [22] for the determination of trace impurities viz., B, Ce, Cd, Co, Eu, Dy, Gd, Mn, Nd, Ni, Sm and Tb in U-Ti, U-Zr and U-Mo by Inductively coupled plasma orthogonal acceleration time of flight mass spectrometer (ICP-oaTOFMS). Solvent extraction

using tributylphosphate (TBP) in carbon tetrachloride (CCl4) was used for the partial removal of matrix elements so as to reduce the matrix effect on these analytes during mass spectrometric analysis. The common analyte internal standard (CAIS) technique was refined and utilized to account for the effect of the remaining matrix elements.

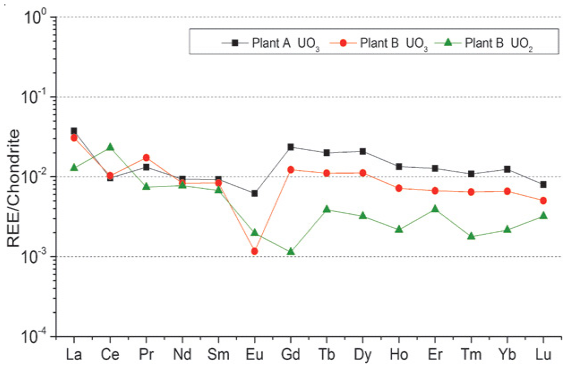

Fig 3. Comparison of the measured REE patterns in UO_3 and UO_2 product samples from Plant A and Plant B.

Aluminum alloy is a preferred material for some structural components in research nuclear reactors. Thermal neutron irradiation of aluminum causes it to undergo transmutation to silicon. The concentration and the isotopic composition of the radiogenic silicon provides information on the irradiation history of the material and operation history of the reactor both of which are important to nuclear forensics and nuclear archaeology. An analytical method had been reported [23] to determine the concentration and isotopic composition of radiogenic silicon using an ICP- SFMS. The measured content of radiogenic silicon in aluminium alloy materials irradiated with known fluence of thermal neutrons agreed well with the theoretically predicted values.

A simple and efficient procedure was reported [24] for the rapid and quantitative extraction of boron (B) from uranium-silicon-aluminium compounds, aided by generation of in-situ accelerator, employing pyrohydrolysis (PH) technique. The PH operating conditions like choice of carrier gas, heating time and sample mass were optimized for rapid and quantitative recovery of B. An ICP-oa-TOF-MS was utilized for the simultaneous determination of B content and its isotope ratio ($^{10}B/^{11}B$). The ICP-oaTOFMS operating parameters like acquisition time, mass bias, long and short term stabilities were optimized and common analyte internal standardization (CAIS) chemometric technique was applied to improve both the accuracy and precision of B determination.

An analytical method had been reported [25] for the quantification of trace amounts of rare earth elements in a zirconium matrix (ZrO2, Zircaloy-2, and Zirconium - 1% Niobium) by quadrupole ICP-MS. Rare earth elements were quantitatively separated from the zirconium matrix by precipitation using Mandelic acid followed by solvent extraction. The analytical methodology was validated by recovery studies with standard addition as well as with an independent gamma spectrometry technique using 141Ce, 147Nd, and 152+154Eu tracers. Recoveries of >90% were reported for nine rare earth elements (La, Ce, Nd, Sm, Eu, Gd, Dy, Yb, and Lu) in both techniques.

U-Zr alloys have potential use in low power or research reactors due to numerous advantages. An analytical methodology was reported [26] for the quantification of trace elements (Al, Ba, Co, Cr, Cu, Ga, Ge,In, Mg, Mn, Ni, Rb, Rh, Sr, W, Y,and Zn) in U-Zr alloys by using ICP-oa-TOF-MS. A dual solvent extraction technique was employed for matrix separation prior to analysis of the trace constituents by ICP-oa-TOFMS. Zirconium was synergistically extracted by 2-thionyltrifluoro-acetone (HTTA) in the presence of tri-butylphosphine oxide (TBPO) in 1,2-dichloroethane, while uranium was separated by the well-established tributylphosphate (TBP)/carbon tetrachloride (CCl4) solvent extraction technique. In order to validate the analytical methodology, recovery studies of the elements were carried out employing the standard addition technique, followed by analysis with ICP-MS. Reproducible recoveries of e"90% were achieved for 17 elements. The separation procedure was further validated for transition elements by an independent gamma spectrometry technique using carrier-free ^{51}Cr and ^{54}Mn tracers with recoveries of >94%.

An analytical methodology was reported [27]for the precise quantification of ten trace rare earth elements (REEs), namely, La, Ce, Pr, Nd, Sm, Eu, Tb, Dy, Ho, and Tm, in gadolinium aluminate (GdAlO3) employing an ultrasonic nebulizer (USN)-desolvating device based ICP-oaTOFMS. A microwave digestion procedure was optimized for digesting the highly refractory oxide. An Ultra Sonic Nebuliser (USN)-desolvating sample introduction system was employed to enhance analyte sensitivities by minimizing their oxide ion formation in the plasma. Individual oxide ion formation yields were determined in matrix matched solution and employed for correcting polyatomic interferences of light REE (LREE) oxide ions on the intensities of middle and heavy rare earth elements (MREEs and HREEs).

Laser Ablation Inductively Coupled Plasma Mass Spectrometry

LA-ICP-MS is one of the most exciting analytical technologies available because it can perform ultra-high sensitive chemical analysis down to ppb (parts per billion) level without any sample preparation. This powerful analytical technique uses the evaporation of sample material by a

focused laser beam (mostly using a Nd–YAG laser with l/4= 266 nm or l/4 =213 nm) in an inert gas atmosphere (e.g. Ar) and ionization of evaporated and ablated material in an inductively coupled plasma - ion source of an ICP-MS. The shorter laser wave-lengths are favoured due to the more uniformed particle size distribution formed after ablation and therefore, fractionation effects are less pronounced. Consequently eximer lasers like ArF are gaining popularity. The details of the instrument are described elsewhere [28].

Both conducting and non-conducting samples can be analyzed by LA-ICP-MS thereby delivering the fastest analysis speed of all analytical techniques.

In contrast to liquid analysis, the quantification is not so easy and straight forward due to the lack of matrix matched reference materials. The quantification of the concentration of samples analysed by LA-ICP-MS is performed by using the relative sensitivity factor (RSF) of an external standard. There are limited papers dealing with the trace element determination of nuclear materials by LA-ICP-MS whereas there are numerous others dealing with isotopic ratios.

It had been reported [29] that elemental impurities in nuclear grade thoria were determined using LA-ICP-MS employing ArF laser (20 ns, 193 nm, 20 Hz). Three certified standards of thoria, prepared in the Department of Atomic Energy (DAE), India were used to find out the RSF of the elements. Magnesium was used as an internal standard for quantification in view of its addition during fuel fabrication. The concentrations determined for 16 different elements (Al, B, Cd, Ce, Cu, Dy, Er, Eu, Fe, Gd, Mg, Mn, Mo, Ni, Sb, Sm and V) were within 20% of the certified values in the standards.

A study [30] had been reported regarding the development of a method for the direct determination of the fission gas (FG) Xe in micro inclusions contained in nuclear fuels using LA-ICP-MS. Two calibration strategies were employed in this study. . The first strategy was based on the direct injection of a known quantity of a reference gas into the LA-ICP-MS carrier gas system. Further, the ablation of a matrix-matched standard of a non-irradiated UO_2 sample, implanted with a known amount of ^{129}Xe was also applied. Using these quantification methods, quantitative LA-ICP-MS measurements were performed on high burnup nuclear fuel. This study demonstrates that direct gas injection is most suitable for the quantification of fission gas in micron-sized inclusions. The direct gas addition is simple and linear calibration curves were obtained. Good reproducibility was obtained and matrix effects were within the uncertainty of the measurements.

It had been reported [31] than an a box integrated laser ablation system coupled to an inductively coupled plasma mass spectrometer was designed and built at the hot laboratory of the Paul Scherrer Institute, for the analysis of highly radioactive samples. A 266 nm Nd:YAG laser based ablation system was separated into beam generation and ablation and sample handling to avoid radiation induced defects of the hardware. The optical beam path is delivered through a window within the a box. The focusing optics and the ablation cell suitable for handling highly radioactive samples are described in detail. The laser ablation system was coupled to a multi- collector ICP-MS and evaluated by applying various laser parameters to ablate uranium dioxide reference materials.

Glow Discharge Mass Spectrometry

Glow discharge Mass Spectrometer (GDMS) is a solid state analysis method for direct trace multi elemental determination. In GDMS an argon gas glow discharge at a pressure of 0.1–10 Torr is used as an ion source. The Ar^+ ?ions formed in low-pressure plasma are accelerated towards the cathode consisting of the sample material. Sample material is sputtered at the cathode surface by Ar^+ ions. Sputtered neutral particles are ionized in the glow discharge plasma (‘‘negative glow’’) by Penning and/or electron impact ionization and charge exchange processes. The detail of the instrument has been discussed elsewhere [32].

Two types of ion sources are differentiated: direct current (dc) GDMS and radio frequency (rf) GDMS. Whereas dc-GDMS is suitable for the direct analysis of conducting samples, rf-GDMS can be used for direct solid analysis of conducting, semi conducting and non conducting material. However dc-GDMS is more widely used as it is a rapid and easy to handle technique for elemental analysis of electrically conducting samples. The non conducting powered samples can be rendered conducting by mixing them with conducting powdered binder (e.g., high purity graphite, Au, Ag, Cu Ga). The instrument has a detection limit in ng g^{-1} concentration range with a relative standard deviation (RSD) of ± 10%.

Like all the direct solid analysis mass spectrometers this technique too is limited due to lack of matrix matched CRM.

It had been reported [33] that traces of boron can be directly determined in Zr-2.5%Nb, Zr-1%Nb alloys and zirconium metals by glow discharge quadrupole mass spectrometer (GDQMS). Zirconium and its alloys are used as structural materials in nuclear reactors. Relative sensitive factor (RSF) values for boron were determined using different solid standard reference materials (Zircaloy and steel). The overall accuracy of the procedure was found to be ±8% at <“0.5 mg kg^{-1} levels of boron using Zircaloy and steel standards. Under optimized experimental conditions the detection limit for boron was found to be ±13 ìg kg^{-1}.

GDMS and ICPMS were employed for the determination of 18 trace elements in nuclear grade graphite [34]. The results from both the methods were found to be consistent.

It is desirable to have the elemental data for construction materials used in nuclear power plants for the prediction of radioactivity induced by neutron irradiation. To evaluate radioactivity in retired Japanese nuclear power plants, it is reported [35] that more than 130 specimens were collected from the structural materials of the Fugen Nuclear Power Plant, which was constructed in the 1970s and whose operation was stopped in 2003. Seventy-six compositional elements in the specimens were analyzed using appropriate chemical analyses and measurement techniques, such as GDMS and ICPMS. These data are expected to become a reference in the establishment of domestic standard data, and they are also expected to be applied to the evaluation of

irradiation-induced radioactivity in the structural materials of reactors that are subject to decommissioning in the future.

Direct current GDMS had been applied for the characterization of different types of nuclear fuels, cladding materials and nuclear-waste glasses [36]. These briefly includes U_3O_8, UO_2, PuO_2, (U, PU)O_2, (Pu, Ce)O_2, UPuZr, UNdZr, two types of nuclear waste glass and Zircaloy cladding materials. For the non-conducting oxide-based nuclear samples the relative sensitivity factors (RSFs), applied for quantitative analysis, are affected by the oxygen content in the matrix. For these samples the effect of 'getter metals.' such as tantalum and titanium as binder material, has been investigated and the results compared with those obtained using silver as the host matrix. Moreover, when tantalum was used as a secondary cathode, it was found to behave as a getter of oxygen. For the quantitative analysis of nuclear-waste glasses the use of matrix specific RSFs was necessary. Comparisons with RSFs obtained from other workers are made in this paper. Metallic alloys were analysed using several analytical techniques. The GDMS results obtained by applying RSFs from the major metallic element uranium were in agreement with those from independent techniques, such as titration, TIMS and ICP-MS.

It had been reported [37] that GDMS was used for determination of 36 elements in four Zircaloy standards including alloying elements, traces and gases. By comparing the mean values of each of these elements with the certified values, of one standard only, a RSF was obtained for each element. This RSF was used to convert the observed ion beam ratio concentration to a normalized concentration. Thereafter excellent agreement is obtained between the normalized and certified values of the elements in the remaining three standards. Likewise four New Brunswick Laboratory (NBL) standards of non conducting U_3O_8 powder were analyzed by GDMS.

Secondary Ion Mass Spectrometry

SIMS is a multi-element mass spectrometric method used for trace analysis on different solid material surfaces or thin layers. This technique is mainly used for depth profiling and determination of lateral element distribution (imaging) on solid surfaces. When solid surfaces are bombarded with ions (e.g. Ar^+, Cs^+, O_2^+, O-, Ga^+) of sufficiently high energy the ions penetrate into the solid to different depths (1-10nm) and transfer their kinetic energy to the atoms of the solid. Part of the energy of the implanted energy is returned to the surface of the solid via impact cascades and causes sputtering of neutral particles and positively or negatively charged secondary ions. In SIMS the secondary ions are analyzed mass spectrometrically (atomic, molecular and cluster ions). SIMS can be used for characterization of bulk material with detection limits down to the low ng g^{-1} (element dependent). The quantification of analytes by SIMS is very difficult due to large matrix effects. Nevertheless, if a matrix matched standard reference material is available then accurate analytical data can be obtained by SIMS. An important application of SIMS is the detection of local enrichment or depletion of chemical elements at the solid surfaces and determination of inhomogeneities in bulk material. This technique is very useful in the cases of refractory nuclear materials where dissolution is difficult. The mass analyzers used in SIMS are quadrupole, time of flight and more often double focusing ones.

SIMS had been used [38] in Nuclear Forensic Analysis for the characterization of plutonium and highly enriched uranium particles. SIMS has been used to obtain a complete spectrum of the trace elements contained in a micro-particle of Plutonium and Highly Enriched Uranium. From the trace elements present and their concentration in microparticles of plutonium and uranium, the history of the sample can be revealed, namely the physical/chemical and / or industrial processes the sample has undergone.

The inert gas xenon is the most abundant fission product produced during irradiation. Xenon retained in bubbles in the fuel has an important impact on the fuel behaviour in terms of heat conductivity and in-pile swelling. It had been reported [39] that SIMS was used for generation of precise data on the partitioning of retained xenon between gas bubbles, grain boundaries and the fuel matrix. Xenon in aUO_2 matrix waste detected by SIMS as Xe^+ by using a O^{2+} primary ion beam. In another report [40] SIMS was used to distinguish between xenon coming from the matrix and from gas bubbles during depth profiling.

Iodine, caesium and tellurium are volatile fission products, which can migrate and leave the fuel during a reactor power ramp. Consequently, to have a better understanding of the fuel behaviour and its evolution during a power ramp, data on the radial distribution of these species after a power ramp are needed. Analyses by SIMS, EPMA and SEM on UO_2 irradiated samples were performed [41] to understand the behaviour and release mechanisms of these fission products during a power ramp. Samples were prepared from a rodlet that had undergone a ramp test in the OSIRIS reactor and analyzed by SIMS. It was found that except at the edge of the sample, iodine forms precipitates during a power ramp, associated with intra- and inter-granular fission gas bubbles. It was also found that iodine is probably released together with the fission gases because they behave very similarly. The behaviour of caesium was found to be very different from iodine in that caesium uniformly coats the grain boundaries near the surface of the fuel. Consequently the authors postulate that in the outer region of the fuel caesium was not present in the gaseous state, but probably as a constituent of a caesium-rich second phase.

Thermal Ionization Mass Spectrometry

Since its inception TIMS is a widely used isotope analytical technique allowing isotopic ratios of long-lived radionuclides to be measured with a precision of better than 0.01% [42]. However quantitative analysis of trace elements in nuclear materials had been carried out by Isotope Dilution Mass Spectrometry (IDMS) in only those cases where spike was available. IDMS was used extensively at National Bureau of Standards, US in the certification of elemental concentrations in Standard Reference Materials [43]. In TIMS a small volume (down to 1 ml) of aqueous solution containing

the analyte in the nanogram to microgram range is deposited on a cleaned filament surface (mostly high-purity Re) and evaporated to dryness. The most frequently applied technique in TIMS works with two heated filaments [44]. One of the filaments is used for the evaporation of sample by thermal heating and the other for ionization of evaporated atoms and molecules on the hot filament surface, i.e. in this arrangement the evaporation and ionization are separated in space and time. TIMS is difficult for elements where the first ionization potential is higher than 8 eV. Chemical elements with a higher ionization potential were analysed as molecular ions (e.g. boron as $Na_2BO_2^+$ [45] or $Cs_2BO_2^+$ [46] ions). Elements or molecules with high electron affinity (e.g. Hf, W, Ru, Mo) were analysed as negative atomic ions [47-50].

Ruthenium is a fission product generated when UO_2 fuel burns up in a nuclear reactor. Its isotopic ratio and the amount in a spent fuel would help us to assess the irradiation behaviour. A method [51]] had been reported for the quantitative determination of Ru in spent fuel by using ^{99}Ru as spike. A single filament was used and the filament current was increased slowly to 5 A to obtain good results. Distillation method was used for separation of Ru from the isobaric elements.

An IDMS method was reported [52] for the determination of traces of iron in zirconium. This was required to study the effects of iron on the irradiation deformation of nuclear alloys. A two-stage purification procedure was developed to avoid the signal suppression and interference caused by the zirconium matrix. After sample dissolution and spiking with ^{54}Fe, the bulk of the zirconium is removed by ion exchange chromatography, and the eluted Fe (III) was further purified by micro-solvent extraction into tributyl phosphate-impregnated resin beads before being analyzed by TIMS.

Hot Vacuum Extraction-Quadrupole Mass Spectrometry

The total gas content and their composition are important specifications for nuclear materials and particularly in the case of fast breeder reactor fuels. Most commonly, total gas content and its composition is determined by hot vacuum extraction-quadrupole mass spectrometry (HVE-QMS). Here the gases are extracted from the sample under static vacuum at high temperature. The gases are then fed into a quadrupole mass spectrometer (QMS) [53].

An investigation on the amount of the occluded gases in sintered, ceramic grade, UO_2 pellets as a function of temperature had been reported [54]. It was been found that the total volume of gases liberated from the pellets at a temperature of 1700 C is in the range of 0.03 cm^3/g which is less than the maximum limit of 0.05 cm^3/g of UO_2 set by American Society for Testing and Materials. The mass spectrometric technique employed for the qualitative and quantitative analysis of the occluded gases shows the presence of H_2, CO, N_2 and CO_2 in the gas mixture.

A hot vacuum extraction technique for the determination of hydrogen in zirconium samples had been reported [55]. The total pressure of the evolved gases were measured and the individual intensities of hydrogen and deuterium were measured using an on-line quadrupole mass spectrometer. Synthetic mixtures of H_2 and D_2, in known concentrations had been analysed by QMS and an analytical expression correlating the measured $[D_2]/[HD]$ intensity ratio with the mole fraction of deuterium in the synthetic mixture has been arrived at. The precision and accuracy in the measurement of hydrogen is about 10% at 50 ppmw level.

The concentration of gases like H_2, N_2, CO, CO_2 and CH_4 in uranium metal was measured [56] by a HVE-QMS system. The isobaric interference between carbon monoxide and nitrogen at m/e = 28 in the mass spectrometric analysis was resolved by considering their fragmentation patterns. Since no standards are available to evaluate the results, only the reproducibility was tested. The precision (relative standard deviation at 3ólevel) of the method is ±5%.

A method had been reported [57]dealing with the optimization of conditions for the determination of hydrogen and deuterium content in a typical Zr-Nb coolant channel employing HVE-QMS and studies on molecular ion formation (H_3^+/D_3^+) in quadrupole mass spectrometer. Reference materials for hydrogen (Ti steel and Zr) were used for standardization and validation. Sliver samples received from irradiated Zr-Nb pressure tubes were analyzed for deuterium determination. The results were reported with a precision of 10%.

A method had been developed [53] for the determination of the total gas content and its composition in PFBR blanket pellets employing HVE-QMS. Sensitivity of the various gases in the QMS had been determined for computing the gas composition. The correction factors were found to be significantly high for He, H2 and O2. Mole fraction of nitrogen and carbon monoxide in the released gas from the sample was determined by considering their cracking pattern. The detection limit of the methodology is 0.001 L/kg at the sample size of 21 g. The relative expanded uncertainty in measurement is 9.2 % (at a coverage factor of 2). The results show that the total gas content observed in these pellets is much less than the specification limit of 0.1 L/kg at STP.

References

1. R. H. Scott, V. A. Fassel, R. N. Kinsely, D. E. Nixon, Anal. Chem. **46** (1974) 75.
2. R. S. Houk, Anal. Chem. **52** (1980) 2283.
3. A.L.Gray, Spectrochim. Acta **40B**(1985) 1525.
4. R. S. Houk, Anal. Chem. **58** (1986) 97.
5. A.L.Gray, Anal. At. Spectrom. **97A**, 58, 1986.
6. R. S. Houk, V. A. Fassel, G. D. Flesch, H. J. Svec, A. L. Gray, C. E. Taylor, Anal Chem. **52** (1980) 2283.
7. D. J. Douglas, L. Kerr, J. Anal. At. Spectrom. **25** (1988)385.
8. M. A. Vaughan, G. Horlick, Spectrochim. Acta **45B**, (1990) 1327.
9. D. C. Gregorie, Spectrochim. Acta **42B** (1987) 895.
10. S. H. Tan, G. Horlick, Appl. Spectrosc. **40** (19986) 434.
11. E. H. Evans, J. J. Giglio, J. Anal, At. Spectrom. **8** (1983) 1.
12. J. Marshall, J. Franks, J. Anal. At. Spectrom. **6** (1991) 591.
13. R. L. Thompson, T. Bank, E. Roth, E. Granite, Spectrochim. Acta **119B** (2016) 76.
14. M. A. Amr, A.F. I. Helal, A. T. A.Kinani, P. Balakrishnan, J. Environ. Radioact. **153** (2016) 73.

15. L. Balcaen, E. B.Fernandez, M. Resano, F. Vanhaecke, Analytica Chimica Acta, **894** (2015) 7.
16. S. D'Ilio, N. Violante, C. Majorani, F. Petrucci, Anal. Chim. Acta, **698** (2011) 6.
17. G.H Tao, R.E Sturgeon, Spectrochim. Acta **54B** (1999) 481.
18. S. D Tanner, V. I. Baranov, D. R. Bandura, Spectrochim. Acta **57B** (2002) 1361.
19. A.E. Eroglu, C.W. McLeod, K.S. Leonard, D. Mc-Cubbin, J. Anal. Atom. Spectrom. 13 (1998) 875.
20. G.M. Hieftje, D.P. Myers, G. Li, P. Manoney, T.W. Burgoyne, S.J. Ray, J.P. Guzowski, J. Anal. At. Spectrom. **12** (1997) 287.
21. J.Krajkó1, Z. Varga, M. Wallenius, K. Mayer, Radiochim. Acta **104** (2016) 471.
22. A. Saha, S. B. Deb, M.K. Saxena, J. Anal. At. Spectrom. **31**(2016) 1480.
23. Y. Shi, C. Broome and R. Collins, J. Anal. At. Spectrom., **31** (2016) 1174.
24. A. Saha, D. Shah, S.B. Deb, M.K. Saxena, V.G. Mishra, B.K.Nagar, B.S. Tomar, Microchem. J. **121** (2015) 56.
25. S.B. Deb, B.K. Nagar, M.K. Saxena, K.L. Ramakumar, Atom. Spectrosc. 31 (2010) 122.
26. A. Saha, S.B. Deb, B.K. Nagar, and M.K. Saxena, Atom. Specrosc. 34 (2013) 125.
27. A. Saha, S.B. Deb, B.K. Nagar, M.K. Saxena, Spectrochim. Acta 94-95B (2014) 14.
28. D. Gunther, B. Hattendorf, Trends Anal. Chem. **24** (2005) 255.
29. D. Alamelu, A.K. Choudhary, S.K. Aggarwal, J. Nucl. Mat.406 (2010) 356.
30. M. Horvath, M. Guillong, A. Izmer, N. Kivel, R. Restani, I. G.Leopold, J. O. Coutureau, , C. Hellwig D. Günther, J. Anal. At. Spectrom.22 (2007) 1266.
31. M. Guillong, P. Heimgartner, Z. Kopajtic, D. Gunther, J. Anal. At. Spectrom. 22 (2007) 399.
32. F.L. King, W.W. Harrison, Mass Spectrom. Rev. 9 (1990) 285
33. R. Shekhar. J. Arunachalam, G.R. Krishna, H.R. Ravindra, B. Gopalan, J. Nucl. Mat. 340 (2005), 284.
34. X. Wang, G. Bhagat K. O'Brien, K.Putyera, *2009 MRS Fall Meeting; Boston, MA US,* 1215 (2010) 113.
35. N. Kawata, Y. Shiratori, K. Maekawa, O. Arai, M. Shimizu, Trans.At. Ener. Soc. Japan 9 (2010) 405.
36. M. Betti, J. Anal. At. Spectrom. 9 (1996) 855.
37. K. Robinson, E. F.H. Hall, J. Met. 39 (1987) 14.
38. M. Betti Gabriele, T. L.Koch, Anal. Chem. 71 (1999) 2616.
39. L. Desgranges, B. Pasquet, Nucl. Instrum. Methods, Sect. B 215 (2004) 545.
40. J. Lamontagne, J. Noirot, L. Desgranges, T. Blay, B. Pasquet, I. Roure, Microchim. Acta, Part B 145 (2004) 91.
41. L. Desgranges, B. Pasquet, X. Pujol, I. Roure, Th. Blay, J. Lamontagne, Th. Martella, B. Lacroix, O. Comiti, L. Caillot, *Proceedings of the NEA/NSC International Seminar on Pellet/Clad Interactions with Water Reactor Fuels*, Aix-en-Provence, France (2004) 241.
42. T. Platzner, Chem. Anal. **145** (1997) 1.
43. J. D. Fasset J Res. Na. Bur. Stand. 93 (1988) 4
44. Roboz
45. R. M. Rao, A. R. Parab, K. S. Bhushan, S.K. Aggarwal, Microchim. Acta **169** (2010) 227.
46. T. Ishikawa, K.Nagaishib, J. Anal. At. Spectrom. **26** (2011) 359.
47. A. Trinquier Anal. Chem. 88 (2016) 5600.
48. K.R. Bermingham, R.J. Walker, E.A. Worsham, Int. J. Mass Spectrom. 403 (2016) 15.
49. E.A. Worsham, R.J. Walker, K.R. Bermingham, Int. J. Mass Spectrom. 407 (2016) 51.
50. Y. Nagai, T. Yokoyama J. Anal. At. Spectrom. 31 (2016) 948.
51. Y.S. Jeon, Park, S. Yang, J.S Kim, S.H. Han, Y.J. Park, Asian J. Chem. 25 (2013) 7044.
52. N.L. Elliot, M.A. Campbell, L.W. Green, J. Anal. At. Spectrom. 146-147 (1995) 99.
53. P. S. Ramanjaneyulu, K. Chandra, A. S. Kulkarni, C. S. Yadav, Abhijit Saha , M. K. Saxena, B. S. Tomar, K. L. Ramakumar, J. Radioanal. Nucl. Chem. 301 (2014) 117.
54. O. Vega, H.G. Riella, C. Rodrigues J. Nucl. Mater. 106 (1982) 121.
55. Y. S. Sayi, K. L. Ramakumar, R. Prasad, C. S. Yadav, P. S. Shankaran, G. C. Chhapru, H. C. Jain, J. Radioanal. Nucl. Chem. 230 (1998) 5.
56. Y.S. Sayi , P.S. Ramanjaneyulu , C.S. Yadav , P.S. Shankaran, G.C. Chhapru, K.L. Ramakumar, V. Venugopal, J. Nucl. Mater. 373 (2008) 75.
57. K. Chandra, P. S. Ramanjaneyulu, C. S. Yadav, A. S. Kulkarni, Y. S. Sayi, K. L. Ramakumar, Analytical Letters, 45 (2012) 2136.

Dr. S.B.Deb is from 42nd batch BARC Training School. He had done his MSc from North Eastern Hill University and PhD from Homi Bhabha National Institute. He has been working in ICP-MS for last 17 years and has developed analytical methodologies for Quality Assurance (QA) of trace metallics in various nuclear materials.

Shri M.K. Saxena joined BARC in 1988 after successful completion of OCES from 31st batch of BARC Training School. Currently he is heading Trace Elements Analysis Section of Radioanalytical Chemistry Division, BARC. He has expertise in various instrumental techniques for chemical quality control of nuclear materials.

Inorganic Mass Spectrometry for Determination of Isotopic Composition in Nuclear Materials

Radhika M Rao

Fuel chemistry Division, Bhabha Atomic Research Centre, Trombay, Mumbai 400085, India

Introduction

Mass Spectrometry is extensively used for characterization of nuclear materials for elemental composition and isotopic abundance for quality assurance of fuel materials and management of radioactive waste. It is used for providing accurate inventories of fissile materials through out the entire nuclear fuel cycle. It is essential for characterizing irradiated fuels for burn-up measurements and for nuclear safeguard purposes. Other than nuclear applications, precise data on isotope ratio are required in various fields of research such as occurrence of natural variations, determination of age of rocks, origin of plants, nuclear forensics, environmental monitoring, characterization of biological samples such as blood, urine etc.

A mass spectrometer creates ions in gas phase from the analyte molecule or atom, separates the ions according to their mass to charge ratio (*m/z*) and measures the abundance of the separated ions. The mass spectrometer consists of five systems : (1) ion source, where ions are produced such as Electron Impact, Thermal Ionization, Inductively Coupled Plasma, etc. (2) mass analyser, which separates the ions according to their mass, such as Quadrupole, Magnetic Sector, Time of Flight (3) detector system, which could be an ion integrator like faraday cup or ion counters like Channeltron, Daly or SEM(Secondary Electron Multiplier) (4) vacuum system, consists of a set of rotary, turbomolecular pumps and high vacuum ion getter pumps with appropriate measuring gauges for creating vacuum of the order $<10^{-8}$ mbar in the mass spectrometer and (5) data acquisition system, which includes software for ion generation, collection and measurement with an interface for integration of all the five systems. The vacuum pumps remove the gaseous ions, for collision free passage of ions to the detector, thereby increasing sensitivity and lowering background.

The technique used for ion formation defines the mass spectrometer. The type of mass spectrometer used depends on the information required from the sample. Multi Collector-Thermal Ionization Mass spectrometry(MC-TIMS) and Quadrupole based Inductively Coupled Plasma Mass spectrometry (Q-ICPMS) are among most sought after analytical techniques in the nuclear industry. MC-TIMS offers accurate and precise data on composition of the nuclide in the sample and Q-ICPMS provide rapid and relevant data on elemental compositions required for quality assurance of nuclear materials. Techniques like Laser ablation-ICPMS (LA-ICPMS), Secondary Ionization Mass Spectrometry(SIMS), Glow Discharge (GDMS) are used for direct isotope analysis of solid samples and for depth profiling, while Gas Source Mass Spectrometry with electron bombardment (GSMS), Resonance Ionization Mass Spectrometry(RIMS) and Accelerator based Mass Spectrometry (AMS) have specific applications in nuclear science and technology. In TIMS ~ 2 µL solution containing submicrogram amounts of the element in pure form is deposited on a filament which is heated, to produce monovalent monoenergetic gaseous ions in the vacuum region of the ion source. A single filament assembly from which sample is evaporated and ionised or multiple filament assembly for independent control of vaporization and ionization processes, wherein the sample is loaded on a vaporization filament are normally used. The formation of ions in TIMS is governed by the famous Saha Langmuir equation which gives the relationship of the ratio of ions to the neutrals in the vapor phase, N^+/N^o á $e^{(f-I)/kT}$ or N^-/N^o á $e^{(E.A-f)/kT}$ where f = work function of filament, I= 1st ionization potential of element or molecule being monitored, E.A = the electron affinity of the monitored negative ion, K= Boltzmann constant, T= temperature in Kelvin which can be anywhere from 1000^o to 2000^o depending on the I.P . The filament material used should be of high purity, refractory, high melting point and must have high work function when positive ions are monitored. Rhenium, tantalum, tungsten and platinum are some of the material used as filaments in TIMS. The isotopic ratios are obtained with a very high precision and accuracy due to the characteristic of the ion source which under the given conditions of analysis produces a steady beam of ions of the element of interest with high specificity. The background is therefore very low resulting in high precision in the isotopic ratios generated. As the ionization process can be suppressed due to presence of impurities, a purification step may be required. Since the ion beams have a low energy spread (~ 0.2 eV), a single-direction focusing magnetic sector analyser is sufficient to achieve high precision isotopic ratios. In addition, the multi-collector faraday cup detector assembly for simultaneous collection of all isotopes of the element, eliminates the effect of time dependent ion intensity drift on the precision of the isotopic ratios measured. In ICPMS the sample aerosol with analyte concentration at ppb/ppt levels is introduced into the high temperature Argon plasma at atmospheric pressure through a nebulizer to produce ions in the plasma region. This feature of ICP decomposes or dissociates the compounds introduced, to produce elemental ions, molecular ions or charged clusters. ICPMS differs from TIMS as it produces a wide spectrum of elemental ions present in the sample covering the periodic table with high efficiency. The efficiency is close to 100% for elements with ionization potential less than 7eV, whereas TIMS is more an element specific technique, making Q-ICPMS popular for elemental determinations and TIMS for element specific isotopic composition determination. Though ease of sample introduction, sensitivity and high sample throughput are the benefits, the limiting factor for high precision in isotopic analysis by ICPMS is the instability of the plasma, formation of isobaric molecular ions and sequential nature of quadrupole

analyzer. This has been largely overcome by combining the ICP ion source with magnetic sector analyzer and multi-collector (MC) detectors for simultaneous collection of ions, referred to as MC-ICPMS. The instrument can also be adapted for solid sample using Laser Ablation-ICPMS. The sample introduction mechanism also makes the technique suitable for coupling of separation techniques like liquid chromatography, ion chromography or capillary electrophoresis to ICP MS for elimination of isobaric and spectral interferences. The feature of high sensitivity and precision for small sample size (ng), makes MC-ICPMS a very useful tool in the area of nuclear forensics and environmental samples. Elements like Mo, Te, Sn, W, Hf, Fe which have high ionisation potential can be analyzed easily by ICPMS but need special loading techniques to be analyzed as positive ions by TIMS else they can be analyzed as an anionic oxide MO_x^- by Negative (N)TIMS. For ICPMS special glove box arrangement to accommodate the sample introduction system is required for analysis of radioactive samples due to the possibility of vapors contaminating the environment. In addition, molecular and elemental interferences from Ar_2^+, Ar_2^+, Xe^+ or element hydrides such as $^{238}UH^+$ etc. and memory effects of the previous sample effect the accuracy of isotopic ratios and have to be addressed. In TIMS, sample dried on the filament is heated in the confines of the evacuated ion source to produce gaseous ions making the instrument appropriate for radioactive samples. Today both TIMS and the high resolution MC-ICPMS are in the forefront of inorganic mass spectrometry for isotopic measurement requirements in various branches of science. This article will be focusing on the roles of MC-TIMS, MC-ICPMS and other mass spectrometric techniques in the nuclear industry for characterization of nuclear materials for their isotopic composition.

The magnetic sector analyzer

Most instruments used for precise determination of isotope ratios are of the magnetic sector type. This type of analyzer is superior to the quadrupole or TOF in this field of research for two reasons. (i) it can be set up for multiple-collector analysis for simultaneous collection of the separated isotopes and (ii) it gives high-quality flat topped peak shapes (Fig. 1).

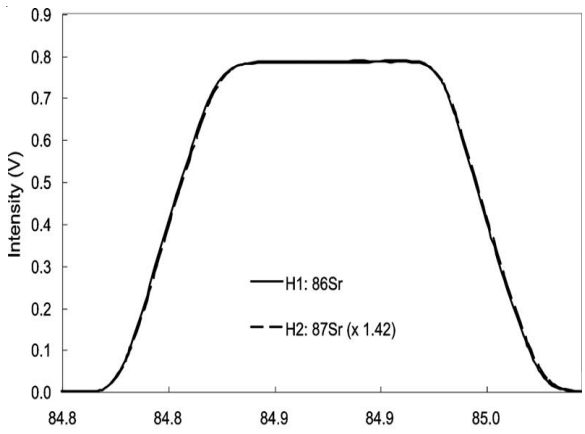

Fig.1. Mass scan showing optimum peak overlap of masses ^{86}Sr and ^{87}Sr.

This ensures that the entire ion beam produced in the source is incident on the detector and that small fluctuations in the position of the ion beam in the focal plane do not result in variations in the measured ion current intensity. Both of these considerations are important for obtaining high precision and accuracy in isotope-ratio analysis. Mono energetic ions formed

in the ion source are accelerated through a potential difference of 8 to 10 kV onto the entrance slit of a magnetic sector field analyzer where they are dispersed into discrete mass components by the field and focused on the focusing plane according to the equation:

$$m/z = r^2B^2/2V$$

where, ***r*** = radius traversed by a singly charged ion *(z=1)* of mass *(m of the isotope)* for constant values of electric potential (V) and magnetic field (B) (Fig. 2). The energy spread in the ions produced by ICPMS and SIMS requires high resolution double focusing action for decreasing the energy spread and resolving the interfering molecular and atomic ions. A typical HR-ICPMS has an electrostatic analyzer placed before/after the magnetic sector analyzer to compensate for the energy spread. Magnet shapes having oblique entry and exit at the pole provide axial focusing in addition to radial focusing, increasing the sensitivity and doubling the dispersion between two masses. The resolution, i.e. the ability of the instrument to separate two close masses given as M/”m is about 450 (at 10% valley between the two masses) which is sufficient for complete separation of U and Pu isotopes. The details of ion optics described elsewhere are beyond the scope of this article[1,2].

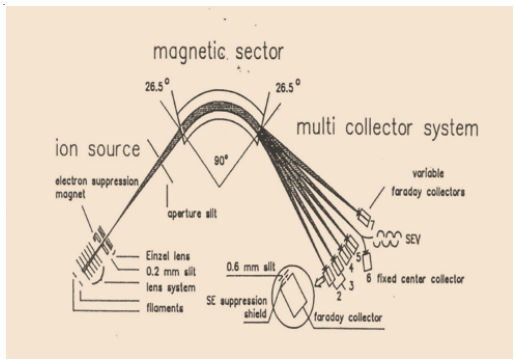

Fig. 2: Formation of ions, separation and detection in a typical MC isotope ratio mass spectrometer.

Ion collectors

The isotopic ions separated by the action of the radial magnetic field are measured by the detector positioned at the exit of the magnetic path (Fig. 2). The faraday cup detector is most suitable for high precision isotopic ratio measurement due to its excellent linearity, stability and reproducibility. The incoming ions are neutralized by electrons, generating a current across the high ohmic resistor of $10^{11}\,\Omega$. It also does not exhibit any mass discrimination effects and has nearly 100% efficiency in collecting ions. However, due to high baseline noise it is not sensitive for minor isotopes of < 0.01% abundance. The multi-collector configurations

exclusively used for high precision isotope ratio measurements (both TIMS and ICPMS) come with nine adjustable faraday cup detectors placed perpendicular to the optical axis of mass spectrometer at positions R"m/M, R is the radius of the sector magnet where ions of mass M are collected and "m the mass difference between ions of mass M from its neighbor. The faraday cup normally integrates the ions for 5 sec in one scan or as defined in the method. 36 to 60 scans are usually obtained for a single analysis. The baseline current is subtracted to obtain accurate ion currents for the isotopic ion. The strength of the integrated ion current produced depends on the abundance of the isotope. Most of the instruments come with an additional ion counting detector such as a secondary electron multiplier for higher sensitivity required for small ion currents ($< 10^{-14}$ A).

Fig. 3: Multicollector movable faraday cup arrays, and miniaturized ion counters identical in size to Faraday detectors mounted on the high mass side (for U on the left) and low mass side (for Pb extreme right).

In customized instruments, mixed array of FAR and multiple ion counters(MIC) for ion counting of minor isotopes are present (Fig. 3). The latest MIC setup has Compact Discrete Dynodes (CDD) instead of Channeltron type detectors with higher dynamic range and longer life similar to the discrete SEMs. In ion counters the measurement is through a secondary process (ions strike the conversion dynode to produce electrons- multiplied by subsequent dynodes) which would require additional calibration to be performed to determine the conversion gain ratio between the SEM to faraday cup. An additional mass bias is introduced in ion counting detectors due to the difference in the velocity of the isotopes striking the first dynode. Nearly ten orders of magnitude of isotope ratio can be covered with this arrangement of ion collection – (ion currents of 0.5 $x10^{-9}$ A giving 50V signal on Faraday to 1 C/sec ~ 10^{-19}A on SEM [3].

Determination of isotopic content, atomic weight and specific activity by TIMS and MC-ICPMS

The fundamental measurement of IRMS is isotopic ratios which is obtained from the ion intensity ratio ($^{m}I/^{n}I$) where ^{m}I and ^{n}I are the ion intensities in amperes of isotopes of mass m and n. The isotopic composition of the element is calculated from the measured isotopic ratio as shown below for natural Uranium.

^{234}U atomic fraction $=(^{234}I/^{238}I) / (^{234}I/^{238}I+^{235}I/^{238}I+1)$

^{235}U atomic fraction$=(^{235}I/^{238}I)/(^{234}I/^{238}I+^{235}I/^{238}I+1)$

^{238}U atomic fraction $= 1 / (^{234}I/^{238}I+^{235}I/^{238}I+1)$

where, $^{234}I/^{238}I$ and $^{235}I/^{238}I$ are the measured ion intensity ratios. Atomic Weight of the element is sum of relative atomic mass fractions of all isotopes $\Sigma A_F Wt_i$ and the Specific Activity of the element is the sum of fractional activities of all isotopes, $\Sigma A_F S_{pi}$ where $A_{F,}$ Wt and S_p are the atomic fraction, relative atomic mass and specific activity of isotope *i*.

The combination of thermal ionization, radial magnetic field for mass based separation of the monovalent ions and faraday cup for measurement of ion intensity, makes TIMS an important tool for accurate and precise determination of different nuclides in the nuclear fuel cycle. Precision better than 0.005% can be obtained for isotopic abundance ratios of 1 to 0.1. Ion source fractionation due to the higher evaporation rate of the lighter isotope can introduce a time dependent systematic error affecting the accuracy. This is addressed by a) analyzing an isotopic reference material with known isotopic ratios under similar condition and cup configuration to obtain the correction factors, i.e. external normalization [4]. The resistor biases and cup efficiencies of the faraday cup are determined in separate measurements. b)The internal normalization method for bias correction in the isotopic ratios is used when the element has two isotopes of invariant ratio for correction of the other variant isotopes, e.g. $^{86}Sr/^{88}Sr$ and $^{144}Nd/^{146}Nd$ are internal standards for the remaining isotope ratios of Sr and Nd respectively or the double spike method where isotopes of known ratio are added to the sample e.g $^{233}U/^{236}U$ of known ratio added to natural uranium for high accuracy and precision of 0.015% in determination of $^{235}U/^{238}U$ in natural U [5]. The fractionation factor per mass unit, β calculated using appropriate fractionation laws (linear, power or exponential) to the measured ratio of the standard, is used to correct the observed isotopic ratios from which absolute isotopic composition and atomic weights are calculated. The dynamic multi-collector mode, a new feature in the software where each ion beam is measured in all cups used for measurement of the isotopes, eliminates the small cup efficiency factor and resistor biases which affect the overall accuracy of the measurement. This along with zoom optics system using quadrupole lenses for perfect peak overlap during dynamic MC mode has further improved the obtainable accuracy and precision using internal normalization correction for elements such as Nd and Sr to 5-10 ppm (1σ) [6]. The latest configuration comes with virtual amplifier which rotates the connection between FAR cups and current amplifier so that effect of bias in the amplifier is nullified in static multi-collection mode [7]. c)Total evaporation (TE) where the data is acquired till the sample is completely exhausted can be performed without an isotope reference material with residual bias of +0.05% for $^{235}U/^{238}U$ ratio and precision of 0.02% [8]. Data obtained by TIMS and in the recent years by MC-ICPMS play a pivotal role in assigning atomic weights to elements accepted by IUPAC's Commission for atomic weights and isotope abundances (CAWIA) as the best value [9].

For measuring minor isotopes with very low abundances, ^{234}U (~ o.oo5%) or ^{230}Th (< 10 ppm), energy filters (Retarding potential quadrupole - RPQ) which lowers the abundance sensitivity, (AS) are provided (AS- a measure of peak tailing from one mass to a neighboring one due to scattering and collision of ions in the ion flight path, measured as contribution of peak at 238 to 237). This arrangement lowers the AS, from 2 ppm to 20ppb. Ion counting detectors are used for measuring these ions of relatively low abundances. The AS of 1.2×10^{-10} at ^{236}U from ^{238}U obtained in the state of art TIMS, made it possible to determine $^{236}U/^{238}U$ ratio of 10^{-8} using μg amounts of U on filament [10]. In the recently developed Modified TE(MTE) protocol developed for TIMS for high accuracies in uranium and plutonium isotope ratio measurement, baseline correction was carried out intermittently between blocks to offset inaccuracies in isotope ratios of minor isotopes caused by back ground and peak tailing from adjacent isotopes resulting in improved accuracies for $^{234}U/^{238}U$ (0.58% for ratio of 5×10^{-5}) and $^{236}U/^{238}U$ (22 % for 10^{-8}) [3]. The Faraday cups in *Triton plus* come with a combination of 10^{12} Ω and 10^{11} Ω feedback resistors for measuring minor isotopes alternatively with RPQ-SEM using MTE method. Due to the increased time requirements of MTE about 2.5 μg of U was required against much smaller requirements of 500 ng for U and 50-100 ng for Pu by TE method.

The sensitivity for TIMS is element dependent unlike in MC-ICPMS where the ion source sensitivities are high for most of the elements, though the ions reaching the detector maybe ~ 1% due to the nebulization and transmission process. The high ion yield of MC-ICPMS makes it possible to analyse samples in ng to pg range with precision comparable to TIMS. For TIMS under normal loading conditions the sample size required for actinides and lanthanides ranges from several ng to a μg for precision of 0.01%. Several loading techniques have been developed to enhance the ion yield and lower the amount of sample required. Ion yield efficiency could be increased from <0.1% to 10% for Plutonium using the resin bead in Re cavity source, possibly due to point source nature of resin bead and increase in surface area to volume ratio allowing the analysis of sub femtogram amount of Pu with precision of 0.1% using single SEM detector. Using the high efficiency cavity source(HEC) for Sr and Nd <1 ng amounts could be analyzed using MC faraday cups with precision of 0.01% [11]. Filament carburization and the micro Porous Ion Emitters(PIE) where the sample resin is dried on a porous alloy of Pt-Re have significantly increased ion yield for both U, Pu and lanthanides leading to analysis of pg size plutonium in environmental samples and for nuclear safeguards using MIC systems [12,13]. Presently Faraday cups with high resistance 10^{13} Ω amplifiers with reduced electronic noise and higher sensitivity are available for both TIMS and ICPMS. Analysis of <100 pg Nd and Sr samples with higher precision compared to ion counters was possible with these detectors[14].

In MC-ICPMS, the space charge effects in the source interface region favors the transmission of heavier isotope into the analyser which results in mass bias affecting the accuracy of the measured isotopic ratio. Since the bias is matrix dependant, complete purification of the analyte from matrix is required unless suitable matrix matched standards are available. The mass bias in ICPMS can be in parts per 100 and can vary with instrument settings, unlike in TIMS where the bias due to fractionation are nearly steady and much lower in parts per 1000 [15]. The mass bias in ICPMS is time independent as fresh solution at a constant flow rate (~0.1 mL/min) is being continuously fed to the plasma. The method of internal normalization using suitable mathematical models is applied to determine accurate isotopic ratios. It is not possible to utilize internal normalization methods for all elements either because the element has only two isotopes or the isotopes are all radiogenic. Alternatively the double spike method is also available for ICPMS. Though TE method cannot be applied in MC-ICPMS, the analyte element can be doped with an element with known isotopic composition having similar mass as internal standard provided it is free from isobars e.g $^{205}Tl/^{203}Tl$ for correcting mass bias in Pb isotopes. This is because the mass bias is independent of the element over a limited mass range for ICPMS. In the case of non-availability of any internal standard, the mass bias will have to be corrected externally, following the std-sample—blank (SSB) protocol called the bracketing method for minimizing the effect of plasma fluctuations on the mass bias with washing between samples for reducing memory effects. Internal normalization methods cannot be considered for irradiated samples as the natural compositions are altered therefore both TIMS and MC-ICPMS have to follow the external calibration method though the option of using TE is available for TIMS. Ion counter configuration similar to TIMS is available in MC-ICPMS with RPQ filters to remove the scattered ions in the vicinity of the high intensity ion beam leading to improved abundance sensitivity [1]. Analysis by MC-ICPMS requires separation of matrix to eliminate the effect of matrix on mass bias and to remove elemental and molecular isobaric interferences. Additionally appropriate sample introduction nebulizers such as micronebulizer with sample uptake of 0.1 mL/min with desolvators are used to suppress hydride and polyatomic ion formation [16]. Due to formation of molecular ions such as UH^+ the AS is poorer to TIMS by a factor of ten [17]. A recent study measuring the compatibility between GSMS, MC-TIMS and MC-ICPMS using certified reference material of uranium, the lowest uncertainty for $^{235}U/^{238}U$ ratio was observed for GSMS (0.02%) measured as UF_5^+ and highest for MC-ICPMS (0.05%). GSMS requires mg amounts of UF_6 with low throughput Vs nanogram amount of U required by TIMS and ICPMS. The minor isotopes measured only by TIMS and ICPMS gave lower uncertainties for TIMS [17]. Analysis of Thorium $^{230}Th/^{232}Th$ by TIMS requires special techniques to increase its sensitivity which is ~ 0.01% as against 0.5% for SIMS and MC-ICPMS. Ir sintered on 'V' shaped Re filament followed by addition of C and Th increased the sensitivity of Th to 0.1% requiring 50-100 ng Th for analyses. The precision obtained by the three methods was < 0.5% [18].

Solid state mass spectrometric techniques for nuclear material

Techniques like LA-ICPMS, SIMS allow direct

determination of isotopic ratios in solid samples, provided suitable matrix matched standards are available for interpretation of spectra and correction of matrix induced mass discrimination. LA-MC-ICPMS uses the ablation of sample material by a focused laser beam in an inert gas atmosphere (e.g., Ar or He) under normal pressure and transfers the ablated material into an inductively coupled plasma ion source of an ICPMS. In SIMS, solid sample surface is sputtered by bombardment with a focused primary ion beam (Ga^+, Cs^+, O_2^+ or O^-), the sputtered ions (secondary ions can be electrons, neutral species, atoms or molecules, or atomic and cluster ions) are separated by a mass spectrometer according to their mass-to-charge ratios. It is mainly used for surface mapping and depth profiling of elements or isotopic ratios. Elements such as N, O, H, P, Se, F which are difficult to analyze by other mass spectrometers can be determined by SIMS. The development of sector field instruments with multi-collector detectors has led to high precision comparable to TIMS in isotope ratio measurement of analyte present in solid matrix. These instruments are operated in high resolution mode (2,000 to 10,000) for separation of the isotope from isobaric interferences of molecular ions such as ^{238}UH ions at ^{239}Pu. The SIMS ion microprobe technique is capable of high spatial resolution of 0.5 to 1 μm, and permits the measurement of isotopic compositions of tiny samples or point analyses[19]. Due to its high depth resolution of less than 1 nm it has been used to obtain the radial isotopic profiles of U and Pu in irradiated pellet to validate the computer code developed to calculate the concentration of isotopes formed during irradiation as a function of radial position within the pellet [20]. Application of LA-ICP-MS which has detection limit in ng/gm level, is largely in the area of elemental and isotopic mapping of biological tissue, nuclear forensic and environmental samples e.g. isotopic analysis of radioactive micro particles was carried out for the rapid and sensitive determination of the ^{235}U/^{238}U, ^{236}U/^{238}U, ^{145}Nd/^{143}Nd, ^{146}Nd/^{143}Nd, ^{101}Ru/(^{99}Ru+^{99}Tc) and ^{102}Ru/(^{99}Ru+^{99}Tc) isotope ratios in the vicinity of Chernobyl [21]. In another example it was used to determine high ^{10}B (90% to 97%) content in steel used in nuclear reactors and in production of radioactive waste storage containers. Reprocessing of these materials may cause changes in the content of ^{10}B, determined using a femtosecond titanium-sapphire laser (795 nm) with a precision of 0.1 to 0.2%[22]

AMS and RIMS for determination of low abundance isotopes

Mass spectrometers capable of detecting very high dynamic range are required for analysis of isotopes with abundances less than 10^9. High isotopic abundance sensitivity to enable the measurement of low-abundant isotopes in the presence of neighboring high abundant ones, with complete removal of isobaric interference, is another very important requirement. AMS and RIMS are two mass spectrometric techniques with high selectivity for ultra trace isotopic analysis. AMS is widely accepted as the best method for the determination of long lived radio nuclides, such as ^{3}H, ^{10}Be, ^{14}C, ^{26}Al, ^{32}Si, ^{36}Cl, ^{41}Ca, ^{53}Mn, ^{59}Ni, ^{129}I, ^{182}Hf, ^{210}Pb and actinides present in nuclear waste which have both environmental waste disposal and nuclear forensic implications. The fundamental instrumentation of AMS consists of two mass spectrometers, the injector and analyzer interjected with a tandem accelerator. A typical configuration consists of a Cs sputter ion source, where negative ions are produced (fraction of negative ions is typically 1%). Since not all elements form negative ions, isobaric interferences are suppressed. The ion beam pre-accelerated to a maximum energy of 80 KeV goes through an ESA (electro static analyzer) for energy selection, the selected monoenergetic beam goes through injection magnetic analyzer for mass selection. The selected ions are accelerated through a stable +3MV tandem accelerator to a gas filled foil stripper where they lose electrons and gain positive charge and are again accelerated through the same potential and in the process gain energy of several MeV. The stripping process dissociates the molecular ions if any. The highly energetic ions are mass analyzed by the double focusing analyzer system for mass separation. These ions are then detected by suitable detector such as gas ionisation detector placed at the focusing point. The whole arrangement allows measurements of isotopic ratios as low as 10^{-15} (e.g. ^{236}U/^{238}U).

In RIMS the solid or liquid samples are vaporized and atomized by an atomic beam source (e.g. thermal vaporization from a hot Re filament or by evaporation of sample using an electron beam). One or more lasers are tuned precisely to the wavelength required for optical excitation of the atoms by resonant absorption of the laser light, realized in a step wise process, followed by ionization of the excited atoms by a resonant photon to obtain highly selective resonance ionization of the element of interest. RIMS offers a number of outstanding properties compared to other mass spectrometric techniques, such as nearly complete isobaric suppression, high overall sensitivity with detection limits in the 10^{-15} to 10^{-18} g range, enabled by the high ionization efficiency, high transmission mass spectrometers and low background ion detection with high abundance sensitivity and optical isotope selectivity. Both these methods are only suited for single element analysis, adaptation to a new element requires elaborate development and till recently no commercial support is available which has restricted their use only to limited laboratories worldwide [23].

Certified isotope reference materials

Relevant Isotope Reference Materials are required for validation of the technique used or a new method developed for isotope ratio determination of an element. In addition the isotopic ratios of all mass spectrometric techniques such as TIMS, ICPMS, SIMS are affected by mass fractionation / mass discrimination which results in a bias in the measured isotope ratio with respect to the true ratio. High purity, Isotope Reference Materials in which the ratios are certified within the specified uncertainties are required for correction of these effects. These reference materials are prepared and distributed by accredited international laboratories such as National Institute of Standards and Technology (NIST), Institute for Reference Materials and Measurements, and BAM, the Federal Institute for Materials Research and Testing, Germany. The correction factor K, is obtained from

the equation, $R_{true,i} = K_i * R_{obs,i}$. The mass discrimination factor per unit mass, â is used for correction of the different measured isotopic ratios of the element. Solid state mass spectrometric techniques like LA-ICPMS, SIMS require matrix matched IRM's for error free analysis [4].

Accurate measurement of isotopic ratios for IDMS

Isotope dilution mass spectrometry (IDMS) is the technique used for accurate and precise determination of the concentration of an element. In this technique a known amount of enriched isotope (often called as spike) of the element, which is absent or least abundant in the sample, is added to the known weight of sample, and the resulting change in isotope ratio is measured by mass spectrometric methods. In IDMS the limiting factor for accuracy and uncertainty in determination of concentration of the element is accuracy and precision in the determination of isotopic ratios in the sample, spike and the spike-sample mixture. Once proper mixing of sample and spike is achieved by chemical treatment to make a homogenous solution, quantitative separation of the analyte from matrix is not required. The combination of the IDMS procedure with TIMS for measuring the change in isotopic ratio makes the ID-TIMS (isotope dilution-TIMS) a very formidable technique due to the high precision and accuracy of better than 0.1% that can be achieved in elemental determination. The method has a large dynamic range $<10^{-15}$ making possible measurement even at femtogram levels [24]. The technique of IDMS is regarded as definitive method and used for certification of elemental concentration at National NIST and IRMM [24]. This method is used for determining the concentration of working standards of U and Pu and to certify the values determined by other techniques such as radiometric or electrochemical method.

Applications of isotope ratio MS is nuclear industry

i) Determination of fissile content, specific activity and important nuclides in nuclear materials

Due to the high precision and accuracy in isotope ratio measurement and small sample requirements of MC-TIMS and MC-ICPMS, they are used extensively in the nuclear fuel cycle for measuring stable as well as radioactive nuclides. TIMS is being used for certification of fissile and fertile content of oxide or metal based fuel materials of Pu, U, Th for several decades. The isobaric interference of ^{238}U in ^{238}Pu is difficult to eliminate in spite of chemical separation and is therefore determined by using alpha spectrometry. The isobaric interference from ^{241}Am at ^{241}Pu can be eliminated by an offline separation step using anion exchange resin. The differences in physico chemical behavior of two or more elements during analysis by TIMS may be used to eliminate isobaric interferences. e.g. The formation of UO^+ at lower ionization filament temperatures and absence of PuO^+ signal is used to obtain $^{235}U/^{238}U$ ratio as UO^+ ions. This information is fed in interfering element correction (IEC) module present in the method file of the software, to subtract the ^{238}U intensity from the total intensity of ($^{238}U+^{238}Pu$) and thereby obtain accurate $^{238}Pu/^{239}Pu$ ratio [25]. The IEC module is available in both TIMS and ICPMS and can be used when the interfering element is from a natural source e.g ^{87}Rb at ^{87}Sr using natural $^{85}Rb/^{87}Rb$ ratios. The corrected $^{86}Sr/^{87}Sr$ gives information on the origin of the mineral/rock. Differences in evaporation and ionization characteristics can be exploited for sequential analysis of two or more elements loaded on the same filament. The analysis is not affected by ion source fractionation if it is carried out at optimum filament temperature for the different elements. (Analysis of Zn and Cd or U and Pu from same filament)[25,26]. TIMS is used for determining the isotopic composition of neutron poisons like boron, gadolinium at procurement stage as well as during reactor operation where the change in isotopic composition of the neutron poison in moderator water is measured intermittently for validating theoretically predicted compositions. U enrichment plant facilities require regular inputs on the ^{235}U isotopic content of process streams. Gas source electron impact mass spectrometry is used continuously, with periodic inputs from TIMS which is used as a reference technique. Similarly enrichment plants of Boron, Lithium also require regular inputs from TIMS to determine the enrichment of ^{10}B or ^{6}Li isotopes at various stages. In the recent years MC-ICPMS is also used due to its high through put and sensitivity.

The molecular beam method using $Na_2BO_2^+$ monitoring ions for determination of $^{10}B/^{11}B$ by TIMS, was suitably modified to minimize the effect of sodium on the accuracy and precision of the isotopic ratios. This was done by adding mannitol and NaCl instead of Na_2CO_3 to the boron sample for formation of sodium borate [27]. $^{10}B/^{11}B$ ratio is determined in different matrices like boric anhydride, borates, carbides, boride alloys etc as $M_2BO_2^+$ (M-Na, Rb, Cs) by direct fusion of sample with alkali carbonate on the rhenium filament. For determination of isotopic ratio of lithium in lithium salts the sample is fused with boric acid for obtaining $Li_2BO_2^+$ and in refractory materials like $LiTiO_2$ sample is fused with sodium borate for formation of $NaLiBO_2^+$ in the ion source [28].

ID-TIMS is used to validate the fissile / fertile fuel and other metallic content in different fuels such as mixed oxide, metallic fuel such as U-Pu-Zr or U-Zr alloy, various candidates for chemical assay standards like $Rb_2U(SO_4)_3$, $K_4Pu(SO_4)_4$, or working standards of U, Pu, Th required for chemical quality control of fuels by electrochemical methods etc[29]. ID-TIMS methodology has been routinely used for the accurate determination of Pu in dissolver solution. This being the first stage of Pu determination, high accuracy is required as smallest of errors will affect the input inventory.

Appropriate spikes (enriched isotope) are used, ^{233}U for natural or enriched Uranium and Uranium standard NIST 950a for ^{233}U. Due to the scarcity of ^{242}Pu spike, high burn-up plutonium is used for spiking low burn up fuel and vice versa. In spite of small difference in the isotopic composition of two Pu samples, the accuracy in concentration is not compromised due to the high accuracy (0.01%) with which $^{240}Pu/^{239}Pu$ ratio in the sample-spike mixture is determined [30]. All analysis are preceded by offline purification of the element from bulk matrix and isobars.

Burn-up determination of different fuels (irradiated thoria, irradiated PHWR fuel, mixed oxide fuel of PHWR) using the fission product monitor technique is normally carried out by TIMS. For a typical UO_2 fuel, the burn-up is computed using the relationship $F_T = 100\,(P/Y)\,/(P/Y+U+Pu)$, P is atom concentration of fission product burn-up monitor, Y is its effective fission yield of the monitor and U & Pu are the atom concentrations of heavy nuclides after irradiation of the fuel. The method needs precise knowledge of concentration of the fission product ^{148}Nd, U and Pu in the sample aliquot, which is carried out by ID-TIMS using triple spike consisting of ^{142}Nd+^{242}Pu+^{233}U. The uncertainty of ~ 1% in ^{148}Nd fission yield is reflected in the calculated burn-up[31].

In the recent years online high-performance liquid chromatographic separation system coupled to a MC-ICP-MS to overcome isobaric interferences for the determination of the plutonium isotope composition and concentrations in irradiated nuclear fuels has been studied with the objective of simplifying sample preparation procedures [32]. For handling radioactive samples, parts of HPLC and sample introduction system of MC-ICPMS were placed in a glove box. About 400 ng of fuel was injected into the HPLC system and the isotope ratio measurements on the transient signals of Pu were performed in the static, low-resolution mode with an integration time of 1.049s per data point. The reproducibility of the Pu isotopic ratios ranged from 0.04 to 0.2%. The same group has studied the various applications of HPLC - MC-ICPMS and LA-MC-ICP-MS for the investigation of nuclear materials for burn-up and fission product analysis as well as the determination of actinide isotope ratios. The isotopic composition of Nd, U and Pu on the transient signals of the separated fractions were used for burn-up determination by IDMS with an uncertainty of ~ 3%. The isotopic composition of fissions products such Sr and Cs were also determined after online separation. LA-ICPMS was used to obtain the local distribution of isotopic ratios of U and Pu close to the fuel cladding interface. The isotopic composition of U and Pu as a function of distance from the clad was obtained using HPLC-ICPMS [32].

ii) Isotopic measurements for determination of fundamental nuclear parameters

Half-life of a radioactive nuclide can be determined using parent decay method for decay schemes with short half lives, daughter growth method for long half life nuclide and the specific activity method using a combination of counting techniques and IDMS.

Mass spectrometry has played a important role in determination of neutron capture cross sections by measuring the change in isotopic abundances of the nuclide, from the relation $N=N_o e^{-\sigma\varphi t}$, where ϕ neutron flux, σ neutron capture cross section, N number of nuclide remaining after time t. $^{10}B/^{11}B$ measurement can be used for determining the neutron flux in nuclear reactors. Mass spectrometry is also used for identifying and measuring the stable isotopes produced at the end of the fission chain and their absolute fission yields by IDMS since this could yield more accurate results than radiochemical methods [1].

Environmental fallout and Nuclear forensics

Besides the naturally occurring radionuclides, a large number of radionuclides have been produced and released to the environment by human nuclear activity, including nuclear weapons testing, operation of nuclear power plants, research reactors, and nuclear fuel reprocessing. For the radiation protection purpose, the level of these radionuclides in various environmental and biological samples needs to be determined. The radionuclides released from the reprocessing plants can also be used as environmental tracer for the investigation of transport of water mass (^{134,137}Cs, ^{99}Tc, ^{129}I) and atmospheric circulation (^{129}I). In decommissioning of nuclear facilities and repository of nuclear waste, inventory of radioactivity or concentration of various radionuclides in the waste samples need to be determined. For nuclear forensic applications sensitive, precise and accurate information on the isotopic content of actinides and various fission products is required in addition to physical parameters, structure, analyte and impurity content, age since the last purification etc. E.g. $^{234}U/^{230}Th$ ratio is an indicator of the time elapsed since purification. The isotopic composition of fission product can give information on the burn-up, the IC of Pu and U on the source of the material etc. It is recognized that ^{236}U along with Pu IC are important signatures to differentiate the source of contamination. This requires techniques with both high sensitivity and abundance sensitivity. MC-ICPMS, MC-TIMS, solid state mass spectrometric techniques, and sensitive techniques such as AMS and RIMS are often being used in the area of nuclear forensics. The sensitivity and reliability of MC-ICPMS for environmental samples was further increased by using 'Jet Interface', which comprises of a high capacity interface pump, Jet sampler cone and X-skimmer cone with high efficiency desolvating sample introduction for production of dry aerosol (DSN-AridusII) for high sensitivity of 1.5% to 2.5%. CIRM was used for measuring peak tail and hydride ion contributions at m±1,m±2 peaks. Prior to analysis by MS, samples were purified and monitored for complete removal of heavy ions for elimination of polyatomic interferences. Using just 0.4 to 0.5 ng U uncertainty of < 0.2% for $^{235}U/^{238}U$ over a wide ratio and 1% for minor isotopes was obtained[33]. Similarly there is a continuing impetus for improvement in sensitivity of TIMS. A recent review has described modified filament techniques for analysis of fg amounts of U, Pu, Am, Nd, Sr, Cs by TIMS [34].

Conclusions

Though MC-ICPMS is a sensitive technique with high throughput, better internal precision and small sample size requirements (CIRM run for mass bias measurements are normally 2.5 pg/mL using MIC detection), the analytical performance depends on the stability of the instrument for unvarying mass bias. The instrument bias is monitored by the SSB protocol with sufficient rinsing between samples to erase memory effects. The dependency of mass bias on the matrix requires separation of analyte from matrix. Mass spectrometric methods for direct analysis of solids such as LA-ICPMS require matrix matched isotope reference materials. The formation of polyatomic ions and hydrides

due to heavy metals in nuclear waste solutions can cause isobaric interferences in the determination of U/Pu Isotopic composition which can be eliminated to some extent by separation. The hydride of the major isotope can also cause interference at mass of minor isotope. Though operation of the instrument with high resolution can be an option, the loss of sensitivity cannot be afforded when minor isotopes have to be accounted. Desolvating nebulizers are used for formation of dry plasma which restricts the formation of oxides and hydrides. MH^+/M ratio obtained from analysis of CIRM are used for correction of such interferences in samples. In the case of TIMS the relatively small mass bias caused by fractionation can be regulated by following analysis protocols and using isotope references for correction. Accuracy of TIMS measurement is not affected by any such polyatomic or hydride interferences and techniques such as TE/MTE with low uncertainties accompanying the measurements can give absolute isotopic abundances.

Acknowledgments

I would like to thank Dr.S.K.Kannan, Head FCD and Dr.B.S. Tomar, Director RC&I Group for their interest and constant encouragement and Dr. P.G. Jaison and Mr. M.K.Saxena for critically reading the manuscript.

References

1. Applications of Inorganic Mass Spectrometry, John R. de Laeter
2. Modern Isotope Ratio Mass Spectrometry, I. T. Platzner
3. Bürger, S., S. D. Balsley, S. Baumann, J. Berger, S. F. Boulyga, J. A. Cunningham, S. Kappel, A. Koepf, and J. Poths, *International Journal of Mass Spectrometry* **311** (2012) 40.
4. Vogl, Jochen, and Wolfgang Pritzkow. *Journal of Analytical Atomic Spectrometry* **25** (2010) 923.
5. S. Richter , R. Eykens , H. Kühn , Y. Aregbe, A. Verbruggen , S. Weyerb, *International Journal of Mass Spectrometry* **295** (2010) 94.
6. Triton Application flash report No. T-4
7. Triton Application Note-30136
8. R.Fiedler, *International Journal of Mass Spectrometry* **146** (1995) 91.
9. Michael E. Wieser and Michael Berglund, *Atomic weights of the elements 2007, Pure Appl. Chem.,* **81** (2009) 2131–2156.
10. S. Richter, A. Alonso, W. De Bolle, R. Wellum, P.D.P. Taylor, *International Journal of Mass Spectrometry* 193 (1999) 9–14
11. Bürger, S., L. R. Riciputi, S. Turgeon, D. Bostick, E. McBay, and M. Lavelle, *Journal of Alloys and Compounds* **444** (2007) 660.
12. Rozle Jakopic, Stephan Richter, Heinz Keuhn and YetundeAregbe, *J. Anal. At. Spectrom.*, **25** (2010) 815.
13. James E. Delmore, *INL/EXT* **10** (2010) 19773.
14. J.M.Koornneef, C.Bouman, J.B.Schwieters, G.R.Davies, *Analytica Chimica Acta* **819** (2014) 49.
15. Thomas Walczyk, *Anal BioanalChem* **378** (2004) 229.
16. J. S. Becker, *Spectrochimica Acta Part B* **58** (2003) 1757.
17. O. Pereira de Oliveira Junior,W. De Bolle, A. Alonso, S. Richter, R. Wellum, E. Ponzevera, J.E.S. Sarkis, R. Kessel, *International Journal of Mass Spectrometry* **291** (2010)48.
18. K.H.Rubin, *Chemical Geology* **175** (2001)723.
19. Maria Betti, *International Journal of Mass Spectrometry* **242** (2005) 169.
20. L. Desgranges, B.Pasquet, Ch. Valot, I. Roure, *J. of Nuclear Materials* **385** (2009) 99.
21. Sergei F. Boulyga, Thomas Prohaska, *Anal Bioanal Chem* **390** (2008) 531.
22. C. Kurta, L. Dorta, F. Mittermayr, K. Prattes, B. Hattendorf, D. Guntherb and W. Goessler, *J. Anal. At. Spectrom*. **29** (2014) 185.
23. Xiao lin Hou, Per Roos, *Analytica Chimica* Acta **608** (2008) 105.
24. K. G. Heumann, *International Journal of Mass Spectrometry and Ion Proc*. **118** (1992) 575.
25. S.K.Aggarwal, *Anal. Methods* **8**(2016) 942.
26. A. S. Ayoub, Brian A. McGaw, A. J. Midwood, *Talanta* 57 (2002) 405.
27. R. M.Rao, A. R. Parab, K. Sasibhushan, and S. K. Aggarwal, *International Journal of Mass Spectrometry* **273** (2008) 105.
28. R. M. Rao, A.R. Parab, Jagadish Kumar, Raju Shah, K. SasiBhushan, D.Alamelu and S.K. Aggarwal, (NUCAR 2015) Paper No. E35, p.371-72.
29. K.L.Ramakumar, M.KSaxena, V.A. Raman, V.L.Sant, V.D. Kavimandan, B.P.Datta and H.C.Jain, *J. Radioanal. Nucl. Chem.,***158** (1992) 158.
30. S.K.Aggarwal, R.K.Duggal, R.Rao and H.C.Jain, *International Journal of Mass Spectrom. Ion Process*, **71** (1986) 221.
31. S.K.Aggarwal, P.G.Jaison, A.R.Parab, BARC/2011/E/012
32. Ines Günther Leopold,NikoKivel, Judith KoblerWaldis& Beat Wernli, *Anal Bioanal Chem* **390** (2008) 503.
33. S.F.Boulyga, A. Koepf, S. Konegger-Kappel, Z. Macsik and G. Stadelmann, *J. Anal. At. Spectrom.,* **31** (2016) 2272.
34. S. Burger, L.R. Riciputi, D.A. Bostick, S. Turgeon, E.H. McBay, M. Lavelle, *Int. J. of Mass Spectrom.,* **286** (2009) 70.

Dr. Ms. Radhika M Rao has been working in the field of inorganic mass spectrometry in particular Thermal Ionisation Mass Spectrometry over a career spanning more than thirty years. She has been associated with providing quality assurance for fissile content of fuel materials and isotopic content of elements of consequence in nuclear materials for various department of DAE. She has contributed substantially towards development of methods for precise and accurate analysis of light elements such as boron and lithium in various nuclear materials. She is the recipient of DAE, Special Contribution Award(2015) for her contribution in the field of Nuclear Science and Technology.

Laser Mass Spectrometry: Nuclear Applications

M. Joseph*, P. Manoravi, N. Sivakumar

Fuel Chemistry group, Indira Gandhi Centre for Atomic Research (IGCAR)
Kalpakkam – 603 102.
Email*: mj@igcar.gov.in

Introduction

Laser coupled with mass spectrometer finds many applications in various fields. Many of these applications are analytical [1]. Because, pulsed lasers suits to time-of-flight mass spectrometers (TOFMS), that essentially use a pulsed source of ions, a large part of the Laser-Mass Spectrometry (LMS) work uses this mass analyzer. In LMS, the laser pulse is generally used for ionization in a gas phase or desorption and ionization from a surface of a thin film or a slurry (matrix) or for vaporization from a solid phase. When the laser is used for gas phase ionization, the process can be mutliphoton ionization or resonance ionization. Desorption & ionization is used generally in the MALDI (matrix assisted laser desorption and ionization) mode, both for organic and inorganic applications. In some LMS studies, laser is used to generate vapor species from solid samples by transient heating to high temperatures and the vapor thus formed is mass analyzed using a suitable mass analyzer. In this article, we will briefly discuss some of the laser-mass spectrometric techniques that are used in nuclear applications.

Nuclear Applications of L-MS

Burn-up determination: As indicated above, since coupling of laser to TOFMS is advantageous, a home- built refletron time-of-flight mass spectrometer (RTOFMS), in a horizontal geometry is coupled to a laser [2]. This RTOFMS was built with the intention of using it as an analytical tool and one of the main objectives was to develop a direct method for the determination of burn-up of an irradiated pellet, so as to dispense with labor-intensive separation procedures being used in conventional methods [3]. Conventional wet chemical methods of determination of burn-up involve very elaborate and time consuming procedures, namely, separation of uranium, plutonium and the rare earths (RE) group fractions, followed by separation of Nd (fission monitor) from RE fission products. Subsequently, isotope dilution studies using Thermal Ionization Mass Spectrometry (TIMS) are used for the determination of the above separated elements [3,4]. Earlier we had reported [5] the use of high performance liquid chromatography (HPLC) for the rapid separation of lighter rare earths, which are potential burn-up monitors. However, this method needs separation of rare earths group from the dissolved fuel solution prior to injection into HPLC columns. Also this method generates more liquid waste. Hence, development of a direct method of determination of burn-up of an irradiated pellet is desirable. Quantitative estimation using laser vaporization/ionization based on the absolute intensities of ions would be difficult for solid samples, as there will be pulse to pulse fluctuations in the laser pulse energy and the sample surface morphology can be different [6]. Though actual partial pressures will be also different, the difference in ionization potential makes it more pronounced for ions. Hence, it would be preferable to use laser for vaporization followed by a suitable ionization method, such as ICP or electron impact ionization. This will make the instrumentation more cumbersome, particularly to handle soild radioactive samples [7]. Other possibility is to use the relative ion signal intensities rather than absolute intensities. The difference in the signal intensities that arise pulse to pulse due to changing surface morphology seem to be reduced by the use of thin films prepared from small volumes of sample solutions that are dried under an infrared lamp. Drying the solution to a solid film has other important advantages, namely: (i) one needs to use a small volume (~ 10 μL) of the dissolved fuel solution as opposed to use of the sample pellet thereby reducing the level of radioactivity to be handled significantly and (ii) one can easily perform isotope dilution (as in TIMS) or addition of internal standards, to ensure desired accuracy.

Schematic of the LMS facility developed in our laboratory is shown in Fig.1. The experimental details can be seen elsewhere [8]. Briefly, a Q-switched Nd:YAG laser of 8 ns pulse duration and mostly TEM_{00} mode was used. The repetition rate was 10 Hz. A home-built reflectron time-of-flight mass spectrometer (RTOFMS), of Mamyrin type [9], was used for mass analysis of the ions produced from the laser heated sample surface. A quartz lens with a focal length of 25 cm was used for focusing the laser beam and the target was positioned after the focus. The power density incident on the sample surface was varied by changing the distance from lens to the sample surface. Either a micro channel plate (MCP) or a fast rise time (< 5 ns) secondary electron multiplier was used as the detector. The signal from the detector was amplified by a fast pre-amplifier and fed to a digital storage oscilloscope. The DSO was triggered by a photodiode illuminated by a stray reflection of the laser beam. The mass spectrum was obtained by sum averaging the signal for 1000 laser shots. The thin film made through drying a few microliter of the sample solution on a metallic plate (steel, platinum, tungsten etc.), was used. A base pressure below $1x10^{-6}$ Torr was maintained by a turbo molecular pump (1000 l/s), in the vacuum chamber containing the sample and the mass spectrometer. The typical mass resolution of our instrument is about 1000, as determined using laser ionization of I_2 in the gas phase, comparable to any commercial instrument [2,8]. We have used RTOFMS to study solid and liquid samples containing UO_2 doped with lighter rare earths, namely, La, Ce, Sm, and Nd as possible burn-up monitors.

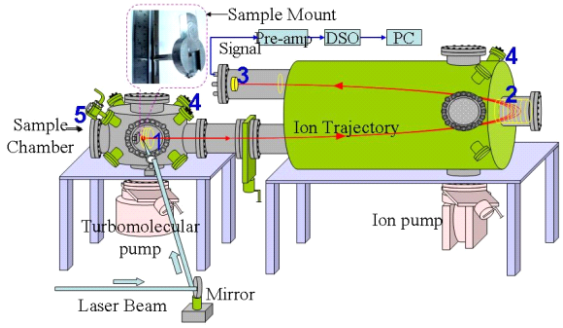

Fig.1. Schematic of Laser- ROTF-MS in horizontal configuration. (1)Ion Extn. & Focus lens; (2) Ion Reflection lens; (3) MCP Ion detector; (4)High Voltage Electrical feedthroughs; (5) Gas inlet leak valve.

Fig. 2 shows a typical mass spectrum of a film prepared from a sample solution containing La, Ce, Nd, Sm and UO_2 with added TBP and methanol [8]. The composition of the sample in terms of number of atoms present in 10 mL of the solution is: U=1.06e19; Nd=4.6e17; Sm=4.97e17;La=2.99e17; Ce=2.93e17. Even though the sample loaded on the metal plate is large, the amount of sample removed per laser pulse will be very low (of the order of nanomoles or less). As can be seen from this figure, all isotopes of the lighter rare earths are well resolved. Keeping in view of the possible burn-up monitors (^{143}Nd, ^{146}Nd and ^{139}La) of natural U and Pu mixed oxide fuel in the fast breeder reactor (FBR), the variation of ion signal intensities for these isotopes and that of UO_2^+ with the number of laser pulses that were incident on the sample film was studied. The signal intensities decrease by a factor of two within 10,000 laser pulses. Rastering of the sample may provide more steady intensities [10], but in the present experiments this feature was not available. Even though, the absolute intensities are reduced by a large factor, the ratio of intensities of RE elements to that of UO_2 remains nearly constant.

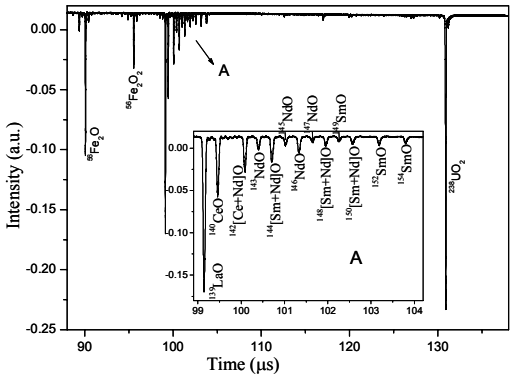

Fig.2. Typical mass spectrum of U, La, Ce, Nd and Sm in TBP/methanol mixture [8].

Using the ratio of the signal intensity of the rare earth oxide ion to that of the heavy elements, the burn-up can be determined as indicated below. Let the fractional fission yield of a selected burn-up monitor (say ^{143}Nd) for the given fuel be Z; and H the total number of residual heavy atoms. The ratio of number of atoms of H to that of number of atoms of ^{143}Nd be K, then the at % fission) = 100/{(K*Z)+1}. For this method of burn-up determination, an error of about ±10% in the intensity ratio would give a corresponding estimated error of ±1 at % burn-up, for a 10 at % fission fuel solution. In this work, only ^{238}U is taken for H as the instrument is not made active yet to handle Pu. The results indicated that this method has potential for direct determination of burn-up of irradiated nuclear fuel solution[8].

Determination of ^{10}B/^{11}B ratio in irradiated boron carbide (B_4C) pellets from control rod

Another RTOFMS in vertical geometry was developed, as this geometry would enable easy sample handling, particularly convenient for large size radioactive samples. This RTOFMS is housed inside a glove box, with the main objective of analyzing the boron isotopic ratio ^{10}B/^{11}B present in the irradiated B_4C pellets of the FBTR control rods. Stack of nine B_4C pellets (39 mm dia and 40 mm length), 90% enriched in ^{10}B contained in stainless steel clad is used as control rod in FBTR. ^{10}B present in these B_4C pellets is burned out to only a small extent, as the rod is kept out of active core level for considerable part of its life in a reactor (life of control rod is determined by the SS clad stability in a radioactive environment) and the maximum burn-up of ^{10}B occurs only in the lower part of the rod. To decide if the pellets from such an irradiated stack can be reused or relocated, one needs to know the ^{10}B/^{11}B ratio present in such irradiated pellets. The accuracy needed for such isotope measurements is about ± 1%. Though neutron irradiated B_4C is not expected to be radioactive, the common trace impurities such as Fe and Eu present in the B_4C pellet can lead to considerable levels of radioactivity. Hence, the method used for the ^{10}B/^{11}B ratio measurements on irradiated B_4C pellets needs to be amenable for remote operation. Furthermore, B_4C is one of the hardest materials known, next to diamond and cubic boron nitride. Any destructive method to analyze isotope ratio of B in B_4C is cumbersome. Hence, a non-destructive method is preferred not only to avoid the difficult dissolution or powdering process, but also because the pellet taken for analysis can be reused, as it is, after the measurement. One such method is laser mass spectrometry (LMS). In LMS, the laser vaporization removes only a few nanograms of the material from the laser-irradiated spot of the surface, without any physical damage to the pellet.

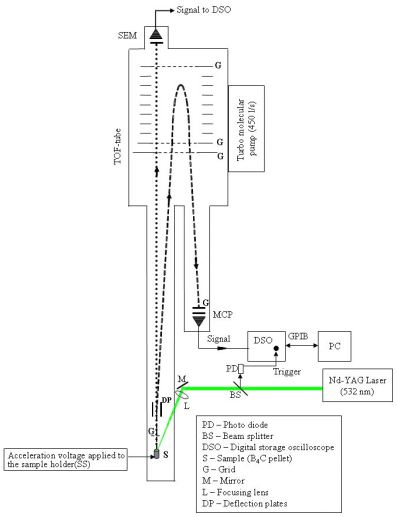

Fig. 3. Schematic of Laser-RTOF-MS in vertical configuration[11]

The experimental layout of vertical geometry RTOFMS is shown in Fig. 3. and the photograph of the same is shown in Fig. 4. The laser used here is common with the horizontal geometry RTOFMS. This vertical system mainly has two additional components (compared to the horizontal unit), namely, remote sample loading and unloading mechanisms, and the sample holding bellow assembly along with X,Y translation stage. Both these are placed inside a glove box. The drift tube, ion mirror region, and detector chambers have slightly different design compared to the one in the horizontal geometry. The sample holding cup (to hold 40mm dia and 40 long B_4C pellets) is made of SS and housed in a Teflon outer cup. Typical mass spectrum obtained for the analysis of B_4C pellets are shown in Fig. 5. The summary of analysis of different pellets taken from different positions in the control rod is given in Fig. 6. The radial distribution of $^{10}B/^{11}B$ ratio in the irradiated B_4C pellets is also measured by scanning the positions of sample and the data are collected at intervals of ~ 2mm and the sampled spot (focused laser) dia is about 0.5mm. More intense ^{7}Li peak is observed at the periphery of the pellet compared to the inner surface area.

Fig.4. Photograph of Laser- ROTF-MS in vertical configuration [12]

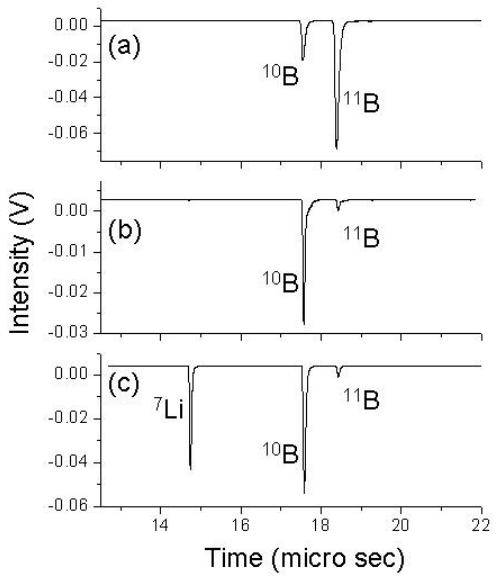

Fig.5. Mass spectra obtained for three different samples of B_4C pellets; (a) natural B_4C; (b) 90% ^{10}B enriched control rod B_4C pellet - unirradiated, (c)- irradiated control rod B_4C pellet [12]

Similar kind of isotopic ratio measurements were done for isotopes of Li from Li_2CO_3 sample, using both picosecond and nanosecond pulse lasers. The results shows marginally better data with picosecond laser compared to nanosecond laser [13].

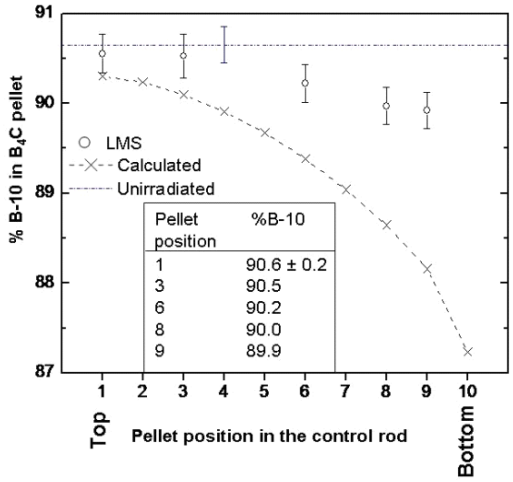

Fig. 6. Measured % ^{10}B in comparison with calculated values (insert indicates the measured values [12]

MALDI type analysis: The experimental facility indicated in Fig 1 is also used for the identification of organic molecules, which are encountered in nuclear applications. For instance, molecular ion of a low vapor pressure compound, 2,6-prydine dicarboxamide dihydrazone was identified from its synthetic mixture (Fig. 7). This compound is a precursor for the synthesis of resin to be used in the minor actinide recovery studies. Similar analyses were done for identification of ionic liquids which are being used in our laboratory for the recovery of noble metals from nuclear waste solution. MALDI type measurements are carried out towards identification of species that are formed on irradiation of extractants such as TBP and TiAP and a typical result obtained with TiAP is shown in Fig 8 [14].

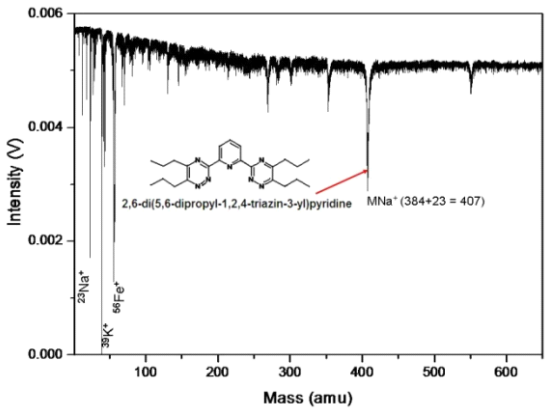

Fig.7. MALDI type mass spectrum of a pyridine derivative obtained using in-house developed LMS facility.

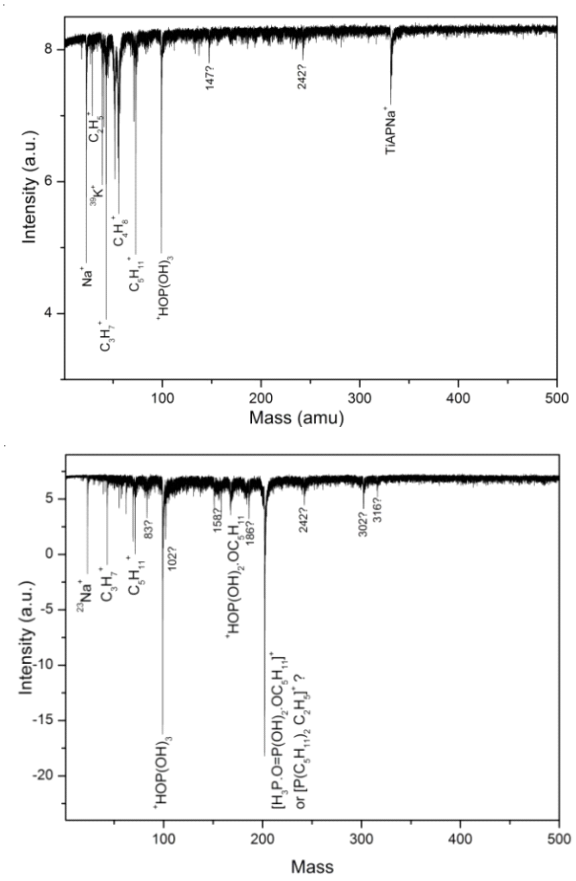

Fig. 8. MALDI type mass spectrum obtained for (a) uniiradiated and (b) g- irradiated TiAP[14].

Failed fuel detection: In a fast reactor, the failed fuel detection and location (FFDL) is very important. In the FFDL technique, fuel pins of each subassembly are tagged with different isotopic ratios of Kr and Xe (Kr and Xe have 6 and 9 stable isotopes, respectively). When a fuel pin of a particular subassembly happen to fail, the Kr & Xe gas come out of the pin and mix in the cover gas. By analyzing the cover gas for the value of isotopes of Xe and of Kr isotopic ratio will indicate the location of the subassembly where the fuel pin has failed. In principle, this can be done for each fuel pin as well. The isotopic ratio measurement of Xe and Kr is done by using Laser-RTOF-MS using resonance ionization. The practical applicability of this technique is demonstrated in JOYO experimental fast reactor in Japan [15].

PLD-TIMS

As indicated in the introduction part, one of the methods for the analysis of solid samples is to generate vapor from the sample by laser ablation (LA) and subsequently analyze by ICP-MS. This technique is generally called LA-ICPMS. Such commercial instruments are finding potential applications in nuclear industry, particularly in identifying spatial profile of different elements across given irradiated fuel pellet or clad materials [7].

Similar analytical information can be generated using PLD-TIMS (Pulsed Laser Deposition coupled with Thermal Ionization), in which thin films of the solid material at different spatial locations can be deposited as a thin film (even at 10^{-2} Torr vacuum, which is advantageous when adopted for hot cell applications) and the film thus obtained can be subjected to TIMS analysis. A typical result on a simulated irradiated UO_2 pellet is shown in Fig. 9 [16].

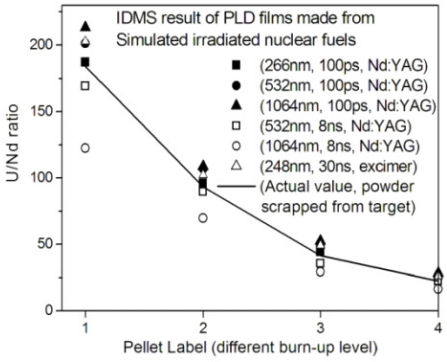

Fig. 9 U/Nd atom ratios obtained from TIMS measurements for pellets with varying elemental composition of U & Nd are compared with those for the corresponding PLD films [16].

Vapor pressure measurements of nuclear fuel materials at Ultra high temperatures

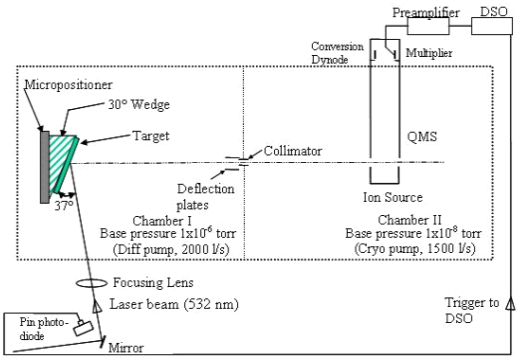

Fig.10a. Schematic of the laser induced vapourisation mass spectrometric (LIVMS) facility [17].

Earlier we have developed a laser induced vaporization mass spectrometry (LIV-MS) facility to study the vaporization behavior of nuclear fuel materials[17]. This was done mainly to obtain the vapor pressure of the nuclear fuel materials at ultra high temperatures (3000-6000 K), a key input parameter for hypothetical core disruptive accident analysis. The schematic of this LIV-MS experimental facility is shown in Fig. 10a and the overall experimental facility (LIV-MS along with RTOFMS, as indicated in Fig 1) is shown in photograph (Fig 10b). As can be seen from the schematic of LIV-MS, the mass analysis is done by ionizing the vapor using an electron impact ionization and subsequent detection by a quadrupole mass spectrometer. Results of such studies are summarized in earlier reports [18] and the vapor pressure data obtained is shown in Fig. 11.

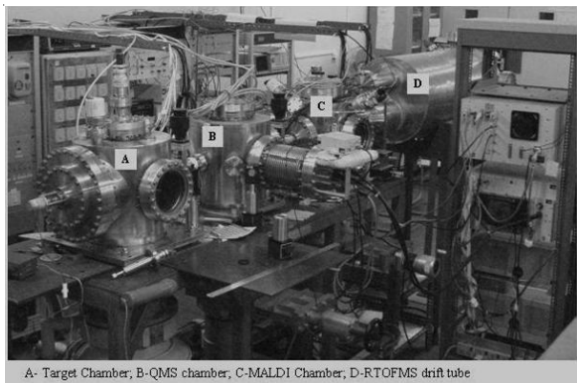

Fig.10b. Photograph of the in-house developed LIVMS facility.

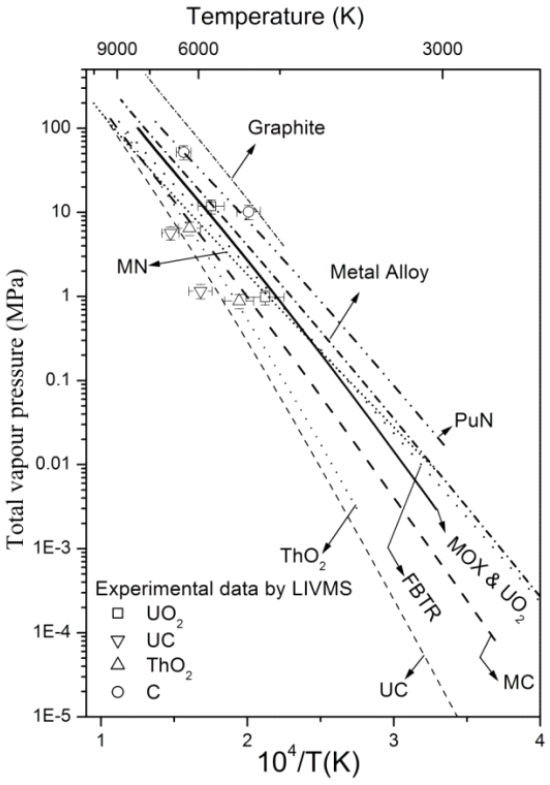

Fig. 11. Vapor pressure for different nuclear materials in their liquid region (line graphs are obtained by principal of corresponding method [18].

Conclusion

Laser mass spectrometric technique finds various applications in nuclear energy research. In this article some of such applications are discussed, with more details on the developments from the authors' laboratory at IGCAR.

References

1. D.M. Lubman (Ed.), Lasers and Mass Spectrometry, Oxford University, New York (1990).
2. N.Sivakumar, M. Joseph, P. Manoravi, R. Parthasarathy, C. K. Mathews, IGCAR report, IGC-183 (1996).
3. Standard Test Method for Atom Percent Fission in uranium and plutonium fuel (Neodymium-148 method) Designation E 321-96 Annual Book of ASTM standards, 12.02, 1996.
4. Saha B, Bagyalakshmi R, Periaswami G, Kavimandan VD, Chitambar SA, Jain HC, Mathews CK (1977) BARC Report-891.
5. M. Joseph, D. Karunasagar, B. Saha, IGCAR report, IGC-184 (1996)
6. M. Joseph, N. Sivakumar, P.Manoravi, R. Balasubramanian, Rapid Commun. Mass Spectrom. **18** (2004) 231.
7. Y.K. Ha , S.H. Han, H.G. Kim, W. H. Kim, K. Y. Jee, Nuclear Engineering and Technology, **40** (2008) 311.
8. M. Joseph, N. Sivakumar, P.Manoravi, R. Balasubramanian, Int. J. Mass Spect. **253** (2006) 98.
9. B. A. Mamyrin, V. I. Karataev, D. V. Shmikk, V .A. Zagulin, Sov. Phys., JETP, **37** (1973) 45.
10. M. Joseph, N. Sivakumar, P. Manoravi, Int. J. Mass and Ion Process, **176** (1998) 237.
11. P. Manoravi, M. Joseph, N. Sivakumar, Int. J. Mass Spect. **276** (2008) 9–16.
12. P. Manoravi, M. Joseph, N. Sivakumar, P.R. Vasudeva Rao, Int. J. Mass Spect. **309** (2012) 148.
13. P. Manoravi, M. Joseph, N. Sivakumar, R.Sajimol, Int. J Mass Spec. **367** (2014) 16.
14. B. Sreenivasulu, A. Suresh, S. Rajeswari, N. Ramanathan, M.P.Antony, N. Sivaraman, M.Joseph, Radiochimica Acta. (in press).
15. Y Iwata, H Harano, C Ito, T Aoyama, Applications of Nuclear Techniques, AIP Conf. Proc. 1412, 295-302 (2011); doi: 10.1063/1.3665327 and references there in.
16. R. Sajimol, P. Manoravi, S. Bera, M. Joseph, Int. J Mass Spec, **387** (2015) 51.
17. M. Joseph, N.Sivakumar, P.Manoravi, High Temp. – High Press **34** (2002) 411.
18. M. Joseph, N.Sivakumar, P.Manoravi, Annals of Nuclear Energy **31** (2004) 1163.

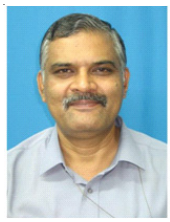

Dr. M. Joseph is currently Associate Director, Fuel Chemistry Group, IGCAR, Kalpakkam. He joined 26th batch of BARC training School and received the Homi Bhabha award. He was a guest Scientist at the National Institute of Standards and Technology during 1988-90 and 1997-98. He was a JSPS fellow at Osaka University during 1998-2000. His area of interest includes laser ablation, vapour pressure measurements of high temperature materials, pulsed laser deposition of thin films, laser-mass spectrometry, ion mobility spectrometry, thermal ionization mass spectrometry, high performance liquid chromatography and equation of state. He received the Science and Technology award of DAE in the year 2006 and Group achievement award in 2013.

Dr P.Manoravi is a Scientific officer, G, working in the Post Irradiation Studies Section of Fuel Chemistry Division of IGCAR, Kalpakam. He joined IGCAR in 1995. Prior to this he was a lecturer in Anna University, Chennai. He was a Swiss National Science Fellow, worked in University of Zurich, Switzerland during 1998-99. His area of specialization is laser-material interaction, mass spectrometry, ion mobility spectrometry, ICP-MS, design of instruments for radioactive sample analysis. He has received the Group achievement award of DAE in the year in 2013.

Dr. N.Sivakumar is currently the Program leader, Mass Spectrometry Studies Section, Fuel Chemsitry Group, IGCAR, Kalpaakm. He was a Post Doctoral research associate at University of Pittsburg during 1986-88 and Visiting fellow at Max-Planck Institut für Festkörperforschung, Stuttgart during 2000-01. His area of interest includes Chemical reaction dynamics (photo dissociation of small molecules, vibrational predissociation of vanderWalls molecules, real time measurement of ultra fast processes, Laser Spectroscopy, Laser-Mass Spectrometry, Ion mobility spectrometry and Pulsed laser deposition of thin films. He has received the Group achievement award of DAE in the year in 2013.

Applications of Mass Spectrometry in Thermodynamic Studies

T. S. Lakshmi Narasimhan

Fuel Chemistry Division, FChG, MC and MFCG, IGCAR, Kalpakkam

Email : tslak@igcar.gov.in

Introduction

Many of the modern technologies are based on the processes that take place primarily at high temperatures. The devices and materials used at high temperatures are constantly under hostile chemical environments. Many of the chemical processes like corrosion, diffusion which are usually not so important at ordinary temperatures become the limiting factors for these materials at high temperatures. A knowledge of mode of vaporisation would be very useful in predicting many of the chemical reactions that occur at high temperatures like those in metallurgical processes, nuclear reactors etc. The study of these evaporation processes helps in understanding the nature and composition of vapour phase, and predicting the nature of phase equilibria that exist between the vapour and the condensed phase. This calls for the generation of thermodynamic data corresponding to both condensed and vapor phases for as many substances as possible. Apart from thermodynamic data of gaseous and condensed phases, the determination of rate of vaporisation enables one to obtain kinetics of vaporisation and condensation processes and also insight to bonding in molecules. In the nuclear technology, irradiation of a reactor fuel results in a chemistry of great complexity, because of the generation of a large number of new elements during fission. This is especially so in the case of fast reactor fuels that would be irradiated to high levels of burn-up resulting in the formation of significant amounts of fission products. High temperatures and steep temperature gradients prevailing in the fuel pins and the occurrence of many competing chemical interactions between fuel and fission products, amongst the fission products themselves, between the fission products and the clad, and finally between the fuel and coolant in the event of a clad failure make the chemistry of the fast reactor fuel a challenging subject of study. Thermo-chemical information is also necessary to understand and establish new methods of reprocessing like pyro-chemical reprocessing etc.

One of the most reliable methods of determining the thermodynamic properties at high temperatures is based on the study of vaporisation equilibria in effusive beam source in conjunction with mass spectrometry. The Knudsen effusion mass spectrometric (KEMS) technique (or very often referred to as high temperature mass spectrometric method) can provide information on the nature and composition of vapour phase and yield thermodynamic data for various reaction equilibria including those of formation of compounds. In the last decades, this method has emerged as the most powerful tool for this kind of investigations. The utility of this method becomes more important at high temperature where the process of vaporisation becomes more complex. Polymeric and complex species, which one would not normally expect based on stoichiometric formula and octet rule, are common in the high temperature vapour in equilibrium with the condensed phase [1]. Though the effusion method for determining vapour pressures was introduced in 1909 by Knudsen [2a,b], the mass spectrometric variant of the method became popular and widespread only after 1948 when Ionov [3] used KEMS to study vaporisation of alkali metal halides. This was followed by the investigations of Chupka and Inghram [4] as well as by Honig [5] to study the free evaporation of carbon. They found that C3 and not C1 , was the major species observed in the vapour phase on heating graphite (carbon filament) to 2500^{o} C. Similarly, to cite a few more examples: $W_3O_9(g)$ was the species observed predominantly over $WO_3(s)$; $V_4O_{10}(g)$ in equilibrium with $V_2O_5(s)$; $Cu_3C_{l3}(g)$ in equilibrium with CuCl(s); and $CLi_6(g)$ over $Li_2C_2(s)$.

Using KEMS almost all groups of inorganic materials were taken into investigations, such as: borides, carbides, nitrates, sulphates, halides, metals, alloys, oxides, glasses and ceramics. Also in recent years, detailed investigations on fullerenes and ionic liquids have also been carried out. The investigations on all these systems were performed primarily to determine the nature and composition of vapour phase, vapour pressure, thermodynamic activities of condensed phases, enthalpies, mixing properties and Gibbs energies of formation. Apart from the ability to detect and analyse the composition of complex vapour, mass spectrometer enables measurement of heat of vaporisation of minor species due to its high sensitivity, and has wide dynamic range, speed and capability to take care of interference from impurities. The extent of research conducted by using KEMS is so enormous that numerous review articles have been periodically written which describe in great detail about this method [6-10]. The review articles and the references quoted therein would reveal the potential and the problem areas of the high temperature mass spectrometric technique. If the greatest potential of KEMS lies in its ability to detect gaseous species in a very large dynamic range of partial pressures, the nagging problem in the conversion of ion intensities into partial pressures lies in the elucidation of the fragmentation processes and in the use of appropriate electron-impact ionisation cross sections. Drowart et al. [11] have very recently critically assessed some of these aspects, paying special attention to the influence of ionisation cross sections. In the last twenty years, internationally more than 350 research papers have been published in this field with contributions from around 45 research groups [9]. In India, BARC [12,13] and IGCAR [14-19] have been actively involved in the high temperature chemistry research employing KEMS.

Hastie et al. [20] developed a new method for

thermodynamic investigations of refractories at very high temperatures beyond 3000 K. A pulsed laser beam is used in this method as a heat source. Mass spectrometer coupled with the laser source enables analysis of vapour species. The advantage of this laser vaporisation mass spectrometer is that no effusion cell is necessary, thereby avoiding the interactions between sample and the Knudsen cell. Such a facility was also built indigenously at IGCAR by Joseph et al. [21]. Recent advances in KEMS technique [22] include a new high temperature furnace that is free of mechanical feeds and also possess very high mechanical stability and a very simple design which can be mounted without tools. The furnace in principle consists of a spherical susceptor in which a spherical Knudsen cell is placed. Two laser beams are introduced via aperture in the susceptor by diffusion and thermal conduction. This system of heating of Knudsen cell overcomes some of the typical technological problems encountered by the standard methods of heating

The method

In the Knudsen effusion mass spectrometric method, vapour in equilibrium with one or more condensed phases (either solid or liquid) is sampled, without disturbing the equilibrium conditions, ionised in an ion source (generally an electron impact ion source), mass analysed and detected by using either an electron multiplier and/or a Faraday cup. The sample chamber consists of a furnace assembly which permits effusion of equilibrium vapour from a cylindrical container called Knudsen cell, (typically 8 to 10 mm dia) in which the sample is placed and heated by some suitable means. The cell can be considered as a closed container but for a small orifice (~0.3 to 1.0 mm dia) of negligible thickness at the top. Inside a closed cell thermodynamic equilibrium is established between the condensed sample and its vapor phase. But in a real cell with an orifice, a small fraction of the molecules (atoms) escape through the tiny orifice. This process is referred to as effusion. The vapour inside the cell is assumed to be isotropic i.e. distribution of molecules is random in all directions and have a constant collisional rate at all surfaces. The vapour species effuse out in all directions following the cosine distribution law. Their distribution in any direction is proportional to the cosine of the angle between the direction and the normal to the orifice. Since the molecules effuse out into vacuum in an effusion set up, they form a molecular beam in which, practically there are no collisions between the molecules. The pressure of the escaping molecular beam can be calculated from Hertz-Knudsen equation [6] which relates the rate of mass loss during effusion to the vapour pressure. The Knudsen cells are generally made of metals like Mo, W, Ta, or ceramic oxides like alumina, yttria or graphite. The Knudsen cell is placed in an outer cup generally made of Mo, W, Ta or graphite. Temperature of the Knudsen cell is usually measured using a thermocouple or using a pyrometer.

An effusion experiment is based on several assumptions:

- The cell is isothermal and the temperature is accurately known.
- The cell is in thermodynamic equilibrium
- The orifice is ideal (zero thickness) or the geometry is well known and the correction factors (known as Clausing factor) are available.
- Pressures measured are in the molecular flow region.

An electron impact ion source, where electron energy can be varied, enables one to measure the ion intensities of various ions as a function of electron impact energy and derive appearance energies. One can study gas phase processes like fragmentation, dissociation etc., with ease. As equilibrium vapour is sampled from the Knudsen effusion cell, it also enables one to study the equilibrium properties (like vapour pressure etc.) and arrive at the thermodynamic properties (like enthalpy, entropy etc.).

Methodology of determination of various properties using mass spectrometer

Different steps involved in any mass spectrometric measurement are:

a) Identification of ionic species present in the mass spectrum

b) Assigning them to respective neutral species

c) Converting the measured ion intensities to partial pressures

d) Determination of thermodynamic quantities

Partial pressure is related to ion intensity by the relation: $p = k I^{+} T /(\sigma \gamma n)$, where k, is instrument calibration constant, σ, the ionisation cross-section γ, the multiplier response *and* n, the isotopic abundance. A number of methods have been employed for determining k, the instrumental constant. Some of them are:
(a) Measurement of the ion intensities of a reference material whose vapour pressure is known; (b) Quantitative evaporation of the sample while monitoring the ion intensities; (c) Employing a reliably known equilibrium constant involving some of the species present in the equilibrium vapour. Sometimes mutilple Knudsen cell configurations are used, which provide the advantage of obtaining in-situ calibration constants.

Determination of Thermodynamic Data

Host of thermodynamic data can be derived from the temperature dependence of partial pressures. One resorts to second-law method or third-law method or both to derive the thermodynamic data [6]. The expressions used for second law method is given below.

$$\ln K_{eq} = -\Delta_r H_T^o / RT + \Delta_r S_T^o / R \qquad (1)$$

where K_{eq} is the equilibrium constant. Measurement of equilibrium constant as a function of temperature can thus yield the enthalpy and entropy of the reaction. The equilibrium constant as a function of temperature is fitted to a straight line by the method of least-squares. Enthalpy

and entropy are derived from the slope and intercept of such equation. The enthalpies derived correspond to the mean temperature of the investigation. If the heat capacity data of all the constituents of the reaction are available, the enthalpy and entropy can be converted to a reference temperature, generally 298.15 K. In the third law method, the reaction enthalpy is derived using the relation :

$$\Delta_r H^o_{298.15} = -RT \ln K - T\{ \sum_{products} fef - \sum_{reactants} fef \} \quad (2)$$

where *fef* is the Gibbs free energy function: $-(G^o_T - H^o_{298.15} / T)$.

fef can be calculated from the heat capacity data and absolute entropy at 298.15 K ($S^o_{298.15}$) by using the relation:

$$fef = (H^o_T - H^o_{298.15})/T - (S^o_T - S^o_{298.15}) - S^o_{298..15} \quad (3)$$

where $(H^o_T - H^o_{298.15})$ and $(S^o_T - S^o_{298.15})$ are enthalpy and entropy increments. These can be calculated from the heat capacity data. For gaseous species these functions can be calculated from molecular parameters and can be experimentally determined by spectroscopic methods. Many of the compilations of thermodynamic data like JANAF tables should be referred to obtain the enthalpy and entropy increments and Gibbs free energy functions. There are methods suggested for estimating these functions when experimental data is either partially available or not available at all.

Vaporisation studies conducted at Chemistry Group, IGCAR over the last 30 years using a Knudsen effusion mass spectrometer (KEMS) included some congruently (elemental composition in the vapor phase and the condensed phase being the same) and incongruently vaporising systems: TeO_2, MnTe, H_3BO_3, and $NaBO_2$ (congruently vaporising systems); binary tellurides of Fe, Cr, Ni, Mo, Mn and the ternary Mn-Te-O and Ni-Te-O (18, 23) (incongruently vaporising systems). A VG Micromass mass spectrometer (MM 30 BK) was employed for the vaporisation studies. It consists of a Knudsen cell furnace assembly which permits effusion of equilibrium vapour, an electron impact ionisation source where the effusing gaseous species are ionised, a 90° sector single focusing magnetic analyser (with a radius of curvature of 305 mm) for mass analysis of the positive ions, and a secondary electron multiplier/Faraday cup for ion detection. Alumina/Mo/Ta Knudsen cells, sometimes with platinum liner, were used to contain the samples. This was placed inside a molybdenum/tungsten cups having a removable but tightly fitting lid made of tungsten with a 3 mm diameter hole collinear with the Knudsen-cell orifice. This assembly was heated by means of electron bombardment from two encircling tungsten filaments. Temperatures were measured by a chromel-to-alumel thermocouple placed at the bottom of the cell. With excellent temperature control, permitted by 'thermocouple control mode' of heating, the temperature measurement was accurate within ± 3 K.

The reason for conducting investigation of so many Te-containing systems is that tellurium is one of the volatile and reactive fission products, generated during a fission in a fast breeder nuclear reactor. Behavior of tellurium is of concern under normal and in transient conditions, especially if mixed uranium plutonium oxide is the fuel, since Te can form a host of compounds with fuel, fellow fission products, and cladding materials [24]. Under off-normal conditions, apart from the chemical reactivity, its vaporisation behavior can also become complex, giving rise to many Te- and (Te + O) bearing species. In order to assess the role played by tellurium in the fuel-cladding chemical interactions, vaporisation thermodynamic studies on tellurium and its compounds with oxygen and/or clad components are of great importance .

The relevance for the KEMS studies of H_3BO_3 and $NaBO_2$ systems comes from the element B being a good neutron absorber and used for control rod-application in nuclear reactors in suitable forms.

Table 1 gives some salient details concerning the different systems studied by using KEMS, the systems classified under "congruent vaporisation'

Table 1: Some salient details concerning the different systems studied by using KEMS, the systems classified under "congruent vaporisation' and "incongruent vaporisation"

System	Condensed Phase	Temp. Range K	Ions detected	Species whose p(i)s were measured
		Congruent vaporisation		
Mn-Te	MnTe	1195 to 1343	Mn^+, Te^+, Te_2^+	Mn, Te, Te_2
TeO_2	TeO_2	805 to 905	Te^+, Te_2^+, $(TeO)_i^+$ (i=1,2), $(TeO_2)_i^+$ (i=1,2),O_2^+	TeO_2, TeO, O_2, Te_2, $(TeO_2)_2$, $(TeO)_2$
H_3BO_3	H_3BO_3	295 to 342	$H_3BO_3^+$, $H_2BO_2^+$, HBO_2^+, $H_3B_3O_6^+$	H_3BO_3
$NaBO_2$	$NaBO_2$(S)	1060 to 1218	Na^+, $NaBO_2^+$, and $Na_2BO_2^+$	$NaBO_2$(g), $(NaBO_2)_2$(g)
		Incongruent vaporisation		
Fe-Te	Fe+$FeTe_{1-x}$	885-1048	Te^+, Te_2^+	Te(g) and Te_2(g)
	$FeTe_{1-x}$+$FeTe_{2-y}$	659-759	Te_2^+	Te_2(g) and Te_3(g)
Ni-Te	Ni+Ni_3Te_2	893-1190	Te^+, Te_2^+	Te(g) and Te_2(g)
Cr-Te	Cr+ $CrTe_{1-x}$	1015-1285	Te^+, Te_2^+	Te(g) and Te_2(g)
Mo-Te	Mo+ Mo_3Te_4	960-1110	Te^+, Te_2^+	Te(g) and Te_2(g)
	Mo_3Te_4+ $MoTe_2$	820-950	Te^+, Te_2^+	Te(g) and Te_2(g)
Mn-Te	Mn + $MnTe_{1-x}$	1120-1250	Mn^+, Te^+	Mn(g) and Te(g)
	$MnTe_{1-x}$+ $MnTe_{2-y}$	650-750	Te_2^+	Te_2(g)
Mn-Te-O	[a]	850-950	Te^+, Te_2^+, TeO^+, TeO_2^+, O_2^+	Te_2(g), TeO(g), TeO_2 (g), and O_2(g)
Ni-Te-O	[a]	850-960 K	Te^+, Te_2^+, TeO^+, TeO_2^+, O_2^+	Te_2(g), TeO(g), TeO_2 (g), and O_2(g)

[a] Over different co-existing phases

and "incongruent vaporisation". The vaporisation behaviors of the four congruently effusing systems studied by us make an interesting comparison. The B-containing systems H_3BO_3(s) and $NaBO_2$(s) vaporise predominantly to monomeric vapor species H_3BO_3(g) and $NaBO_2$(g). Dimeric and trimeric $NaBO_2$ species are also known, but they constitute less than 4 % of the vapor phase. The vapor phase of MnTe(s) [15], on the other hand, consists of elements as Mn(g), Te(g), and Te_2(g), with mole fractions in the temperature range of our study being ~ 0.4, 0.5, and 0.1, respectively. The incongruently vaporising nature of the phases in the M-Te systems led us to 1) obtain an insight to the fundamental concept of monomer-to-dimer ratio of the tellurium vapor species; 2) utilise it to determine the homogeneity ranges of some non-stoichiometric phases in these systems; 3) evaluation of thermodynamic data for the reactions that basically involve Te in the vapor phase; and finally 4) estimation of threshold chemical potential of tellurium that should exist in the fuel-clad gap if the stainless steel cladding were to experience corrosion by the fission product tellurium.

Phase Diagram Information

Incongruent vaporisation provided the means of determining the phase boundaries of many phases in the M-Te systems studied by us. Continuous vaporisation caused continuous composition changes. Combining the Hertz-Knudsen equation (relating pressure with rate of mass-loss) and basic KEMS equation (relating pressure with ion intensity) yields a relation that would facilitate calculation of mass-loss up to any point of time of the experiment. From the knowledge of initial composition and mass, composition of the sample as a function of time could be subsequently derived, and by application of phase rule, the phase boundaries of the phases as well. Table 2 gives information on the phase boundary compositions of some phases deduced by this approach. By a combination of phase equilibration experiments, XRD and isothermal KEMS experiments, one can obtain information about co-existing phases. Figure 1 shows The phase diagram of the Mn-Te-O system around MnO-TeO_2 pesudo binary line determined through such experiments (950 K).

Besides phase diagram information, the vaporisation experiments also yields partial molar thermodynamic quantities across the composition ranges of their existence. Figure 2 shows the results obtained for the phase $MnTe_{2-y}$(s) [16]. The partial molar Gibbs free energies and the integral molar Gibbs free energy of formation of the $MnTe_2$ phase as a function of n(Te)/n(Mn) at T = 650 K are shown in the Figure. While the tellurium activity was obtained from the measured partial pressures of Te_2(g), that of manganese was derived by employing Gibbs-Duhem integration method. The advantage of KEMS in obtaining data at very closely spaced compositions (in situ) was very effective in analysing the activity variations across the single phase.

Table 2: Phase boundary compositions of the various metal tellurides

System	Nominal composition	Te-rich boundary	M-rich boundary (%)
Fe-Te	$FeTe_{0.9}$	68.2±0.3	65.0±0.4
Cr-Te	$CrTe_{1\pm x}$ LTP	-	50.7±0.3
	$CrTe_{1\pm x}$ HTP	-	48.3±0.5
	$CrTe_{4-x}$	78.3±0.2	77.3±0.3
	$CrTe_3$	74.4±0.5	70.5±0.5
	Cr_5Te_8	70.5±0.8	63.6±0.6
Mo-Te	Mo_3Te_4	63.3±0.7	59.4±0.7
Mn-Te	$MnTe_{0.8}$	-	44.3±0.5
	$MnTe_2$	67.0	65.1±0.23

LTP: low temperature phase; HTP: high temperature phase

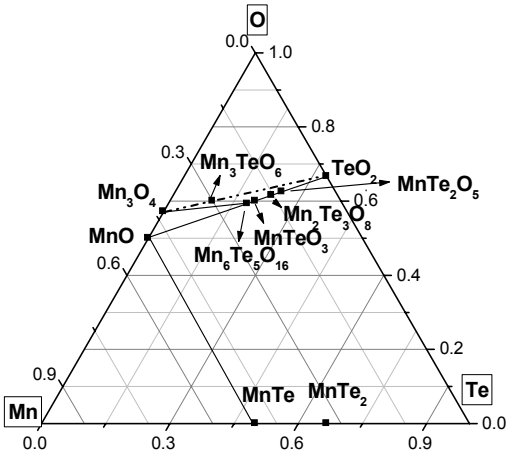

Fig.1. Phase diagram of Mn-Te-O system

Study of unusual vaporisation processes

Vaporisation chemistry associated with condensed phase transitions can be quite fascinating and interesting. During the course of a phase transition in a congruently vaporising system, vaporisation will become incongruent and this change from congruent to non-congruent vaporisation might cause some anomalous changes in vapour phase composition. Unusual and counter intuitive effects like inverse dependence of pressure with temperature or increase in pressure at constant temperature have been observed.

Robert and Searcy [25] , first time have observed such effects over Ga-S system. However, on completion of phase transition, the partial pressures and the total vapour pressures eventually reach values very close to the p-T relations of either phase during congruent vaporisation as dictated by the Clausius-Clapeyron equation. Because of this reason, the changes in vaporisation behaviour due to phase transitions might go undetected or ignored as spurious.

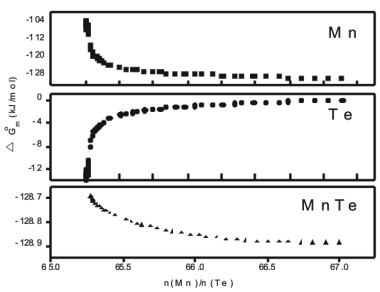

Fig.2. Thermodynamic information for the $MnTe_2$ phase as a function of composition at T = 675 K, the composition change having occurred from 67.0 at. % Te (Te-rich boundary) to 65.2 at. % Te (Mn-rich boundary) due to preferential loss of tellurium. For elements, Mn and Te, the results are chemical potentials $[\Delta\mu(i) = R\,T \ln a(i)]$ and for the $MnTe_2$ phase, the results are molar Gibbs free energy of formation

Such unusual vaporisation behaviour during phase transition is mainly caused, apart from other factors, due to the differences in the compositions of the three phases that are in equilibrium. Such effects can be best investigated by KEMS. During our investigations on Mn-Te [15] (congruently vaporisation) and Mn-Te-O (quasi congruent vaporisation) systems [26], such interesting vaporisation behaviour - associated with condensed phase transitions were observed. In the case of Mn-Te binary system, we observed both a monotonically varying congruently vaporising composition (CVC) and a discontinuous change in the CVC to Te-rich side, the latter associated with the $\alpha \leftrightarrow \beta$ solid state phase transition in MnTe. During the $(\alpha \leftrightarrow \beta)$ (1228 K) phase transition, the vapor phase was relatively richer in manganese in the increasing temperature direction (i.e., as the sample was heated from $T \leq 1203$ K to $T \geq 1238$ K), and was relatively richer in tellurium in the decreasing temperature direction (i.e., as the sample was cooled from $T \geq 1238$ K to $T \leq 1218$ K).

In the Mn-Te-O system, we observed an anomalous vaporisation behavior for the dimeric tellurium vapor species when a three-phase mixture ($MnTeO_3 + Mn_2Te_3O_8 + Mn_3TeO_6$) transformed into a quasi-congruently vaporising two-phase mixture ($MnTeO_3 + Mn_3TeO_6$). This univariant two phase mixture is not very commonly observed or reported in literature. Phase rule consideration warrants four phases (three condensed phases and one gas phase) to be in equilibrium if a sample belonging to a three component system is to vaporise univariantly (invariantly at a fixed temperature). Some ternary compounds exhibit congruent vaporisation behavior due to which one observes univariant two-phase equilibria in ternary systems. Univariant vaporisation behavior is also seen when two condensed phases are in equilibrium in a three component system, when both the phases lie a on a pseudo binary composition line (e.g. mixture of metal halides, many mixed oxide systems).

Fuel-clad Chemical interactions

Apart from serving to obtain basic thermodynamic information, the KEMS data can be used to deduce information of relevance to nuclear technology. For instance, the KEMS

studies on M-Te (M = Fe, Cr, Ni, Mo, and Mn, the major components of stainless steel) and Mn-Te-O and Ni-Te-O systems provided the pertinent information as to under what conditions the fission product Te can cause the chemical attack of 316 stainless steel cladding material used in fast breeder nuclear reactors. From the data obtained on tellurides one can calculate the tellurium potentials required for the formation of various binary metal tellurides and ternary M-Te-O phases across fuel clad gap. Figure 3 shows tellurium potentials Dm(Te) that can exist in the fuel-clad gap as well as the threshold values required for formation of Mn-Te-O phases and binary M-Te phases (at T = 900 K). The available tellurium potential in the fuel-clad gap were calculated based on model available in literature [24]. If threshold Te-potentials for formation of Mn-Te-O or M-Te phases are less than available Te-potentials in fuel-clad interface, then clad attack by tellurium can take place. Positive values of Dm(Te) are also shown in the figure (despite being meaningless) only to enable comparisons amongst different phases. Amongst the four ternary phases considered, threshold $\Delta\mu$(Te) values are the least for Mn_3TeO_6 and the greatest for $Mn_2Te_3O_8$. The values for $Mn_6Te_5O_{16}$ are less than for $MnTeO_3$ when O/M $\geq$ 2 and vice versa when O/M <2. Negative $\Delta\mu$(Te) values exist only for Mn_3TeO_6 (at all three Pu fractions and at O/M = 2.0002 and 2.0004) and for $Mn_6Te_5O_{16}$ (at Pu Fraction = 0.30 and 0.25 and at O/M = 2.0004). When compared with binary tellurides, the values for Mn_3TeO_6 at O/M = 2.0004 are more negative than that for tellurides of Fe, Ni, and Mo. Since it is known that O/M as well as oxygen potential of a MOX fuel increases with burn-up and that the oxygen potential would continue to increase even when the rate of increase in O/M would decrease drastically after a burn-up of 6 at.% fissions, there exists a probability of formation of ternary phases Mn_3TeO_6 and $Mn_6Te_5O_{16}$ on SS clad. Our calculations on Ni-Te-O reveal that these compounds would not be formed on SS clad. While the threshold Te-potential values for formation of M-Te phases do not depend on values of oxygen potential of the mixed-oxide fuel (and thus on Pu-fraction, too), those for Mn-Te-O phases obviously do. This makes it important that study of other M-Te-O systems also are undertaken for a fuller understanding of Te-attack of SS cladding in MOX fuelled FBRs.

High temperature Mass Spectrometry inside Glove box

In order to study the vaporisation behavior of radioactive and air sensitive samples, a high temperature mass spectrometric facility inside an argon atmosphere glove box (HTMS-GB) has been built indigenously at IGCAR. Fig 4 shows the photograph of the facility. Such facility only of its kind in India was hot commissioned and subsequently vaporisation studies on U-Zr [27], U-Ga [28] were carried out. Currently vaporisation studies on U-Pu-Zr system with the composition U-19wt%Pu-6wt%Zr the proposed fuel composition for the metallic fueled fast breeder reactor is being pursued. Pu^+ was the ion observed in the mass spectra of equilibrium vapour and the corresponding neurtal species was ascertained to be Pu(g). Figure 5 shows the preliminary results of temperature dependence behaviour of Pu(g), the species observed over the U-Pu-Zr fuel.

Summary

Knudsen effusion mass spectrometry (KEMS) is a very powerful technique for studying the vaporisation thermodynamics of inorganic systems at high temperatures. Although primarily one examines the vapor phase, information on the condensed phase can also be obtained, if required, through careful measurements and analysis of the results in accordance with the phase rule. This article has shown the capability of KEMS to yield information of practical importance and fundamental interest - essentially by drawing examples from the vaporisation studies on some systems conducted in our laboratory for over two decades.

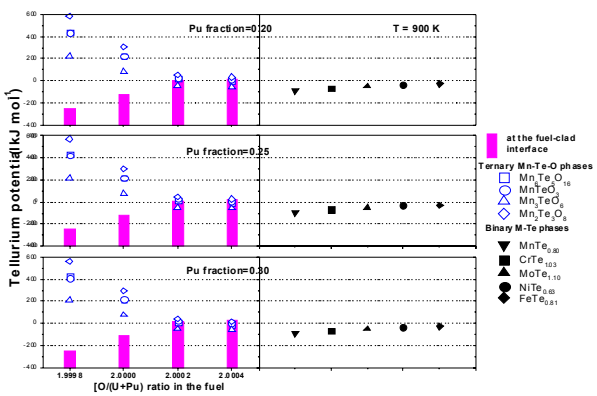

Fig.3. Comparison of tellurium potentials at T = 900 K: threshold $\Delta\mu_{thr}$(Te) for formation of most metal-rich M-Te phases on the SS clad of U-Pu mixed-oxide fuelled fast breeder nuclear reactors (filled symbols); available $\Delta_{\mu f\text{-}c}$ $_{gap}$(Te) in the fuel-clad gap (filled bars); threshold $\Delta\mu_{thr}$(Te) for formation of Mn-Te-O phases (open symbols).

Fig. 4 . Photograph of HTMS-GB facility.

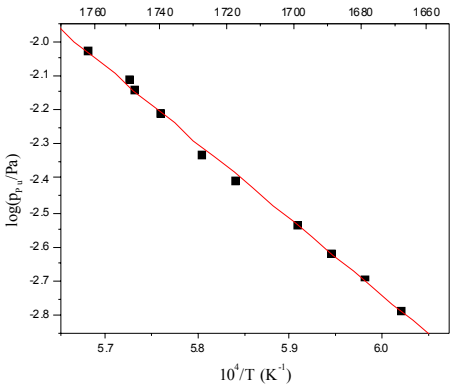

Fig. 5. A typical Plot of log (p_{Pu}/Pa) vs 1/T (K^{-1}) over $U_{19}Pu_6Zr$.

Acknowledgements

The work described is the combined efforts senior and junior colleagues (both past and present) of mass spectrometric studies section. The author express his deep gratitude to the senior colleagues for their guidance and the support and sincerely acknowledges the junior colleagues for their help and support in mass spectrometric measurements.

References

1. L. Brewer, High Temp. Sci. **24** (1987) 173.
2. a) M. Knudsen, Ann. Physik **28** (1909) 75
   b) M. Knudsen, Ann. Physik **28** (1909) 999
3. N.I. Ionov, Dokl Akad Nauk SSSR **59** (1948) 467.
4. W. A. Chupka and M.G. Inghram, J. Chem. Phys. **21** (1953) 371.
5. R.E. Honig, J. Chem. Phys. **22** (1954) 126.
6. R. T. Grimley, The characterisation of high-temperature vapors, J.L. Margrave (Ed.), New York: Wiley, Chapter 8; pp. 195-243, 1967.
7. J. Drowart and P. Goldfinger, Angew. Chem., Intl. Ed. **6** (1967) 581.
8. J. Drowart, in: Mass Spectrometry, Proc. Int. School Mass Spectrom., Stefan Institute, Lubljana, 1969, Ed. J. Marsel, (1971) p. 187.
9. M. Miller, K. Armatys, The Open Thermodyn. Journal, **7** (2013) 2.
10. K. Hilpert, Structure and Bonding 73 (Springer-Verlag Berlin, 1990) p. 97.
11. J. Drowart, C. Chatillon, J. W. Hastie, and D. W. Bonnel, Pure Applied Chem. **77** (2005) 683.
12. V. Venugopal, S.G. Kulkarni, A.A. Banerjee, G.A. Rama Rao, K.N. Roy, D.D. Sood, , J. Nucl. Mater. **238** (1996) 218.
13. S.K. Rakshit, Y. P. Naik, S.C. Parida, V. Venugopal J. of Solid State Chem. **181** (2008) 1402.
14. B. Saha , R. Viswanathan, M. Sai Baba, D. Darwin Albert Raj, R. Balasubramanian, D. Karunasagar, C.K. Mathews, J. Nucl. Mater. **130** (1985) 316.
15. T. S. Lakshmi Narasimhan, R Viswanathan, and R. Balasubramanian, J. Phys. Chem. B, **102** (1998) 10586.
16. T. S. Lakshmi Narasimhan and R. Viswanathan. ECS Transactions **46** (2013) 229.
17. M. Sai Baba, R. Viswanathan, C.K. Mathews, Rapid Commun. Mass Spectrom., **10** (1996) 691.
18. T. S. Lakshmi Narasimhan, M. Sai Baba, and R. Viswanathan J. Phys. Chem. A, **110** (2006) 13705.
19. T.S. Lakshmi Narasimhan, M. Sai Baba, R. Viswanathan, J. Phys. Chem. B **106** (2002) 6762.
20. J. W. Hastie, D.W. Bonnell, P.K. Schenck, Pure Applied Chemistry, **72** (2000) 2111.
21. M. Joseph, N. Sivakumar, D, Darwin Albert raj, C. K. Mathews. Rapi Commun. Mass Spedctrom. **10** (1996) 5.
22. J. Y. Colle, D. Freis, O. Benes and R. J. M. Konings, ECS Transactions **46** (2013) 23.
23. M. G. Adamson, E. A. Aitken and T. B. Lindemer, J. Nucl. Mater., **130** (1985) 375.
24. T.S. Lakshmi Narasimhan, S. Nalini, M. Sai Baba, Thermochim. Acta **600** (2015) 67.
25. J. A. Roberts, Jr. and A. W. Searcy, Science, **196** (1977) 525.
26. R. Viswanathan and T. S. Lakshmi Narasimhan, ECS Transactions, **46** (2013) 153. D. Darwin Albert Raj, R. Viswanathan, P. Manikandan ECS Transactions, **46** (2013) 77

27. D. Darwin Albert Raj, R. Viswanathan, P. Manikandan ECS Transactions, 46 (2013) 77.
28. P. Manikandan, V.V. Trinadh, Suranjan Bera, T. S. Lakshmi Narasimhan, M. Joseph, J. Nucl. Mater. **475** (2016) 87.

Dr. Lakshmi Narasimhan did M.Sc., (Analytical Chemistry) from University of Madras. He joined BARC Training school (31st Batch) in 1987 and Indira Gandhi Centre for Atomic Research (IGCAR), Kalpakkam in 1988. He obtained his doctoral degree from the University of Madras in the area of Physical Chemistry and did his post doctoral research at Forschungzentrum, Julich, Germany during 2004-06. Currently he heads the Mass Spectrometric Studies Section at MC and MFCG, IGCAR.

Applications of Accelerator Mass Spectrometry in Earth Sciences

S. Balakrishnan

Department of Earth Sciences, Pondicherry University, Pondicherry - 60008, India
(Email: sbala.esc@pondiuni.edu.in; Fax: +91-413-2655008; Phone: +91-413-2655008)

Introduction

Accelerator Mass Spectrometry (AMS) is a relatively new technique capable of measuring cosmogenic nuclides invariably found at very low abundances relative to the stable ones (~10^{-14}). Cosmogenic nuclides including ^{10}Be, ^{14}C, ^{26}Al, ^{36}Cl, ^{56}Mn and ^{129}I are useful to understand and quantify Earth's surface processes, determine exposure and burial ages of rocks. They are also used as tracers of crustal recycling by plate tectonic processes. This is largely made possible by developments in (a) AMS measuring techniques, (b) modelling of the present and past production rates of cosmogenic nuclides as a function of latitude and altitude and (c) theoretical basis for interpretation of the data in the context of geological problems.

The Earth is continuously bombarded by nearly a constant flux of cosmic rays which are produced by supernova explosion from distant galaxy. Cosmic rays are mostly made up of protons, alpha particles and at much lower abundances heavier particles. Interaction of these cosmic particles with the atoms of various elements present in the atmosphere and surface of the earth produces an array of cosmogenic nuclides, such as, ^{10}Be, ^{14}C, ^{26}Al, ^{36}Cl, ^{56}Mn and ^{129}I [1]. AMS determinations of ^{14}C has made possible to date a few milligrams of carbon [2] as opposed to about thousand times larger quantity required for counting techniques, which has brought a paradigm shift in understanding human evolution and history.

Challenges faced in the determination of cosmogenic nuclides are their very low abundances at a few thousand atoms per gram of sample and isobaric interference of atomic and molecular species during mass spectrometric analysis. Due to these limitations their measurement is not practicable using conventional mass spectrometers. Radioactive decay counting methods also are not quite effective in detecting cosmogenic nuclei, particularly in the case of cosmogenic nuclides with long half-life (Table 1) as it requires a large amount of sample and enormous time to accurately measure the abundance of radio nuclei.

Table 1: Cosmogenic nuclides rate of production at sea level and high latitude and their half-lives.

Nuclide	Half-life (y)	Production rate atoms (g^{-1} y^{-1})	Target elements	Minerals analyzed
^{10}Be	1.39 *10^6	5	O, Si	Quartz
^{14}C	5720	20	O	Quartz
^{26}Al	716 *10^3	31	Si	Quartz
^{36}Cl	301 *10^3	20-200	K, Ca	K-feldpsar, calcite
^{3}He	stable	120		Olivine, pyroxene
^{21}Ne	stable	20	Mg, Si	Quartz, olivine, pyroxene
^{10}Be, meteoric	1.39 *10^6	106 atoms cm^{-2} y^{-1}	O, Si	sediments, clays

Increasing applications of cosmogenic nuclides to estimate rates of various Earth's surface processes, to date tectonic events and for tracing of groundwater among others are made possible due to improvements in AMS technique during the past three decades [2]. Production of cosmogenic nuclides, AMS measurement techniques, various geological problems that are being addressed and future perspectives are outlined. Interestingly, pioneering work that led to the discovery of cosmogenic nuclides of Be was carried out in India [3]. Lal laid the theoretical framework for application of cosmogenic nuclides to determine the exposure and burial ages and rates of denudation [4]. This prompted several others to refine the production rates and scaling models of cosmogenic nuclides and improve measurement techniques which resulted in better precision and accuracy of ages determined [5,6]. As the usefulness of ^{14}C in earth sciences and archaeology are well documented this review places emphasis on ^{10}Be and ^{26}Al applications aimed to better understand the various Earth processes [4-8].

Cosmogenic Nuclides

Cosmic rays are energetic, subatomic particles that shower on the Earth originating mostly outside of the Solar System. Their energies range from 1 GeV to 10^{20} GeV, however, the flux decreases exponentially with the energy. They are composed of protons (90%), á-particles (9%) and heavier particles (1%) [5]. Most of these particles have energies high enough to cause spallation reactions with target atoms of nitrogen, oxygen and other gasses present in the atmosphere. As a result pions, neutrons and protons are mainly emitted and the charged pions quickly decay to muons. The muons interact weakly with matter and therefore, pass through the atmosphere and penetrate below the Earth's surface (Fig. 1).

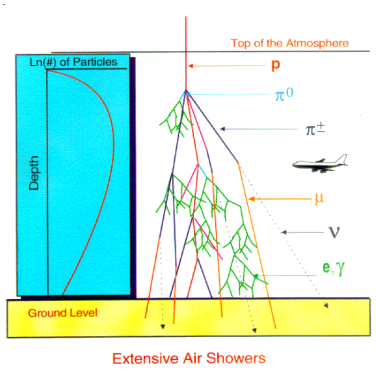

Fig.1. Primary cosmic rays (P) bombard atoms in the air which in turn produce secondary nuclear particles (N, P, π, μ, e and γ). They interact with atoms in the air and on the surface of the Earth and produce cosmogenic nuclides. Maximum cosmogenic nuclide production is at about 16 km above the sea level in the atmosphere. Image from http://www.physics.adelaide.edu.au/astrophysics/hires/uhecr.html

High energy protons and neutrons interact with the atoms in the atmosphere to produce various cosmogenic nuclides by spallation reactions (Table 2).

The rate of production of cosmogenic nuclides is about a million times higher in the atmosphere than at the surface of the Earth [5]. Because the cosmic ray flux is attenuated by the air the flux near the surface of the Earth is only a small fraction of what has entered at the top of the atmosphere. Primary cosmic rays rarely reach the Earth's surface (Fig. 1) and hence most cosmogenic nuclides that are produced in the minerals of exposed rocks and soils by nuclear reactions are caused by neutrons and muons (Table 2).

Table 2: Important nuclear reactions that produce cosmogenic nuclides in the atmosphere and on the Earth's surface.

Nuclide	Target	Reaction type	Reaction
^{3}He	O, Mg, Si, Ca, Fe, Al	Spallation	^{6}Li(n,á)3H'!^{3}He
^{10}Be	O, Si	Spallation	^{16}O(n,4p,3n) ^{10}Be
		Negative muon (μ^-) capture	^{16}O(μ^-,ápn) ^{10}Be
^{14}C	O, Si, N	Spallation	^{16}O(n,2pn)^{14}C ^{17}O(n,á)^{14}C ^{28}Si(n,x)^{14}C ^{14}N(n,p)^{14}C
		μ^- capture	^{16}O(μ^-,2p) ^{14}C
^{21}Ne	Mg, Na, Al, Fe, Si	Spallation	^{16}O(á,n)^{2}1Ne ^{19}F(á,pn)^{21}Ne
^{26}Al	Si	Spallation	^{28}Si(n,p2n)^{26}Al
		μ^- capture	^{28}Si(μ^-,2n)^{26}Al
^{36}Cl	K, Ca, Cl	Spallation	^{39}K(n,2p2n)^{36}Cl ^{40}Ca(n,3p2n)^{36}Cl
		μ^- capture	^{39}K(μ^-,p2n)^{36}Cl ^{40}Ca(μ,2p2n)^{36}Cl
		Low-energy neutron capture	^{39}K(n,á)^{36}Cl ^{35}Cl(n,ã)^{36}Cl

Cosmogenic nuclides produced in the atmosphere are often referred to as 'garden' or 'meteoric' variety whereas, those produced on the surface of the earth and up to about 60 cm depth (assuming density of the rocks as 2600 kg/m^3) are known as '*in situ*' variety [4, 5]. The effective depth of penetration and production of cosmogenic nuclides are inversely related to the density of the soil or rock.

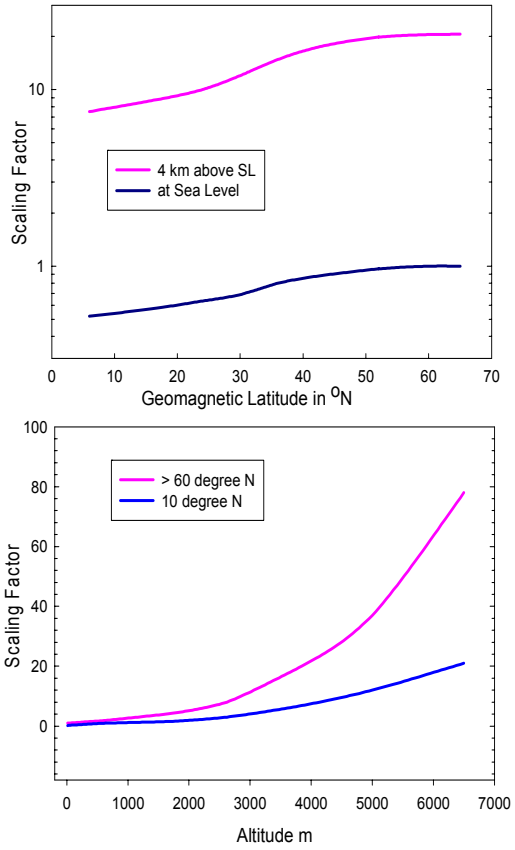

Fig.2. Scaling factor for production of cosmogenic nuclides. (A) Variation of scaling factor as a function of geomagnetic latitude. (B) Variation of scaling factor as a function of altitude which increases more rapidly for higher latitude than lower latitude [9].

The abundance of cosmogenic nuclides in the target minerals steadily builds up with time and hence is useful in determining the exposure age or rate of erosion. Except ^{3}He and ^{21}Ne, all other cosmogenic nuclides undergo spontaneous decay (Table 1) which makes them useful in determining the rate of deposition of sediments and burial age of artefacts.

The rate of production of cosmogenic nuclides depends on altitude, geomagnetic latitude and the strength of the geomagnetic field. As the cut-off magnetic rigidity is much higher at the magnetic equator, cosmic ray flux is much lower at the lower magnetic latitudes than at the higher magnetic latitudes. At the magnetic poles, the field lines are vertical and allow all most all of the cosmic rays to enter, whereas, at the equator cosmic rays are perpendicular to geomagnetic field lines which cuts off about 50 % of the cosmic ray flux. Thus, the rate of production of cosmogenic nuclides increases with magnetic latitude and remains constant beyond 60 degrees. The highest rate of production of cosmogenic nuclides in the atmosphere, at given latitude, is at an elevation of 16 km above the mean sea level and drops exponentially with decreasing elevation [4, 5].

The Earth's magnetic field was not constant in the geological past and witnessed many magnetic reversal

events. The last magnetic reversal occurred about 800,000 years ago and four to five magnetic reversals occur within a million year period. The Earth's magnetic field becomes weaker while approaching the magnetic reversal events. The magnetic field also undergoes 'excursion' typified by weakening of the field and slowly regaining strength without changing the polarity. Evidence for the past magnetic reversals and excursions in its field strength come from spreading mid-ocean ridge basalts, sedimentary rocks and artefacts. During the periods of weak magnetic field strength the cut off rigidity is lowered even at equator allowing a higher flux of galactic cosmic rays to penetrate the Earth's atmosphere. Therefore, the rate of production of cosmogenic nuclides was significantly higher during the periods of geomagnetic reversals or excursions and lower during normal periods [9]. The inverse relationship between the geomagnetic field strength and the rate of production of cosmogenic nuclides in the atmosphere has been demonstrated by several studies on marine sediment cores whose time of deposition has been determined independently by other methods [10]. Appropriate corrections are to be made to the cosmogenic isotope abundance data whenever the duration of event studied spans across magnetic reversal events.

An accurate knowledge about the rate of production of *in situ* cosmogenic nuclides in minerals or their atmospheric fallout flux in case of atmospheric production (meteoric variety) is prerequisite for their application in various fields. Lack of this knowledge had largely impeded growth and advancement in this field in the early stages. Production rates of cosmogenic nuclides were measured for locations mostly in North America and Europe and a few in Australia and New Zealand. The sites suitable for measuring the production rate should meet criteria such as that rocks containing quartz should have been brought to the surface and exposed to cosmic rays and should not have been eroded during the entire duration. The duration of its exposure should be known accurately by some other method. Glacially polished granites are considered one of the best sampling sites for this purpose as the time of glaciations and glacial retreat can be determined independently. If the exposed rock surface also maintains glacial polish it can be assumed that the surface has not been eroded after exposure to cosmic rays. However, such sites are few and they are not evenly distributed throughout the world. Hence there is a need to estimate cosmogenic nuclide production rate for any site of interest by modelling the production rate. Lal [4] and later others [5,9,11-12] have provided scaling models to estimate the production rates of cosmogenic nuclides at various latitudes and altitudes (Fig. 2).

Cosmogenic nuclides produced in the atmosphere have different resident times and their rate of production is higher at higher latitudes as discussed earlier. Hence their distribution in the atmosphere will be uneven unless they are mixed well. In case of ^{14}C, it readily combines with O_2 and forms $^{14}CO_2$ gas which is homogenized in the atmosphere by winds and as a result ^{14}C activity is almost uniform in the atmosphere above any location on the Earth. Whereas, ^{10}Be and ^{26}Al are particle reactive, they get attached to dust particles and aerosols and quickly removed from the atmosphere by way of dust fallout or rainfall. Due to the short residence time their fall out flux is variable depending on the geographic location of the study area and atmospheric circulation patterns. Meteoric fall out flux of ^{10}Be for any location on the Earth has been estimated by Heikkila and von Blanckenburg [13] taking into account atmospheric circulation models of Heikkila et al. [14]. Extent of variation of ^{10}Be fallout flux as a function of longitude and latitude is shown in Fig. 3 using the fallout table of [13]. However, to further improve accuracy and precision further, *in situ* production rate and the atmospheric fallout flux of cosmogenic nuclides need to be measured at various locations, particularly in the Indian sub-continent.

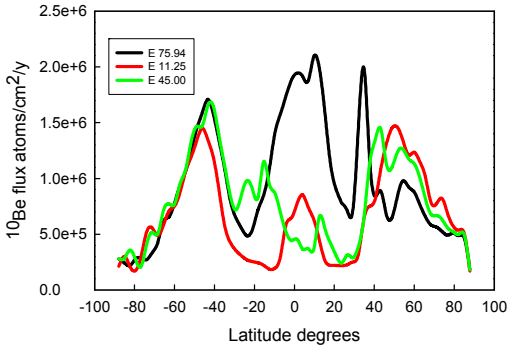

Fig.3. Variations of fallout flux of ^{10}Be as a function of latitude shown for three different longitudes of E75.94°, E11.25° and E45°based on the Fallout table of Heikkila and von Blanckenburg [13].

Accelerator Mass Spectrometry (AMS)

The abundances of cosmogenic isotopes such as, ^{10}Be and ^{26}Al, are very low, typically ratio of atoms of the cosmogenic nuclide to stable ones (e.g. ^{10}Be / ^{9}Be) in a sample varies from 10^{-12} to 10^{-15} requiring highly sensitive detection method. Their low rate of decay (Table 1) and the amount of sample generally available for their measurement precludes their measurement by counting techniques. Furthermore, they need to be separated from the isotope causing isobaric interferences which are far more abundant. For example, the isobars ^{10}B and ^{10}Be need to be separated from each other which cannot be accomplished by normal mass spectrometer. The accelerator mass spectrometer is designed to provide both high selectivity and sensitivity to isolate and measure various cosmogenic nuclides.

The samples to be analyzed are chemically processed to isolate the element of interest from the matrix and interfering elements. The sample is cleaned and digested using strong mineral acids (for *in situ* variety) or leached using suitable solutions or weak acids in case of selective extraction (e.g., adsorbed, authigenic or Fe-Mn oxide species). A known amount of stable isotope of element of interest, typically a few ng, is added. However, addition of the stable isotope tracer is not required with the recent improvements in AMS measurement technique [15]. Concentration of the abundant, stable isotope in the solution is measured using inductively coupled plasma - optical emission or mass spectrometer (ICP-OES or ICP-MS) and passed through cation and anion

exchange columns. The cation and anion exchange columns are pre-calibrated and optimized for separation of ^{10}Be and ^{26}Al from matrix elements with maximum yield and finally precipitated as hydroxide ($Be.OH_2$ or $Al.OH_3$). The precipitate is dried in a quartz capsule and fired in an electrical furnace at 1000°C to convert it to oxide. The oxide powder is mixed with Nb or Ag metal powder to make it conductive and loaded in to cathode target tubes of the AMS. A modern AMS can accommodate multiple sample targets, 40 to 120, and the sample and standards are loaded together in the turret so that they can be analyzed alternatively.

The AMS was developed in the year 1977 to provide ^{14}C measurements on small samples by suitably modifying tandem accelerators used for nuclear physics experiments. These typically had high terminal voltage of 10 to 20 MeV which subsequently was lowered to 3 to 6 MeV in newer equipments [5, 16]. Realizing the vast potential of AMS in measuring not only ^{14}C but a number of other cosmogenic nuclides commercial ventures started making AMS (High Voltage Electric, NEC and HV) from 1990s. To make AMS affordable to more researchers, taking advantage of the recent developments in eliminating molecular background at low energies, the terminal voltage and size of AMS are significantly reduced. The low-energy AMS comes with a terminal voltage as low as 200 keV occupying floor space of 3m by 3m [17] and some of these are dedicated for measurement of ^{10}Be, ^{14}C and ^{26}Al which are more commonly studied.

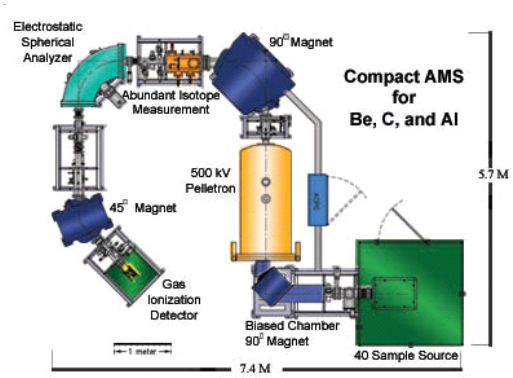

Fig.4. Layout of a low energy Accelerator Mass spectormeter (AMS).

AMS typically consists of a source (Fig. 4) where the target is sputtered by Cs^+ ion beam resulting in the formation of negative ions. Isobaric interference from the elements that cannot form negative ions is eliminated at the source itself, e.g. ^{14}N interference on ^{14}C. The negative ions that pass through an electromagnet (90° magnet) are mass discriminated and the selected mass injected into the accelerator. The negatively charged ions are accelerated and made to pass through a thin metal foil or a gas filled chamber placed in the pelletron (Fig. 4) where they are stripped of electrons to attain charge state of +1 or more (typically +3 in high energy AMS). The interfering light molecules are disintegrated due to Coulomb repulsion. The positively charged ions are repelled by the negatively charged terminal and are again accelerated away from it. These high energy positive ions pass through a series of energy filter, magnetic and electrostatic analyzers and lastly injected into a gas ionization detector (Fig. 4). The gas ionization detector is capable of distinguishing the rare cosmogenic nuclide (e.g., ^{10}Be) from the interfering ones by monitoring the rate of energy loss suffered by them. The interfering isobar that has higher atomic number (^{10}B, Z = 5) will suffer a faster rate of energy loss. The abundant isotope (^{9}Be, ^{27}Al) is injected into accelerator in short pulses and measured by a Faraday cup suitably positioned (Fig. 4). The ratio of counts obtained from the gas ionization detector to the ion current of the Faraday cup gives the ^{10}Be/^{9}Be ratio.

International standards (e.g. NIST SRM 4325 for *Be*) are diluted to cover the range of ratios and repeatedly measured to monitor the instrumental bias. The measured isotope ratios of the samples are corrected for the bias by considering the ratios measured ratios of the standards and certified or reference values.

Applications in Earth Sciences

The Earth is a dynamic planet with its surface undergoing continuous changes and its internal layers, crust, mantle and core recurrently interacting with each other. Sun's energy reaching the Earth drives weathering, transport of sediments, atmospheric and ocean currents and biological activities. Flow of the internal energy of the Earth acquired at the time of its formation and early evolution is responsible for mantle convection, plate tectonics, magmatism including volcanic and plutonic activity and earthquakes. Thus, variation in energy flux from both the sources cause dynamic changes in climate, surface relief and relative amounts of H_2O present in the form of ice, water and vapour. Geological records show that above changes had profound impact on life on the Earth, sometimes wiping out many species in a very short duration known as mass extinction events. An additional complexity is caused by the modern human civilization which reportedly influences natural variations in climate. Knowledge about the rates and timing of various Earth processes that occurred in the recent geological past in comparison to that of the Present day is essential to understand impact of these changes on the life and to predict future rates of change in various environmental conditions like temperature and rainfall. In this regard the cosmogenic isotopes are unique as their rate of formation and decay can be advantageously put to use to quantify various surface processes such as glacial retreat, denudation and sedimentation. Certain key applications of cosmogenic nuclides measured using AMS in different fields of Earth Sciences are discussed below.

Glacial Landforms and Exposure Ages: Earth has witnessed a number of glacial and interglacial periods in the geological past as many as, 30 within the past two million years. During the glacial period ice covered the high latitudes even during summer and each event lasted for about 15,000 years or more. The glacial events occurred due to cooling of the atmosphere and hydrosphere caused by a variety of reasons including changes in orbital parameters, solar activity, volcanism and tectonic activity. During peak glaciations considerable water was locked up in the continental ice sheets resulting in lowering of the sea level, whereas, melting of the continental ice sheets during interglacial or warm periods caused sea level to rise. The timing of glacial retreat indicates

onset of warmer interglacial period and hence, considerable interest in dating glacial landforms (Fig. 5). Glacial landforms taken up for cosmogenic nuclide studies include moraines, erratics, outwash till and glacially polished bedrock [20-22].

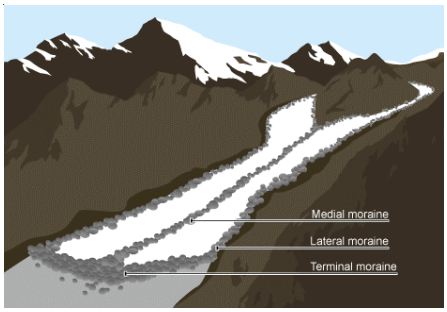

Fig.5.(A) Different types of moraines are shown and among them the Terminal moraines are useful to date glacial retreat events. (B) Erratic is boulder carried by glaciers and left abandoned above unrelated rocks. Their top surface is exposed to cosmic rays after melting of glaciers.[18, 19].

Sediments ranging in size from clay to boulder are transported by glaciers and when melted these are deposited in the valleys and plains (Fig. 5). Most of these sediments were shielded from cosmic rays when covered by glaciers and exposed after melting of the ice (Fig 5). Cosmogenic nuclides (^{10}Be and ^{26}Al) build up in minerals from this time and their abundance is related to duration of their exposure to the cosmic rays (Fig. 6). Similarly, glacially polished bedrock surface can be dated to find out the duration of its exposure after glaciations.

Quartz (SiO_2) is ideally suited for cosmogenic dating as it is ubiquitous in most rocks, resistant to physical weathering (hardness in the Moh's scale = 7) and chemical alteration.

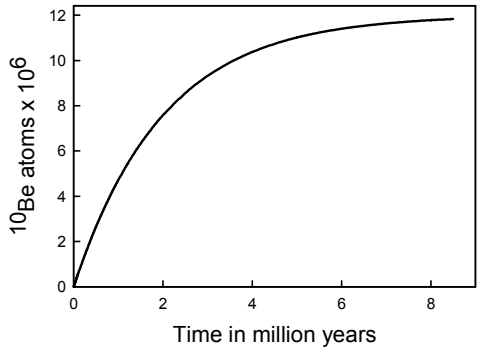

Fig. 6. Build up of ^{10}Be atoms as a function of time in the mineral quartz, which is ubiquitous in the rocks of glacial land forms such as moraines, till and erratics. ^{10}Be growth curve is calculated assuming a production rate of 6 atoms/g of quartz, density of the rock as 2.7 g/cm^3, attenuation length of 157 cm and zero erosion.

By far it is the most common mineral used for cosmogenic nuclide studies although olivine, feldspars and pyroxenes are useful for specific studies as listed in the Table 1. If the sample was not previously exposed to cosmic rays and rock surface not eroding then the number of ^{10}Be atoms present in quartz can be related to its duration of exposure to cosmic rays (t) by:

$$N = (P_o/\gamma)(1 - e^{-\gamma t}) \quad (1)$$

Where, N = number of atoms of cosmogenic nuclide, P_o = rate of production of the nuclide in 1 g of target mineral, t = exposure age and γ = decay constant. Cosmic ray exposure age is determined by solving the equation (1) for t.

Rate of Denudation: The surface of the earth experiences physical and chemical weathering leading to formation of a layer of loose rocks and sediments above the rocks, known as saprolite. Soil is found as the uppermost layer of the saprolite (Fig. 7) and is enriched in carbon and nutrients and sustains plants and other biological organisms in the biosphere. Chemical weathering of rocks leads to removal of CO_2 from the atmosphere and also helps to form and sustain soil and biosphere, thus indirectly responsible for sequestration of CO_2 by the plants.

Fig.7. Weathering profile formed over Archean rocks of Dharwar Craton in southern India. The dark brown layer immediately below the vegetation is soil and below it is the saprolite followed by partly weathered bed rocks dark grey in color. The depth of the above profile is about 4 m.

Thickness of soil in a region depends on the rates of soil formation and removal of soil through denudation. When the rate of denudation equals that of soil formation then 'steady state' is achieved, thickness of the soil will not change with time [23].

Denudation rate of uplands depend mainly on rate of tectonic uplift however, some consider there is a feedback mechanism between denudation and uplift rates to balance the mass removed. Increased rates of denudation are also reported due to increased rainfall, particularly in deglaciated regions. Rate of incision of valley by river, timing of change of river course and age of wave-cut terraces are also of significance to understand tectonic activity of a region.

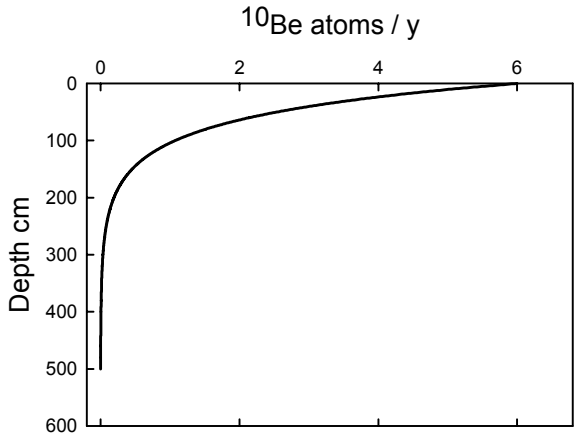

Fig.8. Production of ^{10}Be atoms as a function of depth in rocks with density of 2.7 g/cm^2 assuming that rate of production at the surface is 6 atoms of ^{10}Be/g of quartz and attenuation length of 157 cm.

Cosmogenic nuclides are produced at the surface and varying depths and the rate of production exponentially decreases with depth (Fig. 8). The production rate is reduced by a factor of ~2.72 (e) at an attenuation length which is ~160 g cm^{-2} for ^{10}Be and ^{26}Al, assuming density of 2.6 g cm^{-3} which corresponds to a depth of ~62 cm.

Number of atoms of cosmogenic nuclides increases with time in minerals exposed at the surface but after about four half-lives it remains nearly constant as the rate of decay equals that of production. However, the surface is continuously eroded and the above condition may not be reached in the regions that undergo moderate to rapid denudation.

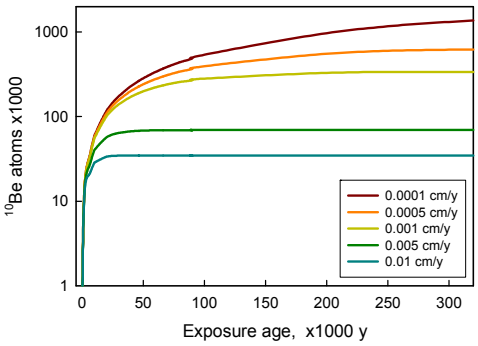

Fig. 9. Number of atoms of ^{10}Be attains steady state depending on its half-life and rate of erosion.The above curves for different rates of erosion were calculated assuming the same parameters given for the Fig.8.

Therefore, the number of cosmogenic atoms present in mineral depends on the rate of its decay and the rate of erosion. Saturation ^{10}Be in quartz is attained sooner in regions undergoing high rate of denudation than in region undergoing moderate rate of denudation (Fig. 9). Thus, the abundance of ^{10}Be in a mineral is related to rate of denudation. As suggested by Lal [4] by using two cosmogenic nuclides with different production and decay rates, usually ^{10}Be and ^{26}Al (or ^{21}Ne), the rate of denudation is determined more accurately than using one (Fig. 10).

An interesting study was carried out by Gunnel et al. [24] on geomorphic evolution of granitoid rock domes that occur as isolated 'islands', 50 to 720 m above the surrounding plains in the Mysore plateau. These geomorphic features are known as inselbergs or bornhardt and are common feature in stable continental regions which are referred to as cratons. Bornharts are often made of granitoid rocks and are also surrounded by similar igneous rocks and occur in regions characterized by tropical, arid or semiarid climates. Their origin is enigmatic and several theories were proposed. Gunnel et al. [24] found that the rates of erosion determined based on the study of *in situ* produced ^{10}Be in quartz are in the order of d"2 m/Ma (Ma=10^6 years) for the granitoid rock domes, whereas, it is considerably higher at 8 to 12 m/Ma for the surrounding low relief planar surfaces. This prompted them to suggest that differential erosion is the potential cause for the origin of granitic domes. From the elevation of bornharts and the rates of erosion determined, the etchplanation (differential erosion) could have been initiated 64 to 68 Ma ago, as early as, Late Cretaceous [24].

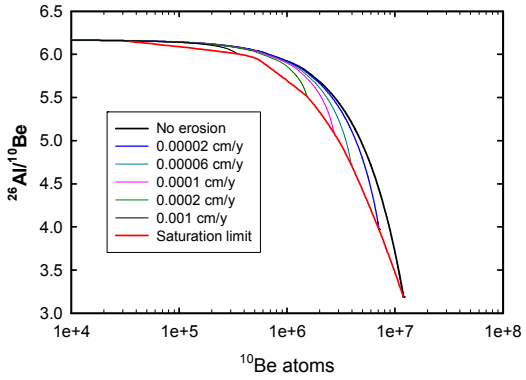

Fig.10. Modelling based on abundance of two cosmogenic nuclides, ^{10}Be and ^{26}Al, for various rates of denudation. Samples that essentially satisfy criteria for determining erosion rate or exposure age will fall between the zero erosion and saturation curves as suggested by Lal [4]. Assumed rate of production of ^{26}Al is 37 atoms/y and other parameters are as given for the Fig. 8.

In contrast to the very low erosion rates, ranging from 0.002 mm/y to 0.01 mm/y, observed in the Dharwar craton of India the erosion rates across Himalayan range varied from 0.1 mm/y to 2 mm/y [25-27]. As the Himalayas are tectonically active its rates of erosion is expected to be higher than that of the stable cratonic regions. Collision of Indian and Eurasian plates resulted in enormous crustal shortening and uplift of the Himalayas. Sliding of rocks along the Main Himalayan Thrust faults is responsible for continued uplift and earthquakes that strike the region frequently. Therefore, it is important to know the geometry of the Himalayan thrust fault which can be constrained using seismic imaging technique or denudation rates estimated across the thrust faults. The rates of erosion determined along N-S sections of the Himalayas starting from Main Frontal Thrust (MFT) to Main Himalayan Thrust (MHT) showed significantly higher values

of 1 to 2 mm/y for the highlands above both the thrust faults while low values of <0.25 mm/y for the intervening areas [25-27]. After careful considerations of the possible influence of rainfall, slope and other geomorphic variables, the major causative factor for the high denudation rates determined for Higher Himalayas was not rainfall intensity but the tectonic activity [27]. Thus, based on ^{10}Be derived denudation rates Le Roux-Mallouf et al. [25] suggested that the Himalayan Thrust Fault steepened below the northernmost Himalayan range and it was responsible for the uplift.

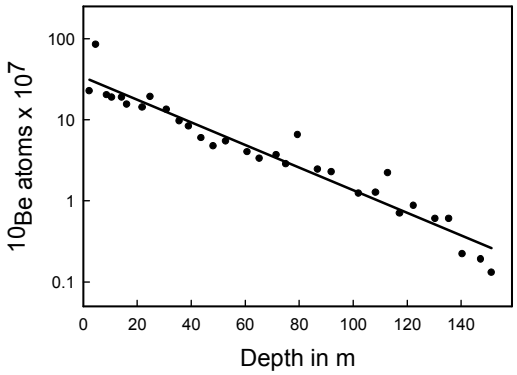

Fig. 11. Variation of ^{10}Be atoms as a function of depth in Arctic ocean sediments reported by Frank et al. [30]. ^{10}Be abundance decreases with depth and slope of the regression line yielded the rate of sedimentation as 14.5 ± 1 m/Ma [30].

Sedimentation Rate and Burial Age: As noted earlier cosmogenic nuclide ^{10}Be produced in the atmosphere is particle reactive and gets attached to aerosols and is washed out by rainfall (or snowfall) and transported to lakes or oceans. It combines with stable ^{9}Be found in water in trace quantities and gets adsorbed on clays and co-precipitates with Fe-Mn oxides that form coatings on coarser mineral grains. Be is removed from seawater (or lake) through formation of authigenic minerals, such as, Fe-Mn nodules and carbonate minerals. After their deposition at the seafloor (or lake-floor) the sediments are insulated from cosmic rays and hence in the absence of new production, ^{10}Be atoms decrease with time as they are radioactive. Therefore, assuming that ^{10}Be flux to sea or lake was constant for the duration of sedimentation and its value is accurately known, the ^{10}Be abundance in sediments would decrease with depth according to the equation:

$$^{10}Be(d) = {}^{10}Be_0 e^{-\gamma t} \quad (2)$$

$$s = d/t \quad (3)$$

Substituting for t in eq. 2 we get,

$$^{10}Be = {}^{10}Be_0 e^{-\gamma d/s} \quad (4)$$

where, ^{10}Be = number of atoms measured at the depth d, $^{10}Be_0$ = number of atoms at the water-sediment interface, γ = decay constant and s = sedimentation rate.

Thus, by determining ^{10}Be abundance at different depths of a sediment core one can estimate age of deposition of sediments at various depths and rate of sedimentation (Fig. 11). Bourles et al. [28] reported ^{10}Be/^{9}Be ratios in marine sediments from different oceans. They reported that ^{10}Be/^{9}Be ratios in the oceans varied according to the distance from continents and thus are influenced by ^{9}Be input from continents. However, ^{10}Be/^{9}Be ratios of authigenic phases of deep marine surface sediments for a given ocean are similar. The above variations could be explained due to lower residence time of *Be* compared to the mixing time of oceans which is ~ 1000 y [28]. They have also found that ^{10}Be/^{9}Be ratios of ~ 24 m long sediment core decreased with the depth of the core. Deviation that cannot be explained by experimental error was noted between independently determined paleomagnetic age and cosmogenic age with half-life of 1.51± 0.06 Ma for ^{10}Be and the authors suggested that one possible reason could be over estimation of the half-life [28]. However, the cosmogenic and paleomagnetic ages agree well using the recently determined half-life of 1.39 Ma [29].

Thus, age and sedimentation rate can be estimated based on the ^{10}Be/^{9}Be measurements in authigenic phases of marine sediment cores, particularly if they are devoid of biogenic material or their age exceed 40 k.y. A 200 m long sediment core has been extracted from Arctic Ocean which essentially consists of detrital sediments with only traces of microorganism. Therefore, ^{14}C dating in not feasible and ^{10}Be/^{9}Be measurements were carried out to establish chronology dating back to 12.3 Ma (Fig. 11) which helped in understanding the variation of climate during the Late Neogene by Frank et al. [30].

Another interesting application of determining variation of ^{10}Be/^{9}Be with depth (or age) is to determine the timing of paleomagnetic reversals. As noted earlier, galactic cosmic rays penetrate deep into the Earth's atmosphere even above equator when geomagnetic field strength is weak. This results in higher rate of production of cosmogenic nuclides. Down core variation of ^{10}Be abundance in arctic and Antarctic ice sheets and marine sediments show inverse correlation with the past geomagnetic field strength [10, 31-33]. Thus these variations in ^{10}Be concentration can be used to correlate ice cores of different continents and also marine sediment cores to derive temporal information.

Age and Rate of Growth of Manganese Nodules: Manganese nodules (also referred as Fe-Mn nodules) are 1-5 cm in diameter, invariably found within top 50 cm of sediment column on the seafloor [34]. When cut into half nodules have a fish tooth, a fragment of rock or any other foreign matter as the core which serve as nucleus for concentric growth by precipitation of Fe-Mn oxy-hydroxides (Fig. 12). In addition to Fe and Mn they have up to few wt. % Cu, Co, Ni and Zn and hence of considerable economic significance [35]. As the manganese nodules slowly grow by direct precipitation from seawater they keep record of past changes in the composition and also the pattern of circulation of ocean currents. For example, Piepgras and Wasserburg [36] reported that the Nd isotope composition (expressed as $[\hat{}_{Nd}$) of Mn-nodules and the seawater are found to be identical and also distinct for each of the major oceans. Based on this several studies were carried out to understand the past ocean circulation and strength of the North Atlantic Deep Ocean Current [37-38]. To understand timing of past changes in

physical and chemical oceanographic parameters precise age and rate of growth of the manganese nodules is required. Initially ^{230}Th disequilibrium dating method was employed but as it has half-life of 7.52×10^4 y only it cannot be used to date interiors of nodules which typically grow few mm to few tens of mm per 10^6 y.

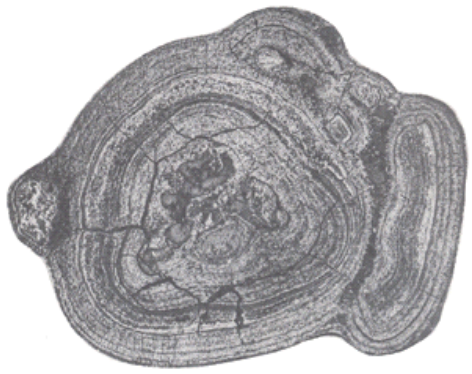

Fig.12. Cross-sectional view of manganese nodule collected from the Indian Ocean at a depth of ~ 4 km. Width of the nodule is 3 cm. Image from [34].

Whereas, ^{10}Be with half-life of 1.39 Ma is ideally suited to date the manganese nodules using an approach similar to the one described above for dating marine sediment core. The manganese nodules sampled using a micro-drill from rim to core are analysed for ^{10}Be using AMS. Applying decay equations similar to 2 & 4 age and rate of growth of manganese nodules found on deep sea bed can be determined. Theoretical and methodological aspects of ^{10}Be dating of Mn-nodules are detailed in Somayajulu [39].

A significant fraction of meteoric ^{10}Be produced in the atmosphere and scavenged by rain over continents ends up in the weathering profile. It is adsorbed or absorbed by fine grained minerals and clay and precipitates as Fe-Mn coating over coarse grains. Pavich et al. [40], You et al. [41] and Brown et al. [42] studied this large inventory of ^{10}Be in soil and weathering profiles and attempted to determine the age of soil profile and quantify denudation rates and rate of transfer of sediments. This approach had large uncertainties as key geochemical behaviour of *Be* was not well understood at that time. Later von Blanckenburg and his co-workers [43] have suggested that instead of using ^{10}Be alone combined use of ^{10}Be/^{9}Be ratios can be modelled to estimate rates of both chemical and physical weathering. Average concentration of ^{9}Be in rocks is 2.2 ± 0.5 ppm [44] and during weathering it is partly released to water present in the weathering profile. Meteoric ^{10}Be found in rainwater infiltrates into the weathering profile and combines with the ^{9}Be already present in the water. Thus, ^{10}Be/^{9}Be ratio of the water and authigenic phases formed from it will be identical and they can be modelled to know relative extents of chemical and physical weathering and total denudation. Details of theoretical consideration and application of this method to determine weathering rates in catchments of major rivers are explained by von Blanckenburg et al. [43] and the results of such study on sediments carried by major rivers of the world are given in [45].

Another important application pertains to determining age of artefacts and sediments buried near river channels, alluvial fans and floodplains as it has significance to human settlement and evolution and paleoseismic and paleo-hazard studies. Typically, in situ produced ^{10}Be and ^{26}Al are used to determine the age of burial as these two isotopes have different rates of decay and thus help to achieve better accuracy and reliability [4].

There are a number of other applications of cosmogenic nuclides such as dating of fault scarps and groundwater and extent and duration of recycling of sediments through subduction of oceanic crust and island-arc volcanism. This is a relatively young field, with the recent developments in AMS technology and the production rate determination, application of cosmogenic nuclides to quantify various Earth processes opens up immense possibilities for new discoveries.

Acknowledgements: I thank Drs. Rajneesh Bhutani and Shreyas Managave for their suggestions after critically going through the manuscript which was useful in revising it. Drs. Sundeep Chopra and Pankaj Kumar, IUAC, New Delhi and my Ph.D. scholars Dr. Jitendra Pattanaik and Mr. Soumya Dhal provided me impetus to understand and appreciate the field of AMS and cosmogenic nuclides.

References

1. D. Lal, B. Peters, In: *Handbook der Physik*, **4/2** Springer Verlag, Berlin (1967) 551.
2. H.A. Synal, International Journal of Mass Spectrometry, **349** (2013) 192.
3. P. S. Goel, D.P. Kharkar, D. Lal, N. Narasappaya, B. Peters, V. Yatirajam, Deep-Sea Res., **4** (1957) 202.
4. D. Lal, Earth and Planetary Science Letters, **104** (1991) 424.
5. T. J. Dunai, N. A. Lifton, Elements, Elements, **10** (2014) 347.
6. M. Christ, R. Wieler, R. C. Finkel, Elements, **10** (2014) 330.
7. F. von Blanckenburg, J. K. Willenbring, Elements, **10** (2014) 341.
8. S. Ivy-Ochs, F. Kober, Quaternary Science Journal, **57** (2008) 179.
9. N. Lifton, T. Sato, T. J. Dunai, Earth and Planetary Science Letters, **386** (2014) 149.
10. Frank, M., B. Schwarz, B., Baumann, S., Kubik, P.W., Suter, M., Mangini, A., Earth and Planetary Science Letters, **149** (1997) 121–129.
11. D. Desilets, M. Zreda, T. Prabhu, Earth and Planetary Science Letters, **246** (2006) 265-276.
12. G. Balco, J. O. Stone, N. A. Lifton, T. J. Dunai, Quaternary Geochronology, **3**, (2008) 174-195.
13. U. Heikkilä, F. von Blanckenburg, GFZ Data Services, (2015)
14. U. Heikkilä, J. Beer, J. A. Abreu, F. Steinhilber, Atmo. Chem. Phys., (2008) 2797.
15. J. Lachner, M. Christl, H-A. Synal, M. Frank, M. Jakobsson, Nuclear Instruments and Methods in Physics Research B **294** (2013) 67.
16. Pankaj Kumar, J. K. Pattanaik, S. Ojha, S. Gargari, R. Joshi, G. S. Roonwal, S. Balakrishnan, S. Chopra, D. Kanjilal, J. Radioanal. Nucl. Chem. (2011) doi 10.1007/s10967-011-1184-x.

17. L. A. Owen, L. Gualtieri, R. C. Finkel, M. W. Caffee, D. I. Benn, M. C. Sharma, J. Quaternary Sci. **16** (2002) 555.
18. S. Ivy-Ochs, J. P. Briner, Elements, **10** (2014) 351.
19. J. D. Shakun, P. U. Clark, F. He, N. A. Lifton, Z. Liu, B. L. Otto-Bliesner, Nature Communications, (2015) DOI: 10.1038/ncomms9059.
20. J. L. Dixon, C. S. Riebe, Elements, **10** (2014) 363.
21. Y. Gunnel, R. Braucher, D. Bourles, G. Andre, GSA Bulletin, **119** (2007) 576.
22. E. W. Portenga, P. R. Bierman, C. Dunan, L B. Corbett, N. M. Kherwald, D. H. Rood, Geomorphology **233** (2015) 112.
23. R. Le Roux-Mallouf, V. Godard, R. Cattin, M. Ferry, J. Gyeltshen, J.-F. Ritz, D. Drupka, V. Guillou, M. Arnold, G. Aumaître, D. L. Bourlès, and K. Keddadouche, Geophys. Res. Lett., **42** (2015) 3257.
24. D. Scherler, B. Bookhagen, M.R.Strecker, J. Geophys. Res. Earth Surf. **119** (2014) 82.
25. D. Bourles, G. M. Raisbeck, F. Yiou, Geochimica et Cosmochimica Acta, **53**, (1989) 443.
26. G. Korschinek, A. Bergmaier, T. Faestermann, U. Gerstmann, K. Knie, G. Rugel, A. Wallner, I. Dillmann, G. Dollinger, C.L. von Gostomski, K. Kossert, M. Maiti, M. Poutivtsev, A. Remmert, Nucl. Instrum. Meth. B **268** (2010) 187.
27. M. Frank, J. Backman, M. Jakobsson, K Moran, M. O'Regan, J. King, B. A. Haley, P. W. Kubik, D. Garbe-Schonberg, Paleocenography, **23** (2008) doi:10.1029/2007PA001478, 2008.
28. Y. Suganuma, Y. Yokoyama, T. Yamazaki, K. Kawamura,C-S Horng, H. Matsuzaki, Earth and Planetary Science Letters, **296** (2010) 443.
29. M. Christl, C. Strobl, A. Mangini, Quatern.Sci. Rev. **22** (2003) 725.
30. G. M. Raisbeck, F. Yiou, J. Jouzel, T. F. Stocker, T.F., (2007), Clim. Past 3, 541–547.
31. http:/www.nio.org?option=com_projectdisplay&task=view&tid=2&sid=15&pid=15
32. R. Mukhopadhyay, A. K. Ghosh, S. D. Iyer, The Indian Ocean Nodule Field: Geology and Resource Potential, Elsevier, (2008) 294.
32. D. J. Piepgras, G. J. Wasserburg, Earth Planet. Sci. Lett., **50** (1980) 128.
34. M. Gutjahr, M. Frank, C. H. Stirling, L. D. Keigwin, A. N. Halliday, Earth Planet. Sci. Lett., **266** (2008) 61.
35. F. Albarède, S. L. Goldstein, Geochimica et Cosmochimica Acta, **61**, (1997) 1277-1291.
36. B. L. K. Somayajulu, Current Science, **78**, (2000) 300-308.
37. M. J. Pavich, L. Brown, J. Klein, R. Middleton, Earth Planet. Sci. Lett., **266** (1984) 61.
38. C. F. You, T. Lee, Y. H. Li, Chem. Geol. **77** (1989) 105.
39. L. Brown, M. J. Pavich, R. E. Hickman, J. Klein, R. Middleton, Earth Suface Processes and Landforms, **13** (1988), 441.
40. F. von Blanckenburg, J. Bouchez, H. Wittmann, Earth Planet. Sci. Lett., 351 (2012) 295.
41. R. L. Rudnick, S. Gao, 2004. In: D. H. Heinrich, K. T. Karl, (Eds.), *Treatise on Geochemistry*. Elsevier, Amsterdam, (1989) p. 1-64.
42. F. von Blanckenburg, J. *Bouchez*, J., Earth and Planetary Science Letters, **387** (2014) 34.

Prof. S. Balakrishnan obtained B. Sc and M.Sc. from Madras University and M.Phil. and Ph.D. from J.N.U., New Delhi. He used Thermal Ionization Mass Spectrometer (TIMS) at the State University of New York at Stony Brook to determine isotope composition of Nd and Pb in geological samples as part of his doctoral and post-doctoral research. He started his career at University of Roorkee (now IIT-Roorkee) and moved to Pondicherry University as professor. A team led by Prof. Balakrishnan successfully established TIMS facility at Pondicherry University in the year 2006 which is being used by researchers from various institutions. He played a significant role in setting up an AMS beam line and a dedicated AMS facility at the Inter University Accelerator Centre, New Delhi.

Applications of Stable Nitrogen and Carbon Isotopes in Oceanography

R. Ramesh* and Arvind Singh

Physical Research Laboratory, Navrangpura, Ahmedabad 380 009.
Email: *rramesh@niser.ac.in
* Present address: NISER(Bhubaneswar), P.O.Jatni, Dist. Khordha 752050, Odisha.

Introduction

Carbon dioxide (CO_2), one of the most important green house gases in the Earth's atmosphere, increased from ~280 ppmv (parts per million volume) to ~400 ppmv during the last ~250 years [1]. Ocean is one of the key components in regulating the Earth's atmosphere as it absorbs around one quarter of the CO_2 emitted. All the processes that influence the oceanic uptake of CO_2 are controlled by climate. Therefore, any changes in climate may alter the uptake of CO_2 by the ocean. However, understanding of the response of ocean CO_2 to changes in climate is inadequate due to the limited data on CO_2 removed by the oceans [2].

Ocean exchanges carbon with atmosphere mainly by two processes. First, cold and dense waters at high latitudes, enriched in dissolved CO_2, sink to the deeper oceans. This localized sinking, associated with the Meridional Overturning Circulation is termed the solubility pump. This sinking flux is approximately balanced by diffuse upward flux of DIC (dissolved inorganic carbon) into tropical

surface waters. The second process is biological through which there is a net removal of (CO_2) from the atmosphere to the deeper ocean, known as the biological pump. This is more efficient in the tropical oceans, e.g., the area of the present study, the northern Indian Ocean.

Marine biological productivity is defined as the rate of carbon fixation during photosynthesis at the ocean surface, measured in units of mg C $m^{-2}d^{-1}$. There is a supply of this fixed carbon from the sunlit layers of the ocean (i.e., the top ~100 m) to the darker, deeper layers through biological pump, termed as export productivity. This is believed to be approximately equal to 'new productivity', the fraction of the productivity sustained by the input of new nutrients into the euphotic zone, over annual time scales [3]. The efficiency of the biological pump is driven by the availability of nutrients, especially macronutrients such as reactive nitrogen (Nr) in the tropics. Nr is known to limit the biological productivity in the surface ocean in many regions [4]. Thus, nitrogen is an essential nutrient for growth of marine biota and hence understanding the processes by which nitrogen is added to the oceans are important. This is the one of the objectives of the present study.

The Marine Nitrogen Cycle

Nitrogen, as a building block in the amino acids, is a fundamental player in marine biogeochemical cycles. The fluxes of nitrogen within and among its reservoirs comprise the global nitrogen cycle. Molecular nitrogen (N_2) is most abundant (78% by volume) in the Earth's atmosphere, but can be directly utilized only by a specific group of marine microorganisms. Most other organisms prefer oxidized or reduced forms of nitrogen, i.e., N_r (e.g., NO_3^-, NH_4^+). Nitrogen enters the surface ocean through the following processes related to the marine nitrogen cycle.

N_2 fixation is a microbial process performed by several types of bacteria and algae. In this process, molecular nitrogen gets converted to ammonium. The surface water of the ocean is deficient in N_r. Nitrate is the main compound present in the surface water on which marine productivity depends. However, in the absence of Nr, a specific group of microorganisms - diazotrophs can utilize N_2, despite the fact that large energy (226 kcal/mol) is required to break the triple bond. These microorganisms convert N_2 into ammonium with their special enzyme, nitrogenase, and in this way 'new' nitrogen is introduced into the ocean. Such microorganisms like *Trichodesmium* occur in the Arabian Sea under favorable conditions, i.e., in the absence of Nr and higher Sea Surface Temperature (SST). Fe is the key micronutrient which may decide the fate of N_2 fixing microorganisms. N_2 fixation has the potential to influence the sequestration of CO_2 by introducing 'new' nitrogen which supports primary productivity. Diazotrophs are involved in a global feedback of the climate system and this feedback exhibits complex dynamics on varying time-scales. The hypothesized feedback mechanisms will have the following components - the rate of N_2 fixation can impact the concentration of atmospheric CO_2; CO_2 concentrations in the atmosphere can influence the climate; the climate system, in turn, can influence the rate of N_2 fixation by controlling the supply of Fe associated with dust, and by influencing the stratification of the upper ocean. Humans play an important role in this feedback cycle by their influence on dust production, through agriculture at the margins of deserts, and by emissions of CO_2 into the atmosphere. These influences can lead to a cyclic feedback system, particularly on longer time-scales. Consequently, a large challenge in the contemporary biogeochemical oceanography is to understand the regional to global scale controls on N_2 fixation in the sea [5].

Nitrification is an aerobic process in which microorganisms obtain energy by converting ammonium to nitrate. This happens in two stages - in the first stage, the oxidation of ammonium to nitrite is performed by a group of organisms called *Nitrosomonas*; in the second stage, another group of organisms-*Nitrobacter*, are responsible for the oxidation of the nitrite to nitrate. Uptake of nitrate by an organism and its incorporation through nitrate reduction is known as assimilatory nitrate reduction It is an important input of nitrogen for many microorganisms. Ammonification (Remineralization) is conversion of organic nitrogen in to ammonium through microbial process. This is part of decomposition of organic matter by heterotrophic microbes.

Denitrification is a multi-step heterotrophic reduction of nitrate to molecular nitrogen, but only when the process leads all the way to N_2 production, it meets the proper definition of denitrification [6]. In addition to nitrogen sink, heterotrophic denitrification is regarded as the major remineralization process in the Oxygen Minimum Zones (OMZs) because heterotrophic bacteria release NH_4^+ from organic matter while respiring NO_3^-.

It is very well established now that apart from denitrification, anaerobic ammonium oxidation (anammox) - chemolithoautotrophic process that fixes inorganic carbon - is also cause for N_r loss from the ocean [7–9]. Anammox mainly occurs if oxygen concentration is less than 1.1 ìM. The occurrence of anammox in seawater was first reported in the Black Sea [7] and Golfo Dulce [10]. Neither oxygen nor sulphide were detectable at the depths where anammox was observed.

Dissimilatory Nitrate Reduction to Ammonium (DNRA) is a microbial process in which nitrate/nitrite is reduced to ammonium. This process has previously been considered unimportant, however, recent research has shown DNRA to be of importance in marine nitrogen cycle [9,11]. The dissimilatory reduction of nitrate to nitrite is the FIrst step in denitrification and DNRA, but it is also an independent process. More microorganisms have potential of reducing nitrate to nitrite without denitrifying or ammonifying [6]. The present study mainly deals with N_2 fixation and denitrification in the northern Indian Ocean.

Ocean gains nitrogen through atmosphere (dry and wet deposition of aerosols) and land (riverine fluxes) besides N_2 fixation [12]. Upwelling/eddy diffusion is another inherent nitrogen source to photic zone of the ocean but this occurs in limited and specific areas of the ocean, e.g., in the western Arabian Sea during summer and in the Bay during the winter [13]. Nitrogen inputs from fertilizer use on land and waste discharge are also probably limited to the coastal regions.

N_2 is the most stable molecule in the Earth's atmosphere. It is chemically unreactive at the atmospheric temperature and pressure and combines with other elements only under extreme conditions or when catalyzed by enzymes. All other forms of nitrogen (oxidized and reduced) are derived from N_2. N_2 is converted to N_r by either N_2 to NH_3 or by converting N_2 to NO via both natural and anthropogenic processes.

In addition to N_2 fixation, lightning is another natural process which converts N_2 to N_r, though this process has less global importance now. With industrial revolution, fossil fuel burning has become the dominant anthropogenic process for N_r creation. The high temperature and pressure provide energy for N_r creation during fossil fuel combustion.

Atmospheric nitrogen deposition

N_r, which is present in the atmosphere, is deposited into the ocean by two ways: wet deposition - aerosols settles with rain over the ocean; and gravitational force leads to dry deposition of N_r [14]. Depositional velocities and scavenging ratio required to estimate wet and dry deposition of N_r have considerable uncertainties as they depend on complex interactions of various parameters, e.g. wind speed, particle size [15]. Atmospheric nitrogen inputs are often poorly represented in the study of the open ocean anthropogenic impacts [15,16], however, potential importance of atmospheric deposition to the new productivity in the open ocean is discussed. Atmospheric deposition of Nr may account for up to ~3% of marine new productivity. Duce et al., (2000) and Bange et al. (2000) have estimated nitrogen deposition through aerosol in the Arabian Sea is to be 1.5 Tg N y^{-1} [17,18].

Nitrogen fluxes through rivers

Nitrogen, in addition to supply of through atmosphere, is also supplied through river via erosion and weathering processes. The most productive areas in the oceans are coastal region because of supply of nutrients through rivers and coastal upwelling [19]. Though the N_r flux through atmosphere and rivers are modest but with increasing human activities they have potential to alter subsurface water chemistry by altering the Redfield Ratio (C:N:P :: 106:16:1). An enigma appeared while estimating the nitrogen loss and gain rates; these are not in balance. Ocean loses ~400 Tg N y^{-1} and fluxes ~200 Tg N y^{-1}. Suggested reasons for the nitrogen deficit are - either there are other less well-studied or currently unknown exist processes that flux substantial amounts of N_r [20]. The loss processes are studied in detail and the possibility of a decrease in the nitrogen loss term in the total nitrogen budget is less likely, while the gain processes are still poorly understood [20]. This motivated to revise N gain processes (e.g., N_2 fixation) with the better tools available now.

Applications of Stable Isotopes

The stable isotopes of C and N, focus of the present study in the biogeochemical cycle, serve as tracers in estimating the carbon and nitrogen fluxes. Isotopic molecules with differences in mass have different reaction rates. This leads to isotopic fractionation [21]. Isotopic fractionation is a physical phenomenon which causes changes in the relative abundances of isotopes due to their differences in mass. Stable isotopes are measured as the ratio of two isotopes of a given element, i.e. R = Abundance of the rarer isotope/ Abundance of the more abundant isotope. For nitrogen, which has two stable isotopes - ^{14}N and ^{15}N, with abundances of 0.99634 and 0.00366, respectively, isotope ratio is given as $R = {}^{15}N/{}^{14}N \sim 0{:}0037$

Measuring an absolute isotope ratio requires sophisticated mass spectrometric equipment. Further, measuring this ratio would lead often to problems in comparing data sets from different laboratories. However, our interest is only in comparing the variations in stable isotope ratios rather than actual abundance, and so a simpler approach is used. Rather than measuring a true ratio, an apparent ratio is measured by gas source mass spectrometry. The apparent ratio differs from the true ratio due to operational variations and will not be constant between machines or laboratories or even different days for the same machine.

However, by measuring a known reference on the same machine at the same time, we can compare our sample with a reference. As fractionation processes do not impart large variations in isotopic concentrations, ä values are expressed as the parts per thousand or per mil (‰) difference relative to the reference.

$$\delta^{15}N = [(^{15}N/^{14}N)_{sample} / (^{15}N/^{14}N)_{air} - 1] \times 1000\ ‰.$$

A ä value that is positive, say +10, signifies that the sample has 10‰ more $^{15}N/^{14}N$ than the reference (air), or is enriched by 10‰. or 1% more $^{15}N/^{14}N$ than the reference. Similarly, the value for a sample depleted relative to the reference by this amount would be expressed as $\delta^{15}N^{sample}_{air} = +10‰$. Artificially enriched (99%) stable isotopes of carbon (^{13}C) and nitrogen (^{15}N) are used in this study. Contribution of ^{15}N tracer in the biogeochemical cycling is well-established, evidences of nitrogen as limiting nutrient are aggregated from ^{15}N studies [22]. ^{15}N tracer is introduced into oceanography to separate the fraction of primary productivity into new and regenerated productivity in the photic zone (oceanic depth upto where 1% of surface sunlight reaches) of the ocean [23]. A conceptual model is introduced assuming the photic zone to be as a close box. The microorganisms present in the zone may obtain nitrogen into two ways - (i) nitrogen is recycled in organic matter decomposition inside the zone, (ii) lateral or vertical transport of nitrogen from outside the zone. Productivity supported by nitrogen produced inside the photic zone is regenerated productivity while that supported by externally added nitrogen is new productivity. It is assumed in this model that the form of new nitrogen is nitrate and that of regenerated nitrogen is ammonium.

^{15}N in the form of gas is used in the present study for measuring N_2 fixation [24]. In addition, ^{13}C is also used for primary productivity (carbon assimilation) estimations [25].

Sampling region

The northern Indian Ocean is divided into two parts - the Arabian Sea in the western and the Bay of Bengal in the eastern side of the Indian subcontinent, both being enclosed in the north at similar latitudes. Though they are like twin seas but are different in many aspects. They form excellent sites to study the variability in the biogeochemistry of the oceans [26]. Unlike other oceans, the northern Indian Ocean, being bounded by the Asian land mass to its north, suffers a strong seasonal reversal in the wind direction, well known as the monsoon circulation. During June-September (the southwest or summer monsoon), strong winds blow from ocean towards land resulting in intense upwelling in the northwestern Arabian Sea. Evaporation over the Arabian Sea (275 cm y^{-1}) is estimated to be higher than that over the Bay of Bengal (250 cm y^{-1}; [27]). River discharge and overhead precipitation together exceed evaporation in the Bay of Bengal. This flux imbalance causes the export (advection) of less saline water to the Arabian Sea [28], e.g., the East India Coastal Current (EICC) transports low salinity water from the Bay to the southeastern Arabian Sea during winter. The West India Coastal Current (WICC) carries this water northward [29–31] and decreases the surface salinity of the eastern Arabian Sea. In contrast, during summer, the eastward owing Indian Monsoon Current carries high-salinity water from the Arabian Sea to the Bay of Bengal [32]. Rainfall over the Indian subcontinent is derived from the northward movement of the Inter-Tropical Convergence Zone (ITCZ) during June-September and its withdrawal during October-November [33]. The rainfall varies seasonally, regionally and annually over the region. Most Indian plains receive a major fraction (~80%) of the annual rainfall during summer. The highest rainfall occurs along the west coast and northeastern regions of the Indian peninsula. During December-February (the northeast or winter monsoon), cool and dry air from the Himalayas enhances evaporation in the northeastern Arabian Sea causing convective mixing [34], while there is little rainfall over most of India; southeastern India gets its major share of rain during this period. Upwelling and winter mixing during summer and winter, respectively, bring nutrient from the deep to the surface in the Arabian Sea which results in enhancing the productivity [34–36]. On the other hand, high riverine fluxes stratify the Bay of Bengal surface water, limiting surface productivity [19,37]. The Arabian Sea is one of most productive regions in the world oceans and also hosts perennially-intensified denitrification zone [34,38]. An interesting study, productivity during summer in the western Arabian Sea show increasing trend from 1997 to 2004 as observed from the ocean color data. This trend has been attributed to the warming of the Eurasian land mass [39]. However, such a trend is not observed in the northeast Arabian Sea; Naqvi et al. [2010] reanalyzed the data and have also ruled out such increasing trend [36,40,41]. These studies suggest that there is still much more to be understood in the Arabian Sea with the improved techniques.

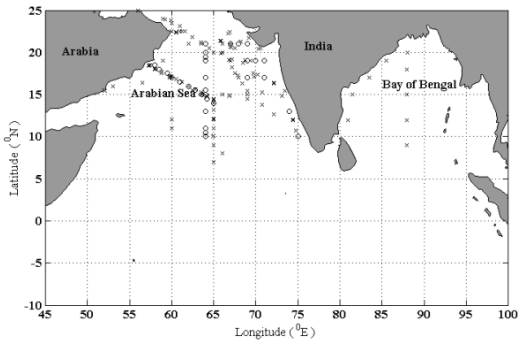

Fig. 1. Primary productivity sampling locations for ^{15}N (in ×) and ^{14}C (in %)

Methodology and mass-spectrometric analysis for estimating ocean productivity

Generally, the tracer used to measure oceanic primary productivity is ^{14}C, which provides an estimation of overall productivity i.e., total rate of carbon fixation. However, this tracer does not provide any information about the export/ new production. The ^{15}N tracer technique [23], besides estimating the primary productivity, yields the new/export productivity as well (i.e. nitrate uptake). In this technique, primary productivity is calculated by sum of the uptake rates of nitrate, ammonia and urea integrated over the photic zone, and using the Red field ratio (C:N:P: :106:16:1). Because of

simultaneous microbial processes occurring in the sunlit layer of ocean, variation in Red field ratio (C:N:P varies from 70:10:1 to 200:27:1) introduces some error in the productivity estimates [42]. Since we compare only nitrogen uptake rates (based on ^{15}N tracer technique) with deposition fluxes, such errors are avoided here. More details of this technique are discussed by [43].

^{15}N tracer technique based new and primary productivity data in the northern Indian Ocean have been obtained from several studies [37,44–51]. ^{14}C tracer technique based primary productivity data are also available [34,52–58] but not used here. Although ^{14}C and ^{15}N based productivity values are comparable [43]; the incorporation of ^{14}C data might increase uncertainties in the nitrate uptake rate estimates while conversion from carbon to nitrogen uptake rates (using the variable Redfield ratio) and then assuming a constant fraction of the primary productivity as new productivity. Productivity measurements also cover almost entire the Arabian Sea (excluding south of 50N), while being spatially limited in the Bay of Bengal. The overall uncertainty in the productivity measurements is less than 10%. This is mostly due to patchiness of the particles and seasonal and inter-annual variations. Hence, our final analysis, based on productivity and atmospheric flux calculations, have less than 25% uncertainty.

A CTD (Conductivity–Temperature–Depth) system along with a rosette sampler is normally used to collect water samples from different depths covering the euphotic zone of the ocean. Sampling locations are shown in Fig. 1. Vertical profiles of temperature and salinity were obtained for the sampling locations. Joint Global Ocean Flux Study (JGOFS) protocol (UNESCO, 1994) was followed to estimate new and regenerated production using the ^{15}N tracer [59]. Total primary production was estimated using ^{13}C tracer [25]. Six sampling depths were chosen to cover the euphotic depth with light intensity corresponding to 100, 80, 64, 20, 5 and 1% of the sea surface irradiance. A photosynthetically-active-radiation (PAR) sensor attached to a portable CTD sensor system was used to measure irradiance levels. Individual water samples were collected in pre-washed polycarbonate bottles (Nalgene, USA) for Carbon (1 L), NO_3^- (2 L), ammonium (NH_4^+; 2 L) and urea (1 L) enrichment experiments, each in duplicate. Samples were also collected at each station for blank corrections for all the tracers. Prior to incubation at 10:00 h local time, tracers containing 99 atom% ^{13}C ($NaH^{13}CO_3$, Cambridge Isotope Laboratories, Inc. USA) and ^{15}N ($Na^{15}NO_3$, $^{15}NH_4Cl$ and $^{15}NH_2$-CO-$^{15}NH_2$, Sigma-Aldrich, USA) were added to the bottles. A constant amount (~0.2 mmol L^{-1}) of $NaH^{13}CO_3$ was added to each bottle for C uptake measurements. NO_3^- ($Na^{15}NO_3$) tracer was added at less than 10% of the ambient concentration. Ambient NH_4^+ and urea could not be measured at several stations because of logistic reasons; a small, constant amounts of $^{15}NH_4Cl$ and $^{15}NH_2$-CO-$^{15}NH_2$ tracers were added (to a final concentration of 0.01 ìmol L^{-1}). To simulate the irradiance at the depths from which samples derived, well-calibrated neutral density filters were put on the sample bottles. Subsequently sample bottles were kept in a big plastic tub and seawater from a depth of 6 m was circulated to regulate the temperature during on deck-incubation from 10:00 to 14:00 h at each station. Immediately after the incubation, samples were transferred to the shipboard laboratory for filtration and were kept wrapped in a thick black cloth and in dark until the filtration were over. All samples were filtered in dark, sequentially through pre-combusted (4 h at 400 °C) 47 mm diameter and 0.7 ìm pore size GF/F filters (Whatmann, GE Healthcare, USA). Samples were filtered under low vacuum (<70 mm Hg) using a manifold filtration unit and vacuum pump (Millipore, USA). Subsequently, filters were dried in an oven at 50 °C overnight and stored for further mass-spectrometric analyses. For blank correction, zero time enrichment was estimated: the same concentrations of isotopically enriched tracers as in samples were added to the individual blank-samples. Immediately after the addition, these samples were likewise filtered and dried for isotopic analysis.

A CarloErba elemental analyzer interfaced via Conflo III to a Finnigan Delta Plus mass spectrometer was used to measure particulate organic nitrogen (and carbon) and atom% ^{15}N (and ^{13}C) in the filters. For nitrogen, calibrated in-house casein and international standards $(NH_4)_2SO_4$ (IAEA-N-2) and KNO_3 (IAEA-NO-3) were used for checking the external precision whereas calibrated in-house starch and international standard ANU sucrose were used for carbon. The external precisions of the measurements were consistently better than 0.5‰. The maximum differences in the duplicate mass-spectrometric measurements of particulate organic nitrogen and carbon were found to be less than 10%. The coefficients of variation in atom% ^{15}N and atom% ^{13}C measurement were less than 1% [60].

For the calculation of nitrogen uptake rates, we used the equation provided by of Dugdale and Wilkerson (1986) [61]; while Slawyk et al. (1977) [25] were followed to estimate carbon uptake rates. The total N-uptake rate is the sum of NO_3^-, NH_4^+ and urea uptake rates. Euphotic-depth-integrated uptake rates were calculated by the trapezoidal method of integration. New productivity was considered equivalent to NO_3^- uptake rate and regenerated productivity, to the sum of NH_4^+ and urea uptake rates; *f*-ratio [3] was the ratio of new productivity to total productivity.

Role of Aerosol deposition and riverine fluxes to new production

The measured concentrations of nitrate, nitrite and ammonium in aerosols are converted into dry and wet deposition fluxes. Dry deposition occurs when particles settle under gravity while during wet deposition particles are scavenged by precipitation. Productivity is estimated on the basis of uptake rates of nitrate, nitrite and ammonium during photosynthesis. These are discussed in detail in the following subsections. Nitrate, nitrite, and ammonia concentrations in aerosols collected over the Arabian Sea and the Bay of Bengal were obtained from the literature (Fig. 2). Deposition of nitrogen occurs through gravitational settling (dry deposition) and precipitation (wet deposition). The dry deposition flux is given by $F_d = V_d * C_d$; where C_d is the measured concentration of substance of interest in aerosol, and V_d the settling velocity of the particle which depends on

complex interactions of various parameters such as wind speed, particle size, relative humidity, and sea surface roughness [15], as a result Vd has large uncertainties. Thus, to simplify estimates of deposition fluxes, the mean values of V_d accounting for the aerosol size distribution, is frequently used. V_d of 1.5 cm s^{-1} for nitrate and 0.05 cm s^{-1} for ammonium are incorporated (because Vd varies with particle size so different rates are used for nitrate and ammonium) in these calculations [14,15]. The wet deposition flux, Fw is given by $P S C_d \rho_a^{-1} \rho_w$, where P represents the rain rate, S the scavenging ratio and ρ_a (1.2 kg m^{-3}), ρ_w (10^3 kg m^{-3}), the densities of air and water, respectively. $S = C_r / C_d$, where C_r is the concentration of the substance of interest in rain. S is 330 and 200 for nitrate and ammonium, respectively [15]. For the estimation of the seasonal wet deposition flux, Bange et al. [2000][18] used a constant P, (780 mm y^{-1} for the Arabian Sea, 2550 mm y^{-1} for the Bay of Bengal) taken from [62]. High interannual and spatial variability of rainfall causes the large uncertainties in such wet deposition fluxes. To minimize these uncertainties, we estimated the wet deposition flux using TRMM (Tropical Rainfall Measuring Mission) rainfall data (http://disc2.nascom.nasa.gov/Giovanni/tovas/rain.GPCP.2.shtml) for each location at the corresponding time. For total deposition flux calculations, the areas of the Arabian Sea and the Bay of Bengal are taken to be 4.93×10^{12} m^2 and 2.93×10^{12} m^2, respectively [18]. The overall uncertainty in the calculated nitrogen deposition flux is less than 20%, mainly caused by the spatiotemporal variability in rainfall over the oceanic regions (uncertainties in wet deposition flux due to rain are also discussed in [63].

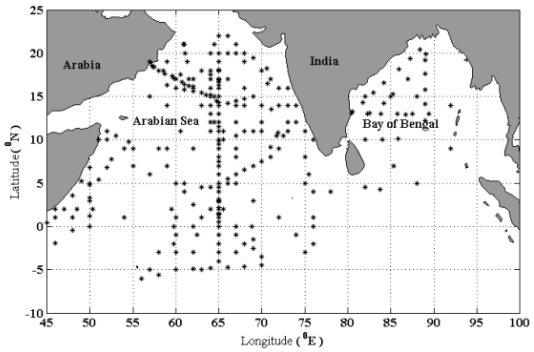

Fig. 2. Sampling locations for aerosol collection.

Major Indian rivers are categorized into four (i) Himalayan, (ii) peninsular, (iii) coastal and (iv) inland. The two largest rivers in northern India i.e. the Ganga (also known as the Ganges) and the Brahmaputra, owing towards east into the Bay of Bengal, originate in the Himalaya and rank the world's third largest river in terms of discharge, after the Amazon and the Congo. The Indus, a major river that flows through Pakistan to the Arabian Sea also originates in the Himalaya (Tibet). In the south, east-bound peninsular rivers i.e. the Mahanadi, Godavari, Krishna and Cauvery; originate in the Deccan plateau and flow into the Bay of Bengal. Coastal rivers such as the Nethravati originate from the Western Ghats flow into the Arabian Sea. Rivers originating inland in central western India, such as the Narmada and the Tapti, discharge into the Arabian Sea [64].

The DIN concentration (C) and water discharge (R) of rivers have been measured at several places on the river courses and estuaries/river mouths and the data are scattered in the literature [65]. The areal influence (extension) of river discharge in the coastal ocean is assumed to be 1°×1°; a significant amount of DIN is unlikely to be transported to the open ocean. Riverine DIN flux is derived as $F = CRA^{-1}$, where A = Area of influence. Nitrate measurements have a maximum error of 6%.

Conclusions

Primary productivity is mostly limited by the unavailability of reactive nitrogen in the sunlit surface layer of tropical oceans. The supply of such new nitrogen to the surface ocean is through upwelling, N_2 fixation by diazotrophs, riverine flux and atmospheric deposition. The relative and absolute importance of these processes in the Indian Ocean was studied. N_2 fixation is estimated directly using the $^{15}N_2$ tracer technique in the Arabian Sea during the spring inter-monsoon 2009. Estimates are double the values reported earlier and can account for a substantial fraction of the nitrogen gained by the Arabian Sea. Further, contribution of atmospheric deposition and riverine fluxes to new productivity in the two biogeochemically different basins of the northern Indian Ocean, the Arabian Sea and the Bay of Bengal, was assessed. An upper bound of the contribution of atmospheric deposition to new productivity in the northern Indian Ocean is ~2.5%. On an average ~1.73 Tg N y^{-1} is deposited into the northern Indian Ocean through dry and wet deposition of aerosols. On the other hand, most of the dissolved inorganic nitrogen (~81% in the case of the Arabian Sea and ~96% in the case of the Bay of Bengal) through riverine flux is not transported to the ocean and is consumed on the course of the rivers or in the estuaries. Coastal Bay of Bengal and Arabian Sea receive ~0.38 Tg N y^{-1} and ~0.06 Tg N y^{-1}, respectively, through rivers. A large variation in the contribution of DIN through river fluxes to new productivity is found in both these basins. Our estimate of nitrogen fluxes through N_2 fixation, aerosols and rivers is a step towards significantly reducing the uncertainty in the global nitrogen budget.

References

1. C. Change, Synthesis Report. Contribution of Working Groups I, II and III to the Fourth Assessment Report of the Intergovernmental Panel on Climate Change, (2007).
2. R. Houghton, Annu Rev Earth Planet Sci. **35** (2007) 313.
3. R. Eppley, B. Peterson, Nature. **282** (1979) 677.
4. W.S. Broecker, Chemical oceanography [by] Wallace S. Broecker. Under the general editorship of Kenneth S. Deffeyes, 1974.
5. D. Karl, A. Michaels, B. Bergman, D. Capone, E. Carpenter, R. Letelier, F. Lipschultz, H. Paerl, D. Sigman, L. Stal, Dinitrogen fixation in the world's oceans, in: Nitrogen Cycle Reg. Glob. Scales, Springer, 2002: pp. 47–98.
6. W.G. Zumft, Microbiol. Mol. Biol. Rev. **61** (1997) 533.
7. M.M. Kuypers, A.O. Sliekers, G. Lavik, M. Schmid, B.B. Jørgensen, J.G. Kuenen, J.S.S. Damsté, M. Strous, M.S. Jetten, Nature. **422** (2003) 608.
8. P. Lam, M.M. Kuypers, Annu. Rev. Mar. Sci. **3** (2011) 317.

9. P. Lam, G. Lavik, M.M. Jensen, J. van de Vossenberg, M. Schmid, D. Woebken, D. Gutiérrez, R. Amann, M.S. Jetten, M.M. Kuypers, Proc. Natl. Acad. Sci. **106** (2009) 4752.
10. T. Dalsgaard, D.E. Canfield, J. Petersen, B. Thamdrup, J. Acuña-González, Nature. **422** (2003) 606.
11. J.A. Brandes, A.H. Devol, C. Deutsch, Chem. Rev. **107** (2007) 577.
12. Y.L. Chen, H.-Y. Chen, Oceanogr. Res. Pap. **53** (2006) 971.
13. A. Singh, N. Gandhi, R. Ramesh, S. Prakash, J. Sea Res. **97** (2015) 5.
14. A. Singh, N. Gandhi, R. Ramesh, J. Geophys. Res. Oceans. **117** (2012).
15. R. Duce, P. Liss, J. Merrill, E. Atlas, P. Buat Menard, B. Hicks, J. Miller, J. Prospero, R. Arimoto, T. Church, Glob. Biogeochem. Cycles. **5** (1991) 193.
16. T. Jickells, Biogeosciences Discuss. **3** (2006) 183.
17. R. Duce, J. LaRoche, K. Altieri, K. Arrigo, A. Baker, D. Capone, S. Cornell, F. Dentener, J. Galloway, R. Ganeshram, Science. **320** (2008) 893.
18. H.W. Bange, T. Rixen, A. Johansen, R. Siefert, R. Ramesh, V. Ittekkot, M. Hoffmann, M. Andreae, Glob. Biogeochem. Cycles. **14** (2000) 1283..
19. A. Singh, R. Ramesh, Int. J. Oceanogr. 2011 (2011).
20. L.A. Codispoti, Biogeosciences. **4** (2007) 233.
21. R. Ramesh, A. Singh, Curr. Sci. **98** (2010) 406.
22. N. Owens, L. Watts, Stable Isot. Integr. Biol. (1998).
23. R. Dugdale, J. Goering, Limnol. Oceanogr. **12** (1967) 196.
24. J.P. Montoya, M. Voss, P. Khler, D.G. Capone, A Simple, Appl. Environ. Microbiol. **62** (1996) 986.
25. G. Slawyk, Mar. Freshw. Res. **30** (1979) 431.
26. A. Singh, R. Ramesh, Prog. Oceanogr. **131** (2015) 138.
27. T. Prasad, Annual and seasonal mean buoyancy fluxes for the tropical Indian Ocean, (1997).
28. R. Rao, R. Sivakumar, J. Geophys. Res. Oceans. **108** (2003).
29. K. Wyrtki, Physical oceanography of the Indian Ocean, in: Biol. Indian Ocean, Springer, 1973: pp. 18–36.
30. W. Han, J.P. McCreary, J. Geophys. Res. Oceans. **106** (2001) 859.
31. F.A. Schott, J.P. McCreary, Prog. Oceanogr. **51** (2001) 1.
32. P. Vinayachandran, Y. Masumoto, T. Yamagata, T. Mikawa, J. Geophys. Res. **104** (1999) 11077.
33. S. Gadgil, Annu. Rev. Earth Planet. Sci. **31** (2003) 429.
34. M. Madhupratap, S.P. Kumar, P. Bhattathiri, M.D. Kumar, S. Raghukumar, K. Nair, N. Ramaiah, Nature. **384** (1996) 549.
35. S. Prasannakumar, T. Prasad, Winter cooling in the northern Arabian Sea, (1996).
36. S. Prakash, R. Ramesh, Curr. Sci. **92** (2007) 667.
37. S. Kumar, R. Ramesh, S. Sardesai, M. Sheshshayee, Geophys. Res. Lett. **31** (2004).
38. S.W.A. Naqvi, H.W. Bange, S.W. Gibb, C. Goyet, A.D. Hatton, R.C. Upstill-Goddard, Prog. Oceanogr. **65** (2005) 116.
39. J.I. Goes, P.G. Thoppil, H. do R Gomes, J.T. Fasullo, Science. **308** (2005) 545.
40. S. Prasannakumar, R.P. Roshin, J. Narvekar, P. Dineshkumar, E. Vivekanandan, What drives the increased phytoplankton biomass in the Arabian Sea?, (2010).
41. S. Naqvi, J.W. Moffett, M. Gauns, P. Narvekar, A. Pratihary, H. Naik, D. Shenoy, D. Jayakumar, T.J. Goepfert, P.K. Patra, The Arabian Sea as a high-nutrient, low-chlorophyll region during the late Southwest Monsoon, (2010).
42. K.R. Arrigo, Nature. **437** (2005) 349.
43. S. Kumar, R. Ramesh, IJMS. **34** (2005) 153.
44. N. Owens, P. Burkill, R. Mantoura, E. Woodward, I. Bellan, J. Aiken, R. Howland, C. Llewellyn, Top. Stud. Oceanogr. **40** (1993) 697.
45. J.J. McCarthy, C. Garside, J.L. Nevins, Top. Stud. Oceanogr. **46** (1999) 1623.
46. L. Watts, S. Sathyendranath, C. Caverhill, H. Maass, T. Platt, N. Owens, Mar. Ecol. Prog. Ser. **183** (1999) 1.
47. L. Watts, N. Owens, Top. Stud. Oceanogr. **46** (1999) 725.
48. R.N. Sambrotto, Top. Stud. Oceanogr. **48** (2001) 1173.
49. S. Prakash, R. Ramesh, M. Sheshshayee, R. Dwivedi, M. Raman, Geophys. Res. Lett. **35** (2008).
50. S. Kumar, R. Ramesh, R. Dwivedi, M. Raman, M. Sheshshayee, W. D'Souza, Int. J. Oceanogr. **2010** (2010).
51. N. Gandhi, R. Ramesh, R. Srivastava, M. Sheshshayee, R. Dwivedi, M. Raman, Int. J. Oceanogr. **2010** (2010).
52. J.H. Ryther, J.R. Hall, A.K. Pease, A. Bakun, M.M. Jones, Limnol. Oceanogr. **11** (1966) 371.
53. S. Qasim, Oceanogr. Res. Pap. **29** (1982) 1041.
54. P. Bhattathiri, A. Pant, S. Sawant, M. Gauns, S. Matondkar, R. Mahanraju, Phytoplankton production and chlorophyll distribution in the eastarn and central Arabian Sea in 1994-1995, (1996).
55. R.T. Barber, J. Marra, R.C. Bidigare, L.A. Codispoti, D. Halpern, Z. Johnson, M. Latasa, R. Goericke, S.L. Smith, Top. Stud. Oceanogr. **48** (2001) 1127.
56. S.P. Kumar, N. Ramaiah, M. Gauns, V. Sarma, P. Muraleedharan, S. Raghukumar, M.D. Kumar, M. Madhupratap, Top. Stud. Oceanogr. 48 (2001) 1115.
57. R. Jyothibabu, P. Maheswaran, N. Madhu, T.M. Asharaf, V.J. Gerson, P. Haridas, P. Venugopal, C. Revichandran, K. Nair, T. Gopalakrishnan, Differential response of winter cooling on biological production in the northeastern Arabian Sea and northwestern Bay of Bengal, in: Indian Academy of Sciences, 2004.
58. M. Gauns, M. Madhupratap, N. Ramaiah, R. Jyothibabu, V. Fernandes, J.T. Paul, S.P. Kumar, Top. Stud. Oceanogr. **52** (2005) 2003.
59. A. Knap, A. Michaels, A. Close, H. Ducklow, A. Dickson, Protocols for the joint global ocean flux study (JGOFS) core measurements, JGOFS Repr. IOC Man. Guid. No 29 UNESCO 1994. 19 (1996).
60. N. Gandhi, A. Singh, S. Prakash, R. Ramesh, M. Raman, M. Sheshshayee, S. Shetye, Glob. Biogeochem. Cycles. **25** (2011).
61. R. Dugdale, F. Wilkerson, Limnol. Oceanogr. **31** (1986) 673.
62. M. Ramesh Kumar, T. Prasad, J. Geophys. Res. Oceans. **102** (1997) 18519.
63. A.R. Baker, T. Lesworth, C. Adams, T.D. Jickells, L. Ganzeveld, Glob. Biogeochem. Cycles. **24** (2010) 1.
64. L. Lambs, K. Balakrishna, F. Brunet, J.-L. Probst, Hydrol. Process. **19** (2005) 3345.
65. R. Krupadam, Y. Anjaneyulu, Res. J. Chem. Environ. **4** (2000) 55.

Dr. Rengaswamy Ramesh, until recently Prof. Satish Dhawan Professor at PRL,is a stable isotope geochemist, who obtained his Ph.D. from PRL, Ahmedabad in 1984. He has more than 200 publications and 4000 citations with a h-index of 30. He is a fellow of all the three Science Academies of India and also the Third World Academy. He won the INSA Young Scientist Medal (1987), S.S. Bhatnagar Prize (1998), Third World Prize (2006), Citation for Nobel peace Prize (2007), K.R. Ramanathan Gold Medal (2011), Performance Excellence Award of ISRO (2016). He has guided 20 student for Ph.D.. Currently he is a Senior Professor at the newly started School of Earth and Planetary Sciences, NISER, Bhubaneswar.

Dr. Arvind Singh completed M.Sc. in Physics from the Rohilkhand University, Bareilly, in 2004 and obtained Ph.D. in Oceanography from Physical Research Laboratory (PRL), Ahmedabad in 2011. He worked as a Nippon Foundation (NF) - Partnership at Bermuda Institute of Ocean Sciences, Bermuda until 2011. He later joined University of Gothenburg, Sweden as a postdoctoral fellow and worked there until 2012. He worked a postdoctoral fellow in GEOMAR Helmholtz Centre for Ocean Research Kiel, Germany during 2012-2015. Presently he is faculty in Physical Research Laboratory, Ahmedabad, where he is trying to understand the impacts of climate change on ocean biogeochemical cycles. His research interests lie in biogeochemical cycles of carbon and nitrogen in the ocean and atmosphere, stable isotopes in the marine environment and oceanographic time-series studies.

Mass Spectrometry: A Versatile Tool for Drug Discovery

Asim Kumar, Tejas M. Dhameliya, Asit K. Chakraborti*

Department of Medicinal Chemistry; National Institute of Pharmaceutical Education and Research (NIPER), Sector 67, S.A.S. Nagar 160 062, Punjab, India

Email: akchakraborti@niper.ac.in; akchakraborti@rediffmail.com

Abstract

The drug discovery and development process have been enriched by the development and enhancement in the mass spectrometry techniques. Drug target identification, proteomics, mechanism of action of small molecules, metabolite identification, off target drug binding sites and quantification of small metabolites could have been possible because of this versatile and magnanimous analytical tool. Last decade has witnessed a paradigm shift in the drug discovery and development process in which mass spectrometry has played a crucial role. Mass spectrometry has inherent advantages over other analytical techniques such as high sensitivity, high speed, high resolution, soft ionization technique and its ability to characterize compounds in the complex mixture of biological sample. High performance liquid chromatography (HPLC) coupled with mass spectrometry (MS) is being used frequently for the screening of new compound libraries and for the identification of new 'hits'. Various physical properties (such as physiological solubility, drug-plasma protein binding, tissue permeability assays) and chemical stability of newly synthesized compounds have been performed efficiently by mass spectrometry. High throughput assay for the permeability studies of the newly synthesized compound on caco-2 cell lines can be performed using HPLC-MS. Drug metabolism and pharmacokinetics (DMPK) assays are performed on HPLC coupled with tandem mass spectrometry (MS-MS). Mass spectrometry has helped in determination of the three-dimensional structure of proteins. Our understanding of drug-protein interactions has grown hand in hand with the development of mass spectrometry. By virtue of its diverse applications mass spectrometry has become an essential component of

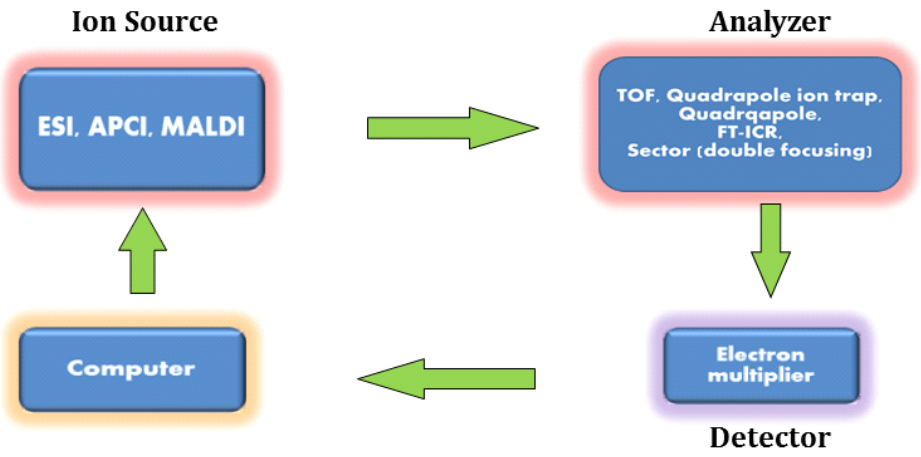

Fig.1. Basic component of mass analyzer. ESI- Electron spray ionization, APCI – Atmospheric pressure chemical ionization, MALDI – Matrix assisted laser desorption ionization, TOF – Time of flight, [1]

medicinal chemist's tool box. Current review highlights and summarizes the role of mass spectrometry in drug discovery process and its advancements.

Introduction

Our knowledge and understanding of chemistry that governs life processes has grown significantly and this has opened new avenues for the identification of new drug targets for the discovery of therapeutic agents.[1] There are various analytical tools available for identification and quantification of various bioactive molecules, bioanalytes, proteins and therapeutic agents. Mass spectrometry is one such indispensable tool in the field of drug discovery and development.[2] Mass spectrometry determines the mass-to-charge (*m/z*) ratio. A mass spectrum is a plot of ion abundance versus *m/z*, although in many cases the *x*-axis is labeled 'mass' rather than *m/z*. The spectrum is presented in terms of Daltons (Da) per unit charge. There are three main components of a typical mass analysis process (a) Ionization which involves conversion of an analyte into gas phase ion (b) Analysis of the ions that are formed during ionization process (c) Detection of the ions.[2]. Figure 1 shows different components of a classical Mass spectrometer.

With the advent of advanced mass spectrometric techniques such as electron spray ionization (ESI), matrix-assisted laser desorption ionization (MALDI), tandem MS-MS, LCMS-NMR, various aspects of drug discovery such as target identification, lead identification, metabolic profiling has been accelerated significantly.[3] Earlier various other

imaging techniques were used to visualize and study any particular biological process such as magnetic resonance imaging, radiography, ultrasonography, radioisotope labeling, microscopy, however they were having their own advantages and limitations.[4] Drug discovery and development has many challenging aspects which needs proper target validation and lead identification.[5] With the help of mass spectrometry proteomics and genomics have witnessed major development during last decade.[6] Mass spectrometry has distinct advantages among other spectroscopic techniques as it requires very less amount of sample and its ability to measure a particular compound in a complex mixture of sample.[7] Mass spectrometric imaging (MSI) is one such methodology available which provides comprehensive analysis of drug distribution studies, metabolite study[8] and quantification of various metabolite in biological fluid.[9] This helps in better understanding of the absorption, distribution, metabolism, elimination (ADME) and pharmacokinetic (PK) of drug.[10] In 1918 J. J. Dempster reports first time the detection of volatile organic compounds using EI-MS (Electron Ionization-Mass Spectrometry).[11] Since then significant progress in ion sources and mass analyzers has been achieved. In terms of the ionization techniques, various sources such as atmospheric pressure ionization (API), electrospray ionization (ESI), atmospheric pressure chemical ionization (APCI), and atmospheric pressure photoionization (APPI) have revolutionized the analysis of low molecular weight compounds (LMWCs) by HPLC-MS.[12] With the discovery and advent of MALDI which was originally developed for the characterization of biomolecules and biopolymers, now been used for identification of drug targets and their metabolites in tissues.[13] Ambient ionization techniques have also gained interest for the same type of applications. Finally, inductively coupled plasma (ICP) mass spectrometry has also been explored as an alternative detector to ^{14}C-labeled drug for drug metabolism studies.[14]

Role of Mass spectrometry in various aspects of drug discovery and development

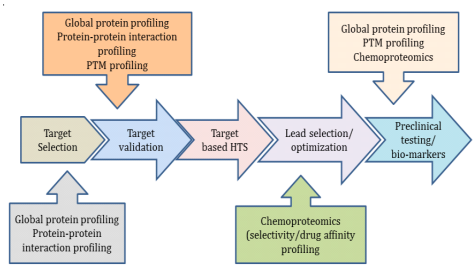

Fig. 2. Target based drug discovery.[16]

Target identification and validation

Target identification of biologically active scaffold is one of the major requirements of medicinal chemistry aspects of drug discovery.[15] The site of action for majority of the small molecule drugs and biologics are proteins present inside our body. These proteins are associated and are in constant interaction with many other cellular components. In order to understand drug-protein interaction properly it is necessary to know the structure and function of proteins. There are different steps involve in the target based drug discovery and needs integration of proteomics. Figure 2 exhibits various steps involved in the target based drug discovery.[16] Affinity Selection Mass Spectrometry (AS-MS) is one such advanced version of mass spectrometry which helps to evaluate the binding interactions of molecules of scaffolds with the receptor or protein. These methods are used in high throughput screening fields as valuable alternatives to conventional drug discovery methodologies. In combination with hyphenated techniques such as liquid chromatography (LC-MS), particularly size based chromatographic techniques, ultrafiltration, gel permeation, or size exclusion chromatography (SEC), AS-MS techniques are widely employed exhaustively for of target identification and validation.[17]

There are two types of AS-MS: one is 'direct' and other is 'indirect' (figure 3). Both involve some common steps which start with the 'affinity selection' stage where a particular protein (receptor or macromolecule) is complexed with one or more ligands through covalent or non-covalent type of interactions. The receptor-ligand complex is separated from a mixture of components of unbound ligands and receptors. The ligands are identified and detected by MS or MS-MS technique. The main difference between these two methodologies is that in case of direct AS-MS technique, receptor-ligand complex is separated within the mass spectrometer whilst in indirect AS-MS the receptor-ligand complex is separated using chromatographic techniques before subjecting it to mass analysis.[18] MS boosts the advantage of speed and sensitivity (nM-pM) over other biophysical techniques such as NMR spectroscopy and analytical centrifugation.[19]

'Direct AS-MS' techniques are utilized for covalent complexes and non-covalent complexes. A fragment based lead discovery methodology has been developed for covalent complexes. Non-covalent complexes are being studied by nano-electrospray-MS, multi-target affinity/specificity screening (MASS), detection of oligonucleotide-ligand complexes by ESI-MS (DOLCE-MS) and ESI-electron capture detection. 'Indirect AS-MS' techniques are also dubbed as hyphenated techniques because they are used in conjunction with other chromatographic techniques viz. size exclusion chromatography and gel permeation chromatography, affinity chromatography, affinity capillary, electrophoresis and ultrafiltration. Automated ligand identification system (ALIS) and SpeedScreen are based on the principle of SEC. Herein, 96-well plates permits high throughput screening HTS (4,00,000 compounds/week) when screened in pools of 400 compounds.[20] Indirect AS-MS employing SEC using ALIS has been demonstrated to purify the chemokine receptor CXCR4 and successfully utilized for the screening of large combinatorial library of small ligands through high throughput AS-MS screens.[21] Frontal affinity chromatography (FAC)-MS technique is based on the principle of solid phase chromatography, wherein ligands with weak affinity elute early and ligands with strong affinity elute later.[22] Affinity capillary electrophoresis (ACE) is not routinely used now-a-days because of requirement of volatile buffers to interface with MS.[23] Solid supported methods require the

immobilization of the receptor which may affect the inherent nature of original macromolecule. Solution based methods tackle this limitation as immobilization of receptor is not necessary. Recently, Muller et al. have demonstrated usefulness of ultracentrifugation-MALDI-TOFMS as a new tool for screening of tubulin binding anticancer agents viz. colchicine alkaloids.[24] The comprehensive coverage of utilization of gel permeation chromatography (GPC)-MS in pharmaceutical industry has been made by Siegel.[25]

Natural products and their derivatives are believed to be one of the major contributors in drug development especially infectious and carcinogenic disease. However, their development as novel drug is hampered due to lack of clear-cut mechanism of action. MS based experiments provides promising unprecedented insights into the mode of action of these natural products.[26] Other development in the drug receptor binding is target identification using drug affinity responsive target stability (DARTS), based upon the affinity between drug molecule under study and its protein target without modifying the drug molecule. When any small molecule binds to any protein, modification in the structure of protein takes place making it resistant to protease enzyme.[27]

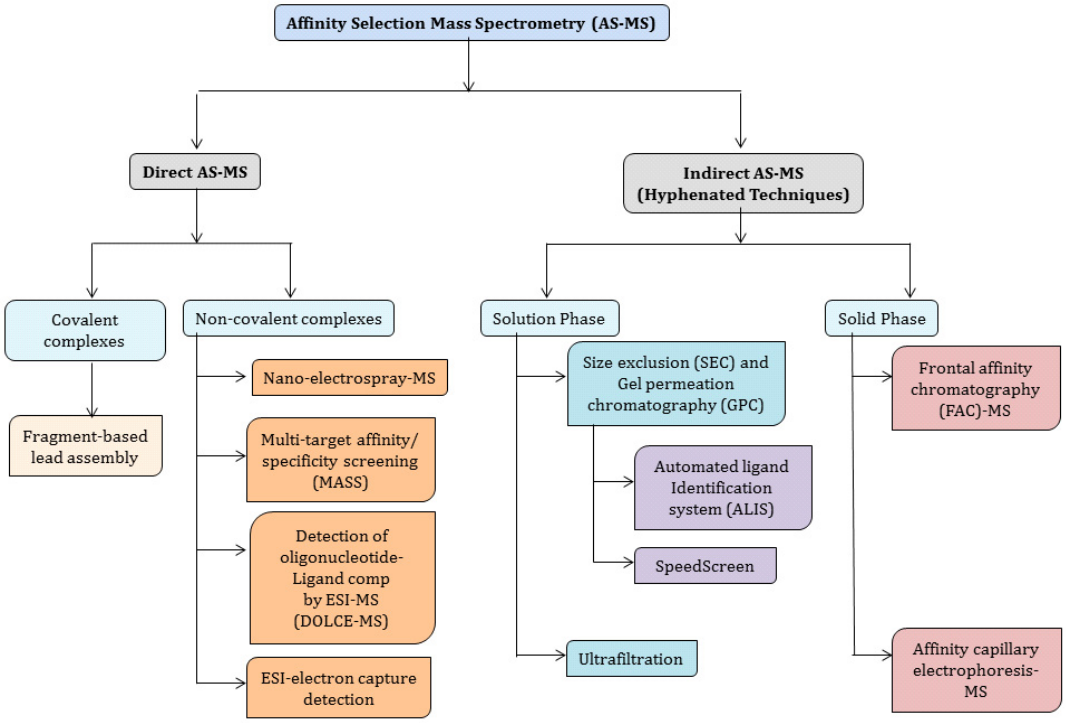

Fig. 3. Classification or different types of Affinity Selection Mass Spectrometry (AS-MS) utilized for identification and validation of biological targets.[18]

ADME and pharmacokinetic studies

Pharmacokinetics (PK) is the study of the absorption (A), distribution (D), metabolism (M) and excretion (E) of the drug molecule within the body. The PK deals with the time of course of drug's concentration in plasma/ blood. So to understand the PK of any drug molecule or drug candidate, properly finding of its concentration throughout the course of its action inside the body becomes quintessential.[28] Such PK characteristics or parameters are area under the curve (AUC), clearance, plasma versus blood clearance, apparent volume of distribution, half-life and bioavailability. According to Kola *et al*. the attrition rates due to PK characteristics in pharmaceutical industry for development of novel drug accounted to 40% in 1991.[29] PK *in vivo* studies are performed on animals such as rats, rabbits etc. where they are dosed with the drug at regular or extended time interval. These studies provide the valuable information regarding bioavailability in certain blood stream or biological fluids, half time and clearance of the drug. These details enable to determine the dosing regimen of the potent active pharmaceutical ingredient.

A quantification study for this purpose is carried out by spectrophotometric methods (UV/Vis) or by fluorescence for over the years. Radiolabelling of the drug molecule with ^{13}C and ^{1}H was one such classical methodology to perform metabolic studies. The mass spectrometry has changed the understanding of the ADME of various drug molecules and in turn the drug discovery and development through its inherent sensitivity, selectivity and speed of detection.[30] In ideal MS studies, the systems involving the chromatographic systems, the analyte must elute from the chromatographic technique, should be vaporized and ionized to the desired polarity (*m*/*z*) under the respective ionization source.

Various research groups have embarked on the

utilization of MS instrument and their advancements for determination of PK characteristics of drug in animal and human models. Yamane *et al*. have demonstrated the successful application of LC-MS/MS to assay of anti-histaminic drug, fexofenadine in plasma after administration of a microdose and a clinical dose to eight healthy volunteers.[31] Recently, HPLC-MS/MS has been adopted for determining the concentration of brazilin, a historical staining red pigment of *Caesalpinia sappan* L. in body fluids of rats to study the PK parameters, distribution and elimination.[32] Recently, super critical fluid chromatography (SFC) coupled with MS (SFC-MS) is gaining popularity as an alternative method to LC-MS/MS or HPLC-UV because of the greater speed/shorter run times and Hoke *et al*. have successfully demonstrated the superiority of super critical fluid chromatography SFC-MS in terms of speed, selectivity, sensitivity and reproducibility over LC-MS/MS for the quantification of the (*R*)- and (*S*)-enantiomers of non-steroidal anti-inflammatory drug (NSAID) ketoprofen in human plasma following oral and topical administration.[33] Similarly, an attractive alternative to HPLC-UV methodology was demonstrated by using SFC-MS considering cost, speed and reproducibility for determination of sulfadoxine level in healthy volunteers via oral dose in combination with pyrimethamine.[34]

Mass spectrometry imaging (MSI) studies has rapidly emerged as precious technology providing the key insight for drug distribution studies in comparison with other traditional methods. A huge number of drugs and their metabolites are studied using MSI via MALDI, Secondary Ion MSI (SIMS), Desorption Electrospray Ionization (DESI), Laser Desorption Ionization (LDI), etc. With this continued development MSI has contributed exhaustively in drug discovery and development workflow.[35]

Enzyme assay and in-vitro studies

Target-identification and mechanism-of-action studies have important roles in drug discovery. Various enzymes present inside the body are the target of most of the drug molecules.[36] In order to study the interactions and to quantify the bioanalytes, mass spectrometry has emerged as panacea for in-vitro drug discovery studies.

Two different quantitative techniques are used for the target identification of small-molecules a) Metabolic labeling and b) Chemical labeling method.[37] Stable isotope labeling by amino acids in cell culture (SILAC) and isotope-coded affinity tag (ICAT) are some of the isotope labeling methods available for the quantitative estimation of the drug-protein interactions. In direct biochemical method isotope labeling and subsequent detection by quantitative MS is carried out. Cells are either labeled with heavy and light isotopes, one compound is mixed with soluble competitor compound and the other without competitor compound and samples are analyzed by quantitative MS.[38] Chemical labeling is also one such methodology to study the small molecule-protein interaction. Brett Lomenic *et al*. in 2009 established a new technique for drug target identification known as drug affinity responsive target stability (DARTS) and identified the molecular target of resveratrol. Figure 4 depicts its mechanism. This is a gel electrophoresis based method where to a complex mixture of protein (cell lysates) any ligand or small molecule to be investigated is added and subsequently its binding to the target protein is identified and analyzed with the help of MS. Examination of the bands of gel electrophoresis by MS reveals the binding of the natural ligand didemnin B (DB) to the EF-1á.[27,39]

Off-target drug binding is an event where the small hydrophobic drugs bind with unintended protein targets other than its normal target, which leads to various untoward side effects. Carol v. Robinson et al in 2016 have shown off-target drug binding of various HIV protease inhibitors (PIs) with the help of MS. A sensitive assay using high-performance liquid chromatography tandem mass spectrometry (HPLC-MS/MS) has been established for the quantitative analysis of cytochrome P450 form-specific activities using warfarin as a probe.[40] In drug metabolism and disposition study there are various assays used such as Quantitative In Vitro ADME assay, assay of oligonucleotides of DNA, uptake and efflux transporter assays, Caco-2 cell permeability assays. For the quantification of bioanalytes and low molecular weight compounds LC-MS/MS, HPLC-MS/MS, MALDI-TOF and ICP-MS (inductively coupled plasma-Mass spectrometry) techniques are being used now a days.[41] Siuzdak *et al*., in 2003 have developed a new technique for quantification of bio analytes by Desorption/ Ionization on Silicon-Mass Spectrometry Using Electrospray Deposition.[42] Antibody–drug conjugates (ADCs) have emerged as a new promising targeted therapy in oncology. The antibodies are conjugated with the cytotoxic drugs for targeted delivery at the tumor site. Characterization, quantification and qualitative analysis of antibody–drug conjugates have been carried out by MS.[43]

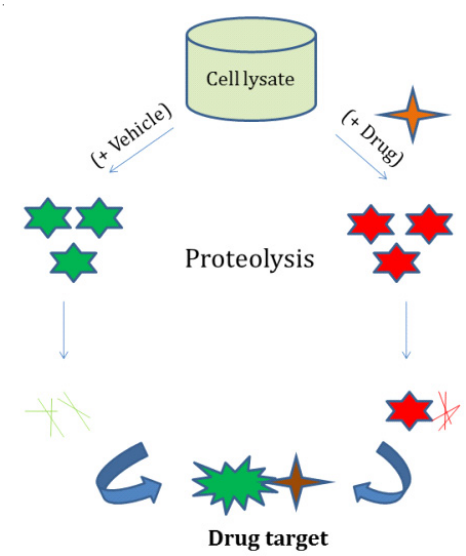

Fig. 4. DARTS method for drug target identification.[27]

Metabolic profiling

Identification of metabolites in a biological sample is a cumbersome procedure given the fact that it contains complex mixture of chemical species and the concentration of any drug related metabolite in bio fluid sample used to be very

less.[44,45] The metabolites are in such a low concentration that it is not possible to detect by total ion current chromatogram.[46] There are various factors that affect the concentration and distribution of metabolites inside tissue and plasma. Some of the factors such as relative tissue and plasma protein binding affinities, pH effects, and membrane transporters cause uneven drug distribution in different tissues.[47] Advancement in the biomolecular mass spectrometry has made metabolic profiling of drugs and low molecular weight compounds easy and comprehensive. HPLC-MS is the key analytical technique for metabolite characterization and quantitative analysis of drugs in modern drug discovery and development. Out of various ionization methods for mass spectrometry APCI is suitable for monitoring drug and metabolite concentrations in samples from animals and humans. The very high sensitivity of APCI further enhances the applicability of this technique in drug analysis.[48]

Advancements and future prospects

The traditional methodology of the mass spectrometry has witnessed tremendous transformation. A range of new techniques for mass spectrometry has been devised such as MALDI–IMS (Matrix assisted laser desorption ionization-imaging mass spectrometry),[49] Liquid Chromatography–Accurate Radioisotope Counting (LC-ARC-MS) Coupled with a Radioactivity Detector and Mass Spectrometer for Metabolite Identification,[50] High-Performance Liquid Chromatography Coupled with Quadrupole-Linear Ion Trap Mass Spectrometry (HPLC-Q-TRAP) for metabolite profiling,[51] SELDI-TOF (surface enhanced laser desorption/ionization-time of flight-mass spectrometry),[52] laser diode thermal desorption-Mass spectrometry (LDTD-MS) for High-Throughput assays.[53] High resolution Two dimensional electrophoresis coupled with MS (2DE-MS) is used for the identification of disease associated biomarkers specially used for anti-cancer drug discovery.[54] Mass spectrometry is playing central role in some of the newer techniques and methodologies of drug discovery such as fragment based lead discovery[55], ligand observed mass spectrometry,[56] drug affinity responsive target stability (DARTS) [27] and spatial profiling of drug distribution within biological tissue by liquid extraction surface analysis-Mass spectrometry (LESA-MS).[57] Mass spectrometry-based proteomics has shown significant promise in preclinical drug discovery setup.[58] These newer variants of mass spectrometry have their own roles and advantages and have streamlined the drug discovery and development process. New ion fragmentation techniques: such as electron capture dissociation, electron transfer dissociation, infrared multiphoton dissociation and their attributes have led the process of identification and quantification of metabolites and bioanalytes to next level. Understanding of these interactions and their mechanism is the key aspects for the drug discovery and development. These mass spectrometric based proteomic studies have not only led to a better understanding of what a small molecule actually does to a biological system but also to a better appreciation of how this information may be exploited therapeutically. To understand the nitty gritty details of some of the complex biological processes of nature, drug-receptor interactions inside biological systems and identification of lead molecules for drug discovery process mass spectrometry could serve as irrefutable analytical tool.

References:

(1) G. L. Glish & R. W. Vachet, Nat. Rev. Drug Discov., **2** (2003) 140.

(2) D. L. Pavia, G. M. Lampman, G. S. Kriz, J. A. Vyvyan, Introduction to Spectroscopy, 5th edition, Cengage Learning, USA, 2008

(3) E. L. Schymanski, J. Jeon, R. Gulde, K. Fenner, M. Ruff, H. P. Singer, and J. Hollender, Environ. Sci. Technol. **48** (2014) 2097.

(4) R. Ramanathan, M. Jemal, S. Ramagiri, Y-Q Xia, W. G. Humpreys, T. Olaha and W. A. Korfmacherc. Mass. Spectrom. **46** (2011) 595.

(5) W. B. Dunn, A. Erban, R. J. M. Weber, D. J. Creek, M. Brown, R. Breitling, T. Hankemeier, R. Goodacre, S. Neumann, J. Kopka, M. R. Viant, Metabolomics, **9** (2013) 44.

(6) J. D. Watrous and P. C. Dorrestein, Nat Rev Microbiol. **9** (2011) 683.

(7) S. Castellino, M. R. Groseclose, D. Wagner, Bioanalysis, **3** (2011) 2427.

(8) (a) T. Greer, R. Sturm, L.J. Li, J. Proteomics, **74** (2011) 2617. (b) E. H. Seeley, R. M. Caprioli, Trends Biotechnol. **29** (2011) 136. (c) P. Chaurand, J. Proteomics (2012). (d) L. A. McDonnell, R. M. Heeren, Mass Spectrom. Rev. **26** (2007) 606. (e) Y. Hsieh, J. Chen, W.A. Korfmacher, J. Pharmacol. Toxicol. Methods **55** (2007) 193.

(9) C. B. Lietz, E. Gemperline, L. Li, Adv. Drug Deliv. Rev., **65** (2013) 1074.

(10) D. T. Rossi, M. Sinz, Mass Spectrometry in Drug Discovery, Marcel Dekker, Inc. 2002, New York, USA.

(11) E. D. Hoffman and V. Stroobant, Mass spectrometry, John Wiley & Sons Ltd, 2007, UK.

(12) Dempster, A. J. Phys. Rev. **11** (1918) 316.

(13) M. M. Gessel, J. L. Norris, R. M. Caprioli, J. Proteomics, **107** (2014) 71.

(14) A. R. Timerbaev, J. Anal. At. Spectrom. **29 (**2014) 1058.

(15) (a) R. B. Silverman and M. W. Holladay, The Organic Chemistry of Drug Design and Drug Action, Academic Press, 3rd edition, Belgium, 2014. (b) M. Schenone, V. Danèík, B. K. Wagner, P. A. Clemons, Nat. Chem. Biol. **9** (2013) 232.

(16) M. Schirle, M. Bantscheff and B. Kuster, Chem. & Biol. **19** (2012) 72-84

(17) (a) D. S. Hage, Clin. Chem. **45** (1999) 593. (b) K. P. Imaduwage, E. P. Go, Z. Zhu, H. Desaire, J. Am. Soc. Mass Spectrometry, **27** (2016) 1870.

(18) D. A. Annis, E. Nickbarg, X. Yang, M. R. Ziebell, C. E. Whitehurst, Curr. Opin. Chem. Biol. **11** (2007) 518.

(19) Y. Saeys, I. Inza, P. Larran˜ aga, BIOINFORMATICS, **23** (2007) 2507.

(20) G. Deng, G. Sanyal, J. Pharm. Biomed. Anal. **40** (2006) 528.

(21) C. E. Whitehurst, Z. Yao, D. Murphy, M. Zhang, S. Taremi, L. Wojcik, J. M. Strizki, J. D. Bracken, C. C. Cheng, X. Yang, G. W. Shipps, M. Ziebell, E. Nickbarg, Chem. High Through. Screen. **15**, (2012), 473.

(22) E. S. M. Ng, F. Yang, A. Kameyama, M. M. Palcic, O. Hindsgaul, D. C. Schriemer, Anal. Chem. **77** (2005) 15495.
(23) C. Schou, N. H. H. Heegaard, Electrophoresis **27** (2006) 44.
(24) P. Hannewald, B. Maunit, J.-F. Muller, Anal. Chem. **78 (**2006) 4390.
(25) M. M. Siegel, K. T. Wanner, G. Hofner, Mass Spectrometry in Medicinal Chemistry, Wiley-VCH, 2007; pp 65–120.
(26) K. Cheng, C. Wong, M. Wang, Q. He, F. Chen, Mass Spectrom. Rev, **29** (2010) 126.
(27) B. Lomenick, R. Hao, N. Jonai, R. M. Chin, M. Aghajan, S. Warburton, J. Wang, R. P. Wu, F. Gomez, J. A. Loo, J. A. Wohlschlegel, T. M. Vondriska, J. Pelletier, H. R. Herschmana, J. Clardy, C. F. Clarke and J. Huang, Proc. Natl. Acad. Sci. **106** (2009) 21984.
(28) G. R. Jang, R. Z. Harris, D. T. Lau, Med. Res. Rev. **21** (2001) 382.
(29) I. Kola, J. Landis, Nat. Rev. Drug Discov. **3 (**2004), 711.
(30) R. Ramanathan, Mass Spectrometry in Drug Metabolism and Pharmacokinetics; John Wiley & Sons, Inc.: New Jersey, 2009.
(31) N. Yamane, Z. Tozuka, Y. Sugiyama, T. Tanimoto, A. Yamazaki, K. Yuji, *J. Chromatogr. B.* **858** (2007) 118.
(32) Y. Jia, H. Wang, Y. Song, K. Liu, F. Dou, C. Lu, J. Ge, N. Chi, Y. Ding, W. Hai, A. Wen. J. Chromatogr. B. **931** (2013) 61.
(33) S. H, Hoke, J. D. Pinkston, R. E. Bailey, S. L. Tanguay, T. H. Eichhold, Anal. Chem. **72** (2000) 4235.
(34) S. I. Bhoir, I. C. Bhoir, A. M. Bhagwat, M.J. Sundaresan, Chromatogr. B. **757** (2001) 39.
(35) B. Prideaux,; M. Stoeckli, J. Proteom. **75** (2012) 4999.
(36) Inglese J, et al. Nat Chem Biol, **3** (2007) 466. (b) L. Burdine, T. Kodakek, Chemist. Biol. **11** (2004)593.
(37) Z. Li, R. M. Adams, K. Chourey, G. B. Hurst, R. L. Hettich, and C. Pan, J. Proteome Res, **11** (2012) 1582. (b) M. schenone, V. danèík, B. K. Wagner & P. A clemons, Nat. chem. boil. **9** (2013)
(38) S-E. Ong, B. Blagoev, I. Kratchmarova, L. J. Foster, J. S. Andersen, and M. Mann, Stable Isotope Labeling by Amino Acids in Cell Culture for Quantitative Proteomics, Mol. Cell. Proteomics, (2002) 376. (b) S. P. Gygi, B. Rist, S. A. Gerber, F. Turecek, M. H. Gelb, and R. Aebersold, Nat. Biotechnol. 17 (1999) 994.
(39) B. Lomenick, G. Jung, J. A. Wohlschlegel, J. Huang, Curr. Proto. Chem. Biol. **3** (2011) 163.
(40) S. Mehmood, J. Marcoux, J. Gault, A. Quigley, S. Michaelis, S. G. Young, E. P. Carpenter and C. V. Robinson, Nat. Chemistry, **8** (2016)1152.
(41) R. B. V. Breemen, Y. Li, Expert Opin. Drug Metab. Toxicol. **1** (2005) 175. (b)
(42) E. P. Go, Z. Shen, K. Harris and G. Siuzdak, Anal. Chem. **75** (2003) 5475.
(43) R. Y.-C. Huang and G. Chen, Drug Discov. Today, **21** (2016) 850.
(44) R. F. Venn, Principles and Practice of Bioanalysis, CRC Press, USA, 2008.
(45) C. Prakash C. L. Shaffer, A. Nedderman, Mass Spectrom. Rev. **3** (2007) 340.
(46) M. Gu, Y. Wang, X-G Zhao and Z-M Gu, Rapid Commun. Mass Spectrom. **20** (2006) 764.
(47) M. S. Lee, M. Zhu, Mass Spectrometry In Drug Metabolism And Disposition: Basic Principles and Applications, John Wiley & Sons, Inc. New Jersey, USA, 2011.
(48) W. A. Korfmacher, Mass Spectrometry For Drug Discovery And Drug Development, John Wiley & Sons, Inc. New Jersey, USA, 2013.
(49) (a) P. M. Angel and R. M. Caprioli, Biochemistry **52** (2013) 3818. (b) M. M. Gessel, J. L. Norris and R. M. Caprioli, J. Proteom. 2014, 71.
(50) A.-E. F. Nassar and S. M. Bjorge, Anal. Chem., 75 (2003) 785.
(51) (a) Y. Q. Xia, J. D. Miller, R. Bakhtiar, R. B. Franklin, D. Q. Liu, Rapid Commun. Mass Spectrom. 2003, 17, 1137. (b) Z. Hu, Z. Wang, Y. Liu, Y. Wu, X. Han, J. Zheng, X. Yan, and Y. Wang, J. Agric. Food Chem. **63** (2015), 8999.
(52) (a) J. D. Wulfkuhle, C. P. Paweletz, P. S. Steeg, E. F. Petricoin 3rd, L. Liotta, Adv. Exp. Med. Biol. **532** (2003) 59. (b) G. Reid, B. S. Gan, Y-M She, Appl. Environ. Microbiol. **68** (2002) 977.
(53) J. Wu, Hughes, C. S.; Picard, P.; et al. Anal. Chem. **79** (2007) 4657.
(54) B. L. Adam, A. Vlahou, O. J. Semmes, G. L. Wright Jr. Proteomics **1** (2001) 1264.
(55) D. C. Rees, M. Congreve, C. W. Murray and R. Carr, Nature 537, 347.
(56) X. Chen, S. Qin, S. Chen, J. Li, L. Li, Z. Wang, Q. Wang, J. Lin, C. Yang and W. Shui, Sci Rep. **5** (2015) 8361.
(57) J. Sarsby, R. L. Griffiths, A. M. Race, J. Bunch, E. C. Randall, A. J. Creese and H. J. Cooper, Anal. Chem. **87 (**2015) 6794.
(58) M. Mann, Nat. Rev. Mol. Cell Biol. **17**, (2016) 678.

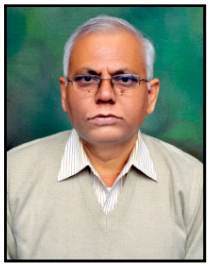

Dr. Asit Kumar Chakraborti received his Ph.D. (Science) under the direct supervision of Dr. U. R. Ghatak from IACS, Calcutta, India. After his post-doctoral work with Dr. Karl Dieter and Dr. Mark Cushman from USA, he joined as Senior Lecturer in the Department of Chemistry, Burdwan University. Currently he is giving his service as Professor and Head of Department of Medicinal Chemistry at National Institute of Pharmaceutical Education and Research (NIPER), S.A.S. Nagar. He has authored over 160 publications in peer reviewed international journals, guided over 30 doctoral and over 110 masters' research students and completed several Govt. (national and International) funded projects. Prof. Chakraborti is Fellow of the Indian Academy of Sciences (FASc), Bangalore, the Indian National Science Academy (FNA), New Delhi and Royal Society of Chemistry (FRSC), Cambridge.

Mr. Asim Kumar obtained his B. Pharm (Bachelor of Pharmacy) from Sam Higginbottom University of Agriculture Technology and Sciences (Formerly AAI-DU), Allahabad in 2011 and M.S. (Pharm.) from National Institute of Pharmaceutical Education and Research (NIPER), S.A.S. Nagar in 2013. He is currently pursuing Ph.D. under the supervision of Prof. Asit K. Chakraborti at NIPER, S.A.S Nagar. His Ph.D. work involves development of new methodologies for the synthesis of bioactive heterocycles via C-H bond activation strategy and development of heterobimetallic nanoparticles catalysed organic transformations.

Mr. Tejas M. Dhameliya completed his B. Pharm. (Bachelor of Pharmacy) from L. M. College of Pharmacy, Ahmedabad, Gujarat Technological University in May 2012 and persuaded post-graduation studies M.S. (Pharm.) from National Institute of Pharmaceutical Education and Research (NIPER), S.A.S. Nagar in June 2014. He is currently pursuing Ph.D. under the supervision of Prof. Asit K. Chakraborti at NIPER, S.A.S Nagar. His area for research includes development of anti-mycobacterial agents using green methodologies of synthesis adopting water and ionic liquid, molecular modeling using 3D-QSAR, docking and quantum chemical calculations.

Applications of Mass Spectrometry in Proteomics

Kranthikumar Yadav[1], R. Srinivas[1] and M. V. Jagannadham*[2]

[1]National Centre for Mass Spectrometry, CSIR-Indian Institute of Chemical Technology, Uppal Road, Tarnaka, Hyderabad-500007, India

[2]CSIR-Centre for Cellular and Molecular Biology, Uppal Road, Tarnaka, Hyderabad-500007, India

(Email: jagan@ccmb.res.in;Fax: +91-40-27160591; Phone: 040-27192572)

Introduction

Proteomics defines the use of quantitative protein level of gene expression to characterise biological processes and interpret the mechanisms that control gene expression. Proteins are vital molecules of living organisms, as they are the main components of the physiological and metabolic pathways of cells. Proteomics refers to the identification of proteins of genome which are expressed by proteins and it's observation of expression, its localisation, functional importance, posttranslational modification and their interaction at specific condition and time too. It is evident that most of the functional information on the genes resides in the proteome, which is the sum of multiple variable processes that include protein trafficking, localization and protein-protein interaction [1]. Therefore proteomics is the rich source of biological information as they are involved in almost all biological activities and also have diverse properties, which collectively contribute to our understanding of biological system.

There was a limit to mass spectrometry for long time to small and thermo stable compounds because of the lack of these soft ionisation techniques to ionize and transfer the condensed phase molecules into the gas phase, without complete fragmentation. The development of two ionization techniques in the 1980s for the formation of molecular ions of intact biomolecules namely electrospray ionization (ESI) [2] and matrix assisted laser desorption/ionization (MALDI) [3] changed this situation. The polypeptides and other biological molecules are subsequently subjected to mass spectrometric analysis. This brought into the development of advanced mass analyzers and complex multistage instruments [for example, combination of quadrupole time-of-flight (Q-Q-ToF) and tandem time-of-flight (ToF-ToF) instruments] (Table 1) invented to the challenges of proteome analysis [4, 5]. Mass spectrometers are used either to measure direct molecular mass (m/z) of a polypeptide or to determine additional structural features including the amino acid sequence determination and post translational modifications.

The various mass spectrometers described here are most often used as base in a range of research scenario in the protein sciences. They alter in their physical conventions, their standards of performance, their capacity to support certain analytical strategies and the mode of operation.

In TOF analyzers and analyte mass to charge ratio is detected from flight time through a specific length tube which is under vacuum. The achievements of TOF analyzers have improved immensely, particular in the area of resolution and mass accuracy [6]. In different mass analyzers TOF is the basis for analytical platforms operated with both ESI and MALDI. For peptides and proteins, MALDI is the affordable technique and is often used to compare the results attained by ESI. Compare with MALDI, ESI is not a tolerant technique to impurities such as salts or detergents.

Fourier transform–ion cyclotron resonance (FT-ICR) mass spectrometers with external ion source [7] represented a step forward in terms of resolving strength and mass accuracy. Measurements in the low ppm, sub ppm range is obtained. Since its resolving power FT-ICR not only produces better quality but also improves peaks sensitivity and thus allows for the observation of more signals rather the instruments with lower resolving power. The development of externally arranged linear ion trap ((LIT, The linear ion trap uses a set of quadrupole rods to confine ions radially and a static electrical potential on the end electrodes to confine the ions axially) in combined FT-ICR device has joined robustness to this platform and allowed common generation of low-resolution MS/MS spectra with accurate mass of the parent ions. FT-MS performed on an LIT-ICR hybrid instrument allows high yields which can also be used for quantification and tandem mass acquisition (MS^2) (not sequential). The only drawback of that is the relatively slow acquisition rate (several sec/cycle) and the limited dynamic range of IT devices. Very recently, a new type of mass analyzer called Orbitrap [8, 9] was developed. It is the new physics principle (ions separation is in an oscillating electric field) based prime analyzer that is introduced in the market. This instrument gives characteristic similar features like resolution and mass accuracy to an FT-ICR spectrometer but without the difficulty of overpriced superconducting magnet. In MS/MS modes of procedure, to know the amino acid sequence of the certain peptide, tandem mass spectrometry is used the most. This technique is available on all types of MS/MS efficient instruments. However, particular instruments (Table. 1) permits variable MS/MS experiments with this recent developments leads new hopes to characterisation of biomolecules. Alternate fragmentation techniques to CID that are depending on electron transfer of the ions present in the collision cell have been improved to get peptide sequencing efficiency. An appropriate, electron capture dissociation (ECD) [10] and electron transfer dissociation (ETD) [11] have been carryout on respective FT-ICR and LIT instruments. These two techniques yield fragments that are complementary to the classical CID fragmentation. They tend to be more evenly distributed over the entire peptide backbone and are particularly useful in localizing posttranslational modifications. ECD and ETD are also applicable extensively to the peptides and proteins.

Table 1: Characteristics and performances of commonly used types of mass spectrometers

	IT-LIT	Q-Q-ToF	ToF-ToF	FT-ICR	Q-Q-Q	QQ-LIT
Mass accuracy	Low	Good	Good	Excellent	Medium	Medium
Resolving power	Low	Good	High	Very high	Low	Low
Sensitivity (LOD)	Good	——	High	Medium	High	High
Dynamic range	Low	Medium	Medium	Medium	High	High
ESI	Available	Available	—-	Available	Available	Available
MALDI	Optional	Optional	Available	—-	—-	—-
MS/MS capabilities	Available	Available	Available	Available	Available	Available
Identification	Good	Good	Good	Excellent	Moderate	Moderate
Detection of modifications	Moderate	Moderate	Moderate	Moderate	—-	Excellent

Identification of Proteins

The "top-down" molecular point of view concentrates excessively on intact protein molecules expressed by cells. As new methods were combined together with genome sequencing for the identification of proteins, more clues were revealed that various protein produced can come from a single gene. The most rigorous definition of a top-down experiment involves high-resolution measurement of with an intact molecular weight value (Mr) and fragmentations of proteins in the gas phase. Better accuracy reduces uncertainties associated with saying that a protein is completely characterized. Top-down fragmentation was primarily demonstrated with electrosprayed ions of ribonuclease A (14 kDa) using a triple quadrupole (QQQ) instrument [12]. Shortly thereafter, Feng and Konishi demonstrated the same approach on a 150-kDa antibody also using electrospray ionization (ESI) with a a triple-quadrupole instrument [13].

Proteins are typically ionized by electrospray ionization and trapped in a Fourier transform ion cyclotron resonance (FT-ICR) [14] or quadrupole ion trap [15] mass spectrometer. Expanded demonstrations of variety of different ESI/ion trap, ESI/Q-TOF and ESI/Q-FTMS (quadrupole-FTMS), MALDI/TOF and MALDI TOF/TOF instruments given in (Table. 2).

The most widespread method for protein identification is peptide mass fingerprinting [16, 17]. The mass of peptides derived from an in gel proteolytic digestion are measured and subsequently searched against a computer generated list obtained from the in silico digestion of a protein database or a translated nucleotide database using the same specific enzyme. Using the mass accuracy now available (1 ppm) this technique alone is sufficient in most cases to identify proteins with high confidence. With the possibility of highly accurate MS instruments, and high throughput handling and preparation of protein samples from 2D gels, the mechanical analysis of complete 2D gels with hundreds and even thousands of protein spots is possible, without human mediation. People are using a probability based protein identification tool [18]. The advantages of this type of scoring are simple rules can be derived for the judgement of significant results, other types of searches can be scored in the same way and the scores can be compared or combined from two types of datasets like fingerprint plus MS/MS data. The program derived from this algorithm (Mascot) supports peptide mass fingerprints, sequences queries and MS/MS ion searches. In several cases the data collected by MALDI mass fingerprints are not sufficient for reliable identification of a protein. To generate additional data, specificity and one can use peptide fragmentation techniques such as valuable sequence information. These possibilities could well be integrated into a high-throughput scheme.

Table 2: Instrumental configurations for the analysis of proteins

Ionization method	Analyzer	Ion fragmentation methods	MS/MS on Mixtures	Resolving power for fragment ions	References
ESI	Triple quad	CID	Yes	10^3	[19]
MALDI	TOF	ISD[a]	No	10^2	[20,21,22]
ESI	Q-TOF hybrid	CID	Yes	10^4	[23]
ESI	Ion trap	CID[b]	Yes	10^3; 10^4 possible	[24,25,26]
ESI	FTMS	CID, IRMPD, ECD	Yes	10^5; 10^6 possible	[27,28,29,30,31]
ESI	Q-FTMS hybrid	CID, IRMPD, ECD	Yes	10^5; 10^6 possible	[32]

CID, Collisions induced dissociation; IRMPD, IR multi photon dissociation; ECD, electron capture dissociation.

[a]MALDI with ISD has been extended very recently by using a TOF/TOF for MS/MS of c and y ions. [b]IRMPD has been demonstrated on peptides in an ion trap.

Table 3: Published uniform resource locators (URLs) to access tools for protein identification

URL	Description
http://www.matrixscience.com/	MASCOT
http://thompson.mbt.washington.edu/sequest/	Sequest program, database searching
http://www.prospector.uscsf.edu	MS-Tag (Protein Prospector)
http://www.expasy.ch/tools/findmod/	FindMod program for post-translational modifications
http://base-peak.wiley.com/msi/msres.html	Useful site which lists MS links
http://thegpm.org/TANDEM/index.html	X!Tandem (The GPM)
http://hs2.proteome.ca/prowl/knexus.html	Sonar
http://pubchem.ncbi.nlm.nih.gov/omssa/index.htm	OMSSA
http://bart.scripps.edu/public/search/pep_probe/search.jsp	PepProbe
http://phenyx.vital-it.ch/pwi/login/login.jsp	Phenyx
http://proteomics.ucsd.edu/LiveSearch/	InsPect
http://www.maxquant.org.	Andromeda

Software tools

Proteomics would not be possible without the proper software tools. There have been numerous improvements ranging from instrument control of mass spectrometers to data interpretation, database searching, and bioinformatics algorithms. Due to the increase in popularity of the World Wide Web, many of the tools are publicly available, several of which are summarized in Table. 3.

Post-translational Modification

Post-translational modifications (PTM) on a protein are catalysed by enzymes. Generally these are referred to the addition of a functional group by a covalent bond to a protein as in phosphorylation [33]. Methylation, glycosylation, proteolysis, N-acetylation, and lipidation, are some more examples for post-translational modifications. The ribosomes translate the mRNA molecule into polypeptides by using genetic code. Ones the polypeptide is synthesised, it is usually modified before it actually becomes a mature and active protein. Such modifications are known as post-translational modification.

Phosphorylation: Certain amino acids, such as threonine, serine and tyrosine, found on the polypeptide chain can be modified via phosphorylation by enzymes called protein kinases. This type of modification plays a crucial role in the cell cycle and signal transduction.

Methylation: Methyl groups can be added onto the amino acids by an enzyme called methyltransferase. Methylation usually increases the hydrophobic character of the amino acid. Methylation is utilised in epigenetic regulation, which is the regulation of gene expression.

Glycosylation: This is one of the major ways in which polypeptides are modified. This process involves adding sugar components to the proteins. This can affect the proteins conformation and folding. One example of proteins that are glycosylated are membrane proteins that acts as acceptors for important biological molecules.

Proteolysis: Certain proteins are synthesised in their inactive (zymogen) form, in order to activate them, enzymes called proteases must break certain bonds. Many of the digestive enzymes in the small intensive use this type of post-translational modification.

N-Acetylation: N-acetylation is the transfer of an acetyl group onto the nitrogen on amino acids. This process can takes place when the ribosome is still translating the polypeptide chain. In most eukaryotic cells, when transaction is still taking place, the first amino acid (methionine) is usually removed and replaced by an acetyl group. N-acetylation plays a crucial role in gene expression. Histones, the proteins that assist in condensing DNA into chromatids can be acetylated, which reduces their ability to fold and opens up the DNA for transcription.

Lipidation: Lipidation is the process by which lipid components are added onto the polypeptides. Usually those proteins that are destined to be in membranes, such as the ER membrane, mitochondrial membrane or plasma membrane undergo this process. It increases the proteins hydrophobic character, which in turn increases the proteins affinity to membranes.

Protein post-translational modifications play a key role in many cellular processes such as protein degradation [34], cellular differentiation [35], signalling and regulatory processes [36], protein-protein interaction and regulation of gene expression. Post-translational modifications can occur at the protein's C- or N- terminal amino acid and side chains too [37]. These post-translational modifications generate diversity, heterogeneity and complexity of gene products, and their study became one of the main task of research in proteomics. Recent improvements in mass spectrometry based approaches for systematically studying modified proteins helped in understandings the dynamics and regulation of protein activities by post-translational modifications. MS-based techniques standardised for separation and sequencing of peptides are complementary to gel electrophoretic methods for separation of intact proteins. With the help of these technologies the detection,

quantitation, and characterization of PTMs is possible [38–40]. Subsequently several phosphoproteins from the 2DE gel were identified by matrix-assisted laser desorption/ ionization time-of-flight (MALDI TOF) MS, nano electrospray MS/MS and liquid chromatography (LC)-MS/MS analysis [41].

Mass spectrometry continues to evolve, for higher sensitivity, resolution and mass accuracy, increased duty cycle and more efficient MS/MS fragmentation of peptides. Electrospray ionisation (ESI) MS/MS has been used for several years for peptide sequencing. Generation of diagnostic, PTM-specific reporter ions or fragments by MS/MS using parent ion scans [42-44] or neutral loss scans [45] is an efficient and highly sensitive method for selective and specific detection of modified peptides, including glycopeptides, phosphopeptides. However, further improvements and refinements of sample preparation techniques, mass spectrometer software and hardware is required to make these scanning methods applicable to the analysis of the highly complex peptide mixtures generated in many proteomics experiments. MALDI instruments have now emerged and proven efficient MS/MS for sequencing of post-translationally modified peptides (e.g. phosphopeptides) [46–48]. The main attributes of MALDI are robustness and high sensitivity and there is an increasing interest in combining MALDI MS/MS methods with peptide separation techniques. In situ liquid-liquid extraction is a simple and rapid method for the separation of hydrophilic and hydrophobic peptides before MALDI MS and MS/MS [49]. This method may enable more efficient detection and sequencing of modified, hydrophobic peptides, markedly for acylated peptides. Graphite columns permit capture of mainly hydrophilic peptides, glycopeptides and phosphopeptides for their analysis by MS [50].

Fourier transform ion cyclotron resonance (FT-ICR) MS inherently provides high mass accuracy and resolving power and is bound to make an impact in proteomics. Linear ion traps combined to FT-ICR improve the duty cycle and data quality attainable in LC-MS/MS by combining efficient ion build up and fragmentation with accurate mass determination for improved LC-MS/MS performance [51]. Electron capture dissociation (ECD) FT-ICR MS is a novel technique suited for sequencing of post-translationally modified peptides as it breaks merely the peptide backbone while leaving the modified amino acid side-chains intact [52]. Thus, ECD enables dynamic sequencing of phosphopeptides, glycopeptides and other types of modified peptides as well as of intact, modified proteins up to 45 kDa [53, 54]. Advances in intact protein separation techniques for MS [55,56] point towards future 'top-down' proteomic strategies for determination of PTMs. Combinations of affinity-based enrichment and extraction methods, multidimensional separation technologies and mass spectrometry are particularly useful for systematic investigation of post-translationally modified proteins in proteomics.

De novo Sequence

A well-known definition for "*de novo* peptide sequencing" is, peptide sequencing performed without prior knowledge of the amino acid sequence. *De novo* derives a peptide sequence from the mass spectrum without the need of a sequence database; this makes *de novo* sequencing the preferred method for identifying novel peptides and the study of organisms, whose genome sequence is not known. Even when the peptide sequence is available in a database, *de novo* sequencing can greatly help to improve the database-search based peptide identification, since the similarity between the *de novo* sequence and the database sequence explains the correctness of the identification for each amino acid of the *de novo* sequence. This permits the result filtration at the amino acid level. PEAKS search engine is available commercially, that also features a commonly used *de novo* sequencing program. In order to compare computer-generated results to manually sequenced data. PEAKS additionally calculates the ALC (average local confidence) and TLC (total local confidence) scores for each peptide by averaging and summing up to the local confidences.

Peptide fragmentation rules and nomenclature were established with these techniques. The first nomenclature was given by Roepstorff and Fohlman [57], but the recently accepted terminology was made by Biemann [58]. This time period was prime time for the peptide *de novo* sequencing, and most analysis was done by manually. Burlingame was the other well-known leading researcher in *de novo* sequencing using high-energy CID [59, 60]. Hunt et al., were the most famous users of low-energy CID data [61, 62]. The newest *de novo* sequencing trend is the combination of various MS/MS activation techniques. High resolution CID and ECD spectra provided enough information for the de novo sequencing of a bacterial protein [63].

De novo sequencing is possible by Edman degradation chemistry. However, at low quantities, gaps and uncertainties are often encountered, even with Edman sequencing. Mass spectrometers do have the advantage when it comes to generating sequence data in a low femto mole quantities of peptides. MS/MS sequencing does have difficulty with isobaric or near isobaric masses, for example K from Q telling in a low resolution, low mass accuracy mass spectrometers. Another advantage is that MS/MS sequencing is never hindered by a blocked amino terminus. The approach to *de novo* sequencing requires expertise to understand all of its challenges and also to all of its advantages. As scientists/ researchers need to have a faith in the derived *de novo* sequence without knowing the sequence, especially when software is involved. An excellent tutorial on *de novo* sequencing with an emphasis on software was published recently as part of a set of tutorial articles commissioned by the HUPO committee of education [64] and applications of *de novo* in large scale complex proteomics datasets published recently [65]. There is also an earlier review that could be useful for the interpretation of covalently modified peptide spectra [66].

It is very important to know that learning more about peptide fragmentation rules, and how to manually interpret and annotate data, is first step for everyone who is engaged in proteomic research. It would be especially important for all those who develop tools that enable researchers to process

the huge amount of data acquired in today's high-throughput experiments to have a thorough understanding of the data they analyze. Mathematical tools cannot work optimally unless their developers comprehend the physical, chemical, and biological complexity of the data. At the same time, challenging the users of these programs to develop a better understanding of the data analysis [67-73], as well as of the tools [74-78] used to decipher them. A closer collaboration between the two sides would be desirable for improving the confidence of the data.

Conclusions

Protein analysis and more specifically, proteomics have driven the development of mass spectrometry for the past decade. Advanced technology have translated into major improvements in mass accuracy, resolving power, LOD, and accuracy of quantification and new experimental strategies aimed at the routine and comprehensive analysis of whole proteomes. Though these mass spectrometry technologies have been driven by protein research, they also equally useful to other types of biomolecules, including metabolites, lipids, and carbohydrates and so on. Mere protein identification will become more straightforward as more genomes are sequenced, complete protein characterization will continue to require *de novo* techniques, thus *de novo* peptide and protein sequencing by MS is likely to have a bright future. It can therefore be anticipated that the use of mass spectrometry in the life sciences will become even more diversified.

References

1. M. A. Alaouli-Jamali, Y. J. Xu, J. Zhejiang university, Science B. **7** (2006) 411.
2. J. B. Fenn, M. Mann, C. K. Meng, S. F. Wong, C. M. Whitehouse, Science. **246** (1989) 64.
3. M. Karas, F. Hillenkamp, Anal. Chem. **60** (1988) 2299.
4. R. Aebersold, D. R. Goodlet, Chem. Rev. **101** (2001) 269.
5. R. Aebersold, R. M. Mann, Nature. **422** (2003) 198.
6. M. Vestala, P. Juhasza, **9** (1998) 892.
7. M. W. Senko, C. L. Henderickson, M. R. Emmett, S. D. Shi, A. G. Marshall, J. Am. Soc. Mass Spectrom. **8** (1997) 970.
8. M. Hardmanand, A. Makarov, Anal. Chem. **75** (2003) 1699.
9. Q. Hu et al., J. Mass Spectrom. **40** (2005) 430.
10. R. A. Zubarev, N. L. Kelleher, F. W. McLafferty, J. Am. Chem. Soc. **120** (1998) 3265.
11. J. E. P. Syka, J. J. Coon, M. J. Schroeder, J. Shabanowitz, D. F. Hunt, Proc. Natl. Acad. Sci. U.S.A. **101** (2004) 9528.
12. J. A. Loo, C. G. Edmonds, R. D. Smith, Science. **248** (1990) 201.
13. R. Feng, Y. Konishi, Anal. Chem.**65** (1993) 645.
14. B. Bogdanov, R. D. Smith, Mass spectrometry reviews. **24** (2005) 168.
15. N. John Louris, R. Graham Cooks, E. P. John Syka, E. Paul Kelley, C. George Stafford Jr. F. J. John Todd, Anal. Chem. **59** (1987) 677.
16. W. J. Henzel, T. M. Billeci, J. T. Stults, S. C. Wong, C. Grilely, C. Watanabe, Proc. Natl. Acad. Sci. USA. **90** (1993) 5011.
17. P. James, M. Quadroni, E. Carafoli, G. Gonnet, Bio-chem. Biophys. Res. Commun. **195** (1993) 58.
18. P. Berndt, U. Hobohm, H. Langen, Electeophoresis. **20** (1999) 3521.
19. J. A. Loo,C. G.Edmonds, R. D.Smith, Science. **248** (1990) 201.
20. D. C.Reiber, T. A.Grover, R. S.Brown, Anal. Chem. **70** (1998) 673.
21. R. R.Loo, et al. Anal. Chem. **73**(2001) 4063.
22. J. J.Lennon, K. A.Walsh, Protein Sci. 8 (1999) 2487.
23. J. F.Nemeth-Cawley, B. S.Tangarone, J. C. Rouse, J. Proteome. Res. **2** (2003) 495.
24. G. E.Reid, S. A.McLuckey, J. Mass Spectrom. **37** (2002) 663.
25. J. L. Stephenson, et al., Curr. Opin. Biotechnol. **13** (2002) 57.
26. G. E. Reid, et al., J. Am. Chem. Soc. **124** (2002) 7353.
27. N. L. Kelleher, et al., J. Am. Chem. Soc. **121** (1999) 806.
28. M. W. Senko, S. C. Beu, F. W. McLafferty, Anal. Chem. **66** (1994) 415.
29. Y. Ge, et al., J. Am. Soc. Mass Spectrom. **14** (2003) 253.
30. P. A. Demirev, J. Ramirez, C. Fenselau, Anal. Chem. **73** (2001) 5725.
31. S. K. Sze, et al., Proc. Natl. Acad. Sci. U.S.A. **99** (2002) 1774.
32. F. Meng, et al., Anal. Chem. **74** (2002) 2923. Morch, G. J. Hughes, K. L. Williams, D. F. Hochstraser, Electrophoresis. **19** (1998) 1960.
33. C. T. Walsh, Englewood, Colorado: Roberts and Company (2006).
34. R. G. Friedlander, F. Melchior, Nat. Rev. Mol Cell Biol. **8** (2007) 947.
35. G. Grotenbreg, H. Ploegh, Nature. **446** (2007) 993.
36. R. S. Morrison, Y. Kinoshita, M. D. Johnson, T. Uo, J. T. Ho, J. K. McBee, T. P. Conrads, T. D. Veenstra, Mol. Cell. Proteomics. **1** (2002) 553.
37. P. D. Voet, G. J. Voet, W. Charlotte, N. J. Hoboken, Wiley. **105** (2006).
38. M. Mann, O. N. Jensen, Nat. Biotechnol. **21** (2003) 255.
39. R. E. Schweppe, C. E. Haydon, T. S. Lewis, K. A .Resing, N. G. Ahn, Acc. Chem. Res. **36** (2003) 453.
40. J. G. Zimmermann, L. R. Brown, Curr. Opin. Mol. Ther. **5** (2003) 241.
41. N. V. Bykova, A. Stensballe, H. Egsgaard, O. N. Jensen, I. M. Moller, J. Biol. Chem. **278** (2003) 26021.
42. H. Steen, M. Mann, J. Am Soc. Mass Spectrom. **13** (2002) 996.
43. H. Steen, B. Kuster, M. Fernandez, A. Pandey, M. Mann, J. Biol. Chem. **277** (2002) 1031.
44. J. Jebanathirajah, H. Steen, P. Roepstorff, J. Am Soc. Mass Spectrom. **14** (2003) 777.
45. R. H. Bateman, R. Carruthers, J. B. Hoyes, C. Jones, J. I. Langridge, A. Millar, J. P. Vissers,-J. Am Soc. Mass Spectrom. **13** (2002) 792.
46. C. H. Lee, M. E. McComb, M. Bromirski, A. Jilkine, W. Ens, K. G. Standing, H. Perreault, Rapid. Commun. Mass Spectrom. **15** (2001) 191.
47. M. A. Baldwin, K. F. Medzihradszky, C. M. Lock, B. Fisher, T. A. Settineri, A. L. Burlingame, Anal. Chem. **73** (2001) 1707.
48. K. L. Bennett, A. Stensballe, A. V. Podtelejnikov, M.

Moniatte, O. N. Jensen, J. Mass Spectrom. **37** (2002) 179.
49. S. Kjellstrom, O. N. Jensen, Anal. Chem. **75** (2003) 2362.
50. M. R. Larsen, S. J. Cordwell, P. Roepstorff, Proteomics. **2** (2002) 1277.
51. M. J. Chalmers, J. P. Quinn, G. T. Blakney, M. R. Emmett, H. Mischak, S. J. Gaskell, A. G. Marshall, J. Proteome Res. **2** (2003) 373.
52. F. W. McLafferty, D. M. Horn, K. Breuker, Y. Ge, M. A. Lewis, B. Cerda, R. A. Zubarev, B. K. Carpenter, J. AmSoc. Mass Spectrom. **12** (2001) 245.
53. F. Kjeldsen, K. F. Haselmann, B. A. Budnik, E. S. Sorensen, R. A. Zubarev, Anal. Chem. **75** (2003) 2355.
54. S. K. Sze, Y. Ge, H. Oh, F. W. McLafferty, Proc. Natl. Acad Sci. USA. **99** (2002) 1774.
55. C. F. Taylor, N. W. Paton, K. L. Garwood, P. D. Kirby, D. A. Stead, Z. Yin, E. W. Deutsch, L. Selway, J. Walker, I. R. Garcia et al., Nat. Biotechnol. **21** (2003) 247.
56. S. Peri, J. D. Navarro, R. Amanchy, T. Z. Kristiansen, C. K. Jonnalagadda, V. Surendranath, V. Niranjan, B. Muthusamy, T. K. Gandhi, M. Gronborg et al. Genome. Res. **13** (2003) 2363.
57. P. Roepstorff, J. Fohlman, Biomed. Mass Spectrom. **11** (1984) 601.
58. K. Biemann, **193** (1990) 886.
59. K. F. Medzihradszky, B. W. Gibson, S. Kaur, Z. H. Yu, D. Medzihradszky, A. L. Burlingame, N. M. Bass. Eur. J. Biochem. **203** (1992) 327.
60. D. X. Wen, B. D. Livingston, K. F. Medzihradszky, S. Kelm, A. L. Burlingame, J. C. Paulson. J. Biol. Chem. **267** (1992) 21011.
61. D. F. Hunt, J. R. Yates III, J. Shabanowitz, S. Winston, C. R Hauer. Proc. Natl. Acad Sci. USA. **83** (1986) 6233.
62. D. F. Hunt, N. Z. Zhu, J. Shabanowitz, Rapid. Commun. Mass Spectrom. **3** (1989) 122.
63. R. M. Branca, G. Bodo, C. Bagyinka, L. Prokai. J. Mass Spectrom. **42** (2007) 1569.
64. B. Ma, R. Johnson. Mol. Cell. Proteomics. **11** (2012) 1.
65. A. Devabhaktuni, J. E. Elias, J. Proteome. Res. **15** (2016) 732.
66. K. F. Medzihradszky. Methods. Enzymol. **402** (2005) 209.
67. D. F. Hunt, J. R. Yates 3rd, J. Shabanowitz, S. Winston, C. R. Hauer. Proc. Natl. Acad. Sci. **83** (1986) 6233.
68. I. A. Papayannopoulos, Mass Spectrom. Rev. **14** (1995) 49.
69. S. E. Martin, J. Shabanowitz, D. F. Hunt, J. A. Marto. Anal. Chem. **72** (2000) 4266.
70. M. J. Schroeder, J. Shabanowitz, J. C. Schwartz, D. F. Hunt, J. J. Coon. Anal. Chem. **76** (2004) 3590.
71. J. E. Syka, J. J. Coon, M. J. Schroeder, J. Shabanowitz, D. F. Hunt. Proc. Natl. Acad Sci. U S A. **101** (2004) 9528.
72. R. Deutzmann, Methods. Mol. Med. **94** (2004) 269.
73. J. J. Coon, J. E. Syka, J. Shabanowitz, D. F. Hunt. Biotechniques. **38** (2005) 519.
74. D. M. Horn, R. A. Zubarev, F. W. McLafferty, Proc. Natl. Acad. Sci. **97** (2000) 10313.
75. R. Bruni, G. Gianfranceschi, G. Koch. J. Pept. Sci. **11** (2005) 225.
76. Y. Han, B. Ma, K. Zhang, J. Bioinform. Comput. Biol. **3** (2005) 697.
77. M. M. Savitski, M. L Nielsen, F. Kjeldsen, R. A. Zubarev, J. Proteome. Res. **4** (2005) 2348.
78. H. Zhong, L. Li. Rapid. Commun. Mass Spectrom. **19** (2005) 1084.

Mr Kranthikumar Yadav G completed M. Sc in Organic chemistry at Kakatiya university, in the year 2008. Later he qualified CSIR-UGC-NET exam and was selected in the UGC Fellowship scheme since August 2012. He is pursuing PhD as SRF under the supervision of Dr. R. Srinivas at CSIR-IICT. He is working in proteomics, particularly improving the de novo sequencing efficiency of peptides and bacterial membrane proteins whose genome sequence is not known by using mass spectrometry.

Dr. R. Srinivas obtained his Ph.D. from I.I.T. Chennai in 1985. He joined the mass spectrometry division, IICT, as a scientist in 1984. He was a post-doctoral fellow at T.U. Berlin and a Visiting scientist at TU, Berlin and University of Wurzberg. He has guided 11 PhDs, around 35 MS/MSc dissertations and published more than 165 research papers in peer reviewed international journals. He is the editorial board member of international journals viz. "Journal of Mass Spectrometry" "Open Spectroscopy Journal". He is a Fellow of A.P./Telangana Akademi of Sciences; Fellow of Royal Society of Chemistry (London), Advisory board member of National Authority of Chemical weapons convention, New Delhi: DBT-Taskforce committee member. Currently he is the Chief Scientist & Head, Mass & Analytical Division, Indian Institute of Chemical Technology.

Dr. M.V. Jagannadham is working as a senior principal scientist and project leader at the CSIR-Centre for Cellular and Molecular Biology. He published several research papers in internationally reputed scientific journals. He trained several students, conducted meetings and workshops in proteomics. He received "Bharat Jyothi" award from India International Friendship Society, New Delhi in 2014 and "Eminent Mass Spectrometrist" award from the Indian Society for Mass spectrometry (ISMAS) in 2015. His current research Interests are proteomics, particularly in improving the *de novo* sequencing efficiency of peptides using MS techniques, structural and functional studied of outer membrane vesicles of Gram-negative bacteria.

RNI MAHENG / 2002 / 7152

For Limited Circulation Only

Printed & Published by :
Dr. Raghunath Acharya, Secretary, Indian Association of Nuclear Chemists and Allied Scientists (IANCAS)
(Registration No. MAH 232/1984 GBBSD) on the behalf of IANCAS, C/o. Radiochemistry Division,
Bhabha Atomic Research Centre, Mumbai 400 085. Email : secretaryiancas@gmail.com

Printed at
Perfect Prints, 22/23, Jyoti Industrial Estate, Nooribaba Dargah Road, Thane 400 601.
Tel. : (022) 2534 1291 / 2541 3546, E-mail : perfectprints@gmail.com

Edited by
Dr. A. Dash
Bhabha Atomic Research Centre, Department of Atomic Energy, Mumbai